THE EFFECTIVENESS OF MULTI-STAGED SWIRLING FLUIDIZED BED

S. FAUZAN ASHRI

MECHANICAL ENGINEERING

UNIVERSITI TEKNOLOGI PETRONAS

DECEMBER 2012

The Effectiveness of Multi-Staged Swirling Fluidized Bed

by

S. Fauzan Ashri

Dissertation submitted in partial fulfillment of

the requirements for the

Bachelor of Engineering (Hons)

(Mechanical Engineering)

DECEMBER 2012

Universiti Teknologi PETRONAS

Bandar Seri Iskandar

31750 Tronoh

Perak Darul Ridzuan

CERTIFICATION OF APPROVAL

The Effectiveness of Multi-Staged Swirling Fluidized Bed

by

S. FAUZAN ASHRI
14632

A project dissertation submitted to
Mechanical Engineering Department
Universiti Teknologi PETRONAS
as partial fulfillment of requirements for the
BACHELOR OF ENGINEERING (Hons)
(MECHANICAL ENGINEERING)

Approved By,

_____
Ms. Chin Yee Sing

UNIVERSITI TEKNOLOGI PETRONAS

TRONOH, PERAK

DECEMBER 2012

CERTIFICATION OF ORIGINALITY

This is to certify that I am responsible for the work submitted in this project, that the original work is my own except as specified in the references and my acknowledgement, and that the original work contained herein have not been undertaken or done by unspecified sources or persons.

_____

S. FAUZAN ASHRI

ACKNOWLEDGEMENTS

First of all, I would like to thank my saviour the Almighty GOD for giving me the strength and ability to achieve what I have done and guide me throughout my life.

I am deeply indebted to my supervisor, Chin Yee Sing for her invaluable advices and exceptional guidance during my study and my final year project.

I would also like to extend thanks to the faculty members, lecturers and post graduate students who have helped in my final year project for their time, suggestions and comments, especially Ahmad Shukrie M. Yudin, Prof. Dr. Vijay R. Raghavan, Mr. Vinod Kumar and Mr. Anggara Warsita. Special thanks to my junior fellow Indonesian students who willingly assisted me to conduct experiments. Thanks to all who have supported me in one way or another.

Finally, thanks to all my parents and my brothers for their support and encouragement. Special thanks is reserved to my parents, S. Fadlan Akhyar and Sy. Fatimah who support me at all times during my study in Universiti Teknologi PETRONAS; without their patience, constant support and encouragement, my achievements would not be possible and meaningful.

ABSTRACT

Fluidization is defined as an operation through which fine solids are transformed into a fluid like state through contact with either a gas or a liquid. Circulating fluidized beds are used mostly in the chemical process industry, mineral processing, pharmaceutical production, energy related processes and catalysts process in the petroleum industry and also for drying. Although it has been investigated by many researchers, a good understanding in the effects of different design parameters on it is yet to be established. In fluidized bed processes, the effectiveness of fluidization process is necessary as it determines how much energy or power required by means of improvement in residence time distribution and bed pressure drop. The aim of the project is to combine multi-staging with counter-flow operation in the novel Swirling Fluidized Bed. In this study, the experiments were conducted utilizing one bed particle shape and size (spherical plastic beads with a diameter, d_p = 2.99mm), with four different bed weights (500 g, 1000 g, 1500 g and 2000 g) as well as with various distributor blade overlap angles (9°, 12° and 15°) at constant blade inclination of 10°. The experimental set up has two stages and it has been tested and to work properly. A particular set of variables that include bed weight and blade overlap angle were set to analyze the results of two-staged swirling fluidized bed. During hydrodynamics study, it was found that the bed pressure drop ΔP_b for both stages increases with superficial velocity and bed weight. Moreover, a distributor with 15° blade overlap angle showed the lowest pressure drop when compared to 12° and 9°. The experimental results of solid residence time distribution have shown that as the bed weight increases, the area under the tail of curve increases and it shifts the peak of the distribution towards the higher value of θ (moving the curve to the right) with the value of dimensionless age distribution $E(\theta)$ reduce. Concurrently, the blade overlap angle affects the value of $E(\theta)$ with no significant change on the value of θ. Thus, the experiment set up is shown to be highly versatile and capable of representing widely different conditions depending on the variables from the parameters.

TABLE OF CONTENTS

CERTIFICATION OF APPROVAL ii

CERTIFICATION OF ORIGINALITY iii

ACKNOWLEDGEMENT iv

ABSTRACT v

LIST OF FIGURES x

LIST OF TABLES xiii

LIST OF SYMBOLS AND ABBREVIATIONS xiv

1. CHAPTER 1 INTRODUCTION

1.1 Background of Study 1

1.2 Problem Statement 3

1.3 Objectives and Scope of Study.....3

2. CHAPTER 2 LITERATURE REVIEW

2.1 Fluidized Concept 4

2.1.1 Ergun Equation 4

2.1.2 Particle Characterization and Dynamics 6

2.2 Single-Staged Swirling Fluidized Bed 6

2.2.1 Hydrodynamics and Operating Parameters 7

2.2.2 Studies on Annular Distributor and Bed Behaviour 8

2.3 Multi-Staged Swirling Fluidized Bed.....8

2.3.1 Pressure Drop Theory Over Heights 9

2.4 Design Specific Research and Recent Findings 10

2.4.1 Operating Velocity 10

2.4.2 Aspect Ratio 11

2.4.3 Distributor 11

2.4.4 Downcomer 13

2.4.5 Valves 13

2.5 Residence Time Distribution 14

2.6 Residence Time Distribution (RTD) Measurement Method 16

3. CHAPTER 3 METHODOLOGY

3.1 Flow Chart 17

3.2 Project Work 18

3.2.1 Physical Representation of the Bed Behaviour 19

3.2.2 Residence Time Distribution Density Function 20

3.2.3 Mean Residence Time 20

3.2.4 Dimensionless Residence Time Distribution Density Function 20

3.3 The Construction of Multi-Staged SFB 21

3.3.1 Pressure Monitoring 25

3.3.2 Solid Feed and Solid Discharge 26

3.3.3 Sample Collector 28

3.3.4 Bed and Tracer Material 31

3.3.5 Residence Time Distribution Experimental Condition 32

4. CHAPTER 4 RESULTS AND DISCUSSION

4.1 Introduction 36

4.2 Experimental Results 36

4.2.1 Pressure Drop 36

4.2.2 Residence Time Distribution of Solids in the Bed 41

5. CHAPTER 5 CONCLUSION AND RECOMMENDATION

5.1 Conclusion 47

5.2 Recommendation for Future Work 48

REFERENCES 49

APPENDICES 52

Appendix A - Project Gantt Chart and Project Milestone 53

Appendix B - Residence Time Distribution Experimental Procedure 54

Appendix C - 1st (Lower) Stage Pressure Drop Data Collection 58

i. 9° Blade Overlap Angle 58

ii. 12° Blade Overlap Angle 60

iii. 15° Blade Overlap Angle 62

Appendix D - 2nd (Upper) Stage Pressure Drop Data Collection 64

i. 9° Blade Overlap Angle 64

ii. 12° Blade Overlap Angle 66

iii. 15° Blade Overlap Angle 68

Appendix E - Residence Time Distribution of Solids Data Collection 70

i. 9° Blade Overlap Angle 70

ii. 12° Blade Overlap Angle 74

iii. 15° Blade Overlap Angle 78

Appendix F - Project Recognition 74

i. Acceptance from 2nd International Conference on Advanced Materials and Engineering Materials 2012 (ICAMEM2012) 82

ii. Acceptance from International Conference on Mechatronics and Computational Mechanics 2012 (ICMCM2012) 83

Appendix G - Calculation of Superficial Velocity 84

LIST OF FIGURES

Figure 1.1 (a)-(c) A Fluidized Bed Demonstrates All Characteristics of a Fluid [Reproduced from 5] 1

Figure 2.1 Basic Configuration of Swirling Fluidized Bed [Reproduced from 2, p.2] 6

Figure 2.2 Annular Spiral Distributor [Reproduced from 15, p. 2] 12

Figure 2.3 Downcomers of a Multi-Staged Fluidized Bed [Reproduced from 11, p.2] 13

Figure 2.4 Schematic Diagram of Non-Mechanical Valves [Reproduced from 16] 14

Figure 3.1 Physical Observation for the Operation of Multi-Stage SFB (a) Second Stage (b) First Stage 20

Figure 3.2 Close-Up View of Experimental Apparatus of SFB 22

Figure 3.3 Photograph of Multi-Stage SFB Experimental Set Up 23

Figure 3.4 Schematic Diagram of The Experimental Set Up 23

Figure 3.5 Simple Schematic Diagram of Experimental Set Up 24

Figure 3.6 Experimental Test 25

Figure 3.7 Feeder Hopper 26

Figure 3.8 Close-Up View of Feeder Hopper 27

Figure 3.9 (a)-(b)Close-Up View of Salt-and-Pepper Dispenser Mechanism 27

Figure 3.10 Sample Collector with Tubes 29

Figure 3.11 Top View of Sample Collector 29

Figure 3.12 Ball Bearing and Slot Mechanism of Sample Collector 29

Figure 3.13 Schematic Drawing of Sample Collector (In Unit of mm) 30

Figure 3.14 White Bed Particles of 2.99 mm 31

Figure 3.15 Dark Blue Tracer of 2.98 mm 31

Figure 3.16 Distributor [Reproduced from 2, p.4] 33

Figure 3.17 Shapes of Blades Used in this Experiment 33

Figure 3.18 Multi-Staged SFB Detailed Design (In Unit of mm) 33

Figure 3.19 Detailed Blade Drawing of 9° Blade Overlap 34

Figure 3.20 Detailed Blade Drawing of 12° Blade Overlap 34

Figure 3.21 Detailed Blade Drawing of 15° Blade Overlap 35

Figure 4.1 Bed Pressure Drop vs Superficial Velocity in the 1st Stage for 2.99 mm Spherical Particles with 9° Blade Overlap. 37

Figure 4.2 Bed Pressure Drop vs Superficial Velocity in the 1st Stage for 2.99 mm Spherical Particles with 12° Blade Overlap 38

Figure 4.3 Bed Pressure Drop vs Superficial Velocity in the 1st Stage for 2.99 mm Spherical Particles with 15° Blade Overlap 38

Figure 4.4 Bed Pressure Drop vs Superficial Velocity in the 2nd Stage for 2.99 mm Spherical Particles with 9° Blade Overlap 39

Figure 4.5 Bed Pressure Drop vs Superficial Velocity in the 2nd Stage for 2.99 mm Spherical Particles with 12° Blade 39

Figure 4.6 Bed Pressure Drop vs Superficial Velocity in the 2nd Stage for 2.99 mm Spherical Particles with 15° Blade Overlap 40

Figure 4.7 Bed Pressure Drop vs Superficial Velocity of Single-Staged SFB for 2.99 mm Spherical Particles with 12° Blade Overlap [Reproduced from 17] 40

Figure 4.8 RTD Density Function for 2.99 mm Spherical Particles with 9° Blade Overlap 41

Figure 4.9 RTD Density Function for 2.99 mm Spherical Particles with 12° Blade Overlap 42

Figure 4.10 RTD Density Function for 2.99 mm Spherical Particles with 15° Blade Overlap 42

Figure 4.11 (a)-(h) Comparison of RTD Density Function between Multi-Staged SFB (Left) and Single-Staged (Right) for 2.99 mm Spherical Particles with 12° Blade Overlap 43

Figure 4.12 The Original Design of Downcomer 44

Figure 4.13 The Modified Design of Downcomer 45

Figure 4.14 Schematic Diagram of Modification on The Height Downcomer 45

Figure 4.15 Dimension of the Modified Downcomer Design 45

Figure 4.16 Details of the Modified Downcomer 46

Figure 4.17 Simple Working Principle of Flexible Duct 46

LIST OF TABLES

Table 2.1 Breakdown of Ergun Equation 5

Table 3.1 Major Equipment for Experiments 24

Table 3.2 Solid Feed Calibration Data 28

Table 3.3 Properties of Bed and Tracer Particles Used in the Experiments 31

Table 3.4 Experimental Conditions 32

List of Symbols and Abbreviations

ΔP	pressure drop
L	height of the bed
μ	fluid viscosity
ε	void space of the bed
U_0	fluid superficial velocity
D_p	particle diameter
ρ	density of the fluid
ϕ_p	surface area of volume-equivalent sphere)/surface area of particle
V_p	volume of a single non-spherical particle
A_p	surface area of particle
A_{sp}	surface area of the equivalent-volume sphere
$E(t)$	RTD density function
$E(\theta)$	dimensionless age distribution
Mt_i	tracer weight
CFB	conventional fluidized bed
RTD	residence time distribution
SFB	swirling fluidized bed
t_i	measure clock time
3D	three dimensional
CATIA	computer aided three-dimensional interactive application
Ph.D	doctor of philosophy
d_p	particle diameter
PVC	polyvinyl chloride
SD	standard deviation

CHAPTER 1
INTRODUCTION

Fluidization is a process in which solid particles are converted into fluid-like form by means of injected gas or liquid. It is one of the eminent techniques used in industry to have an interchange of solids and fluids for wide possibility applications. There have been many outpourings to publicize fluidized beds since the late 1970s and it has conveyed the environmental advantages to petro-chemical industry.

1.1 Background of Study

Fluidization is a process where solid particles behave like fluid, mixing with other particles and flows like liquid or gas [1]. Faizal et al. [2] stated that swirling fluidized bed (SFB) is a recent development in the field of fluidization. In swirling fluidization, momentum is transferred radially and tangentially to the bed particles, increasing the fluidization quality and reducing the particle elutriation [2]. It can best be described by means of a simple experiment where, particles such as sand are poured into a tube provided with a porous plate distributor. Gas or liquid is then forced upward through the particle bed. This flow causes a pressure drop across the bed, and when it becomes sufficient enough to support the weight of the particles it is said to be at minimum fluidization. [3, 4]

Particles under the "fluidized" state experience a gravitational pull which is counter-acted by the fluid drag on them. Thus the particles remain in a semi-suspended condition. A fluidized bed displays characteristics similar to those of a liquid, as shown in Figure 1.1. [3, 5]

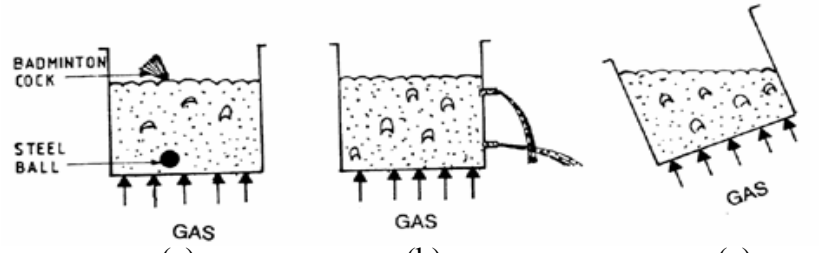

(a) (b) (c)

Figure 1.1 (a)-(c) A Fluidized Bed Demonstrate All Characteristic of A Fluid

[Reproduced from 5]

The characteristics of fluid are described as follow:

- The static pressure *(P)* at any height is approximately equal to the weight of bed solids *(F)* per unit cross section *(A)* above that level, $\boldsymbol{P = F/A}$, like Figure 1.1(a).
- The solids from the bed may be drained like a liquid through an orifice at the bottom or on the side like Figure 1.1(b).
- The bed surface maintains a horizontal level, irrespective of how the bed is titled; also the bed assumes the shape of the vessel like Figure 1.1(c).
- An object denser than the majority of the bed will sink, while the one lighter than the bed will float (e.g. a steel ball sinks in the bed, while a light shuttlecock floats on the surface) like Figure 1.1(a).
- Particles are well mixed, and the bed maintains a nearly uniform temperature throughout its body when heated.

An increase in the gas velocity through a bed of granular solids brings about changes in the mode of gas-solid contact in many ways. With changes in gas velocity the bed moves from one state to another.

These regimes arranged in order of increasing velocities are [3, 4]:

- Packed bed (fixed)
- Bubbling bed
- Turbulent bed
- Fast bed
- Transport bed (pneumatic or entrained bed)

It may also achieve slugging or dense phase suspension flow under certain conditions.
There have been many different types of fluidization with more being advanced and innovated as time goes towards modern age. There is a standard homogeneous fluidization which is used commonly throughout the petro-chemical industries. Gas fluidized beds are widely used in combustors for steam. [3, 4]

The uses of fluidized beds are generally for:

- Mostly, the interaction of solids and fluids
- Drying

- Chemical processing
- Torrefaction
- Energy efficient method using air as medium and power from a blower
- Used to produce gasoline and other fuels, along with many other chemicals

Circulating fluidized beds are used mostly in the chemical process industry, mineral processing, pharmaceutical production, energy related processes and catalysts also for drying.

1.2 Problem Statement

In industrial processes involving gas-solid contact, it is important to ensure correct residence times distribution (RTD) and pressure drop for optimal performance and maximum yield in the process. To design such a system, the principles of multi-staging are useful. In addition, counter-flow operation is required for effective use of the driving potential.

1.3 Objectives and Scope of Study

The project objectives are:

1. To apply the concept of serial processing to the SFB via multistage.
2. To combine multi-staging with counter-flow operation in the novel SFB.
3. To improve the fluidization process by enhancing quality of processing with a gain in residence time.
4. To compare the experimental results of pressure drop and RTD of solids for multi-stage SFB with single-stage SFB experimental results.

The scope of the study includes:

1. Design and construct two-stage of a counter-flow, multi-staging SFB.
2. Base the design on the study of SFB and model a system that is energy, time and cost efficient.
3. Study and characterize the behavior of SFB in multistage mode of operation.
4. Straight blades are used in this project.

CHAPTER 2
LITERATURE REVIEW

2.1 Fluidization Concept

2.1.1 Ergun Equation

The fundamental energy balance of the particles at the point of fluidization can be represented by: $F_{Drag} = W_{Bed}$ where F_{Drag} is the drag force exerted by the fluid on the particles and W_{Bed} is the gravitational force exerted on the particle bed.

However, the mathematical relationship of how the particles act in the fluidized state is far vaster than the above equation. Pressure drop is the determining value in order to achieve reasonable fluidization. As mentioned before, the pressure drop is the product of the force exerted with the area occupied by the bed. This initially would mean that the pressure is dependent on the velocity of the fluid, as velocity increases (above minimum fluidization velocity) on the contrary the effect on the pressure would be significantly low as it is now affected by the weight of the particle bed. [2]

Sasi et al. [6] stated that the onset of fluidization occurs when: *(pressure drop across bed) * (cross-sectional area of bed) = (Volume of bed) * (fraction of solids) * (Specific weight of solids)*.

They agree that the equation above lacks many parameters for accurate results and interpretation and there are several factors that need to be considered, which are rate of fluid flow, viscosity and density of fluid, closeness and orientation of packing, and the last one is factors on their size, shape and surface of particles. These factors are related to Ergun's equation in which the equation has a co-relationship with the aforementioned all parameters over the distance of a packed column. [6]

Previously, the observation made by researchers stated that the pressure drop was proportional to velocity (U) at low gas flow rates and proportional to the square of the velocity (U^2) at high gas flow rates. Subsequently, it was formulated into the resistance by friction on the motion of fluid by Osbourne Reynolds to recapitulate these two conditions. Following this, Carman and Kozeny found that for viscous flow, the change in pressure was proportional to $(1- \varepsilon)^2 / \varepsilon^3$. It was also experimentally determined, by way of 640 experiments, that a constant of 150 was also a factor in the equation. These findings

resulted in the Carman-Kozeny equation for change in pressure under viscous flow. At the same time, Burke and Plummer discovered that change in pressure at turbulent flow, resulting from kinematic energy loss, was proportional to $(1-\varepsilon) / \varepsilon^3$. There was also a constant of 1.75 found to be relevant at the turbulent flow, resulting in the Burke - Plummer equation for change in pressure at turbulent flow. After having gone through much experimentation, Ergun and Orning were able to put the two equations above together and they found that it was accurate for a wide range of Reynolds numbers. [6]

Table 2.1 Breakdown of Ergun Equation

CONTRIBUTOR	***FORMULA***	***CRITERIA RESOLVED***
Osbourne Reynolds	$\frac{\Delta P}{L} = aU + b\rho U^2$ where a and b are representatives of packing and fluid properties	Resistance by fluid flow friction
Carman and Kozeny	$\frac{\Delta P}{L} = \frac{150\left(1-\varepsilon\right)^2 U\mu}{\varepsilon^3\ \phi^2\ \left(D_p\right)^2}$	Change in pressure for viscous flow
Burke and Plummer	$\frac{\Delta P}{L} = \frac{1.75\left(1-\varepsilon\right)\ \rho\ U^2}{\varepsilon^3\ \phi\ D_p}$	Change in pressure for turbulent flow
Ergun and Orning	$\frac{\Delta P}{L} = \frac{150\left(1-\varepsilon\right)^2 U\mu}{\varepsilon^3\ \phi^2\ \left(D_p\right)^2} + \frac{1.75\left(1-\varepsilon\right)\ \rho\ U^2}{\varepsilon^3\ \phi\ D_p}$	All Criteria combined. ϕ is the particle shape factor.

Where:

ΔP = pressure drop

L = height of the bed

μ = fluid viscosity

ε = void space of the bed

U_0 = fluid superficial velocity

D_p = particle diameter

ρ = density of the fluid

2.1.2 Particle Characterization and Dynamics

The study of the particles is immensely essential in which every aspect of the particle, such as the size, shape, density, and surface type, needs to be taken into consideration and to be correctly defined.

In order to best describe shape, Leva (1959) defined the particle diameter of an arbitrary shape in terms of sphericity by:

$$D_p = \frac{6V_p}{A_p \phi_p} = \frac{6V_p}{A_{sp}}$$

Where: ϕ_p = (Surface area of volume-equivalent sphere) / surface area of particle,

V_p = Volume of a single non-spherical particle

A_p = Surface area of particle

A_{sp} = Surface area of the equivalent-volume sphere

2.2 Single-Staged Swirling Fluidized Bed

SFB utilizes annular distributor with an annular bed and inclined injection of gas through the distributor and this setup will result in swirling motion of the particles inside the bed. It was first studied analytically by Sreenivasan and Raghavan [7]. According to Sreenivasan and Raghavan [7], the gas entering the bed will have horizontal and vertical components. The vertical component results in fluidization while the horizontal component results in swirling motion of the particles.

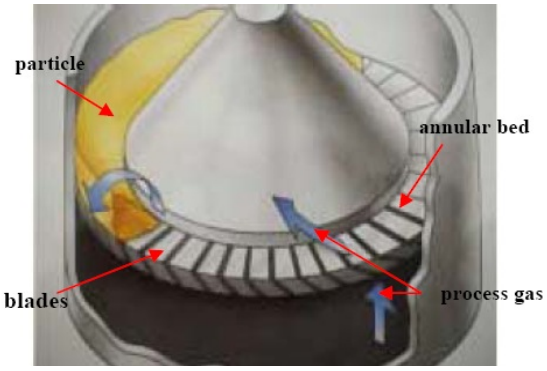

Figure 2.1 Basic Configuration of Swirling Fluidized Bed [Reproduced from 2, p. 2]

Further investigation on the fluidizing pattern by [8], they deduced that an innovative swirling fluidizing pattern generated by a multi-horizontal nozzle distributor has been proven to produce a remarkable improvement on the fluidization quality and reduce elutriation. Their analysis shows that with an increasing distance above the distributor the bubbles are distributed more evenly cross-sectional due to the decay of centrifugal forces. Thus, comparing the conventional axial fluidization, the swirling fluidization pattern exhibits high frequency and low-amplitude pressure change characteristics. Their main finding states that by modifying the fluidizing pattern, it is possible to improve fluidization quality and reduce elutriation simultaneously without the need of auxiliary equipment.

2.2.1 Hydrodynamics and Operating Parameters

Sreenivasan and Raghavan [7] stated that the advantages of swirling fluidized bed overtake that of the conventional system. The swirling motion allows for the diminishing of visible bubbles and prevents gas bypassing. The moment a particle enters the feed, it disperses rapidly and thoroughly without the need of bubbles. Additionally, for all distributor of the swirling fluidized bed can vary according to required results. The percentage useful area of the distributor was about 95% in the inclined blade type distributors, while it was 64% in the perforated plate type distributor. When the distributor pressure drops for each of the distributors were compared, the perforated plate type distributor had much higher pressure drop when compared with the inclined blade type. [9]

Raghavan and Sreenivasan [6] also concluded that the superficial velocity and blade angle have greater influence on the swirl characteristics more than the other parameters. When the inclined blade type distributors were compared, it was noticed that the distributor pressure drop was slightly more in the case of three-row type and that was due to the blade holders fixed in between the rows. [9]

2.2.2 Studies on Annular Distributor and Bed Behaviour

Recent studies show that the principle of operation is based on the simple fact that a horizontal component of gas velocity in the bed creates horizontal motion of the bed particles. The cyclone-like features resulting from the swirling motion of bed particles also contribute to this low elutriation. Therefore, it is possible to fluidize very fine particles and a wide variety of shapes of particles in this kind of fluidized bed. [2]
The flow regimes in swirling fluidized bed are packed bed, minimum fluidization, swirling regime, two-layer regime and finally elutriation or transport regime. Thus the bed behaviour can be summarized as [2]:

- The pressure drop of the swirling fluidized bed increases with the mass flow rate of fluidizing gas.
- Larger particles have lower pressure drop and capable of withstanding higher superficial velocity and hence, larger swirling regime.
- Increasing the overlapping angle of the distributor blades causes air to flow through higher resistances which initiates higher pressure drop. This also reduces elutriation by increasing the swirling region.
- Particle size, bed weight and the number of blades (60) are the most important variables that have more influence on the bed behaviour.

2.3 Multi-Stage Swirling Fluidized Bed

The idea behind the design of a multi-stage swirling fluidized bed is based mostly on the principle of residence time in the process. Since the residence time plays a huge role in the efficiency of a fluidized bed, by increasing that time and decreasing the amount of work done, by adding multiple stages of fluidization, fluidization can be improved. The absence of back-mixing and the large solids residence time per segment offers the opportunity to combine separated processes (e.g. gas-solids reactions), spatially divided, in a single reactor. [10]

- To prevent back-mixing of gas-solids

  Due to its specific shape, a fluidized bed arises in the bottom cone of each segment and back-mixing of gas and solids between the segments is prevented effectively.
- To enlarge the solids residence time

  The concept of several fluidized beds operated co-currently in series results in a ratio between the solids residence and the gas residence time being much higher than for a normal circulating fluidized bed (CFB).
- To provide serial processing for efficient outcomes

  The concept in which different processes are carried out in separate segments of the same reactor has huge benefits.

Continuous fluidized beds can be operated as a single-stage or multistage system. The limitations of a single-stage continuous fluidizer can be summed up in terms of wide distribution of residence time of solids and low efficiency of operation both with respect to gas and solid phase besides the chances of slugging in deep beds. [11]

2.3.1 Pressure Drop Theory Over Heights

Based on the previous study by researchers [12], it was found that the pressure drops across different heights were measured to be approximately the same (with variation less than 2%) and all the stages were identical in their operation as well as performance. Moreover, it was found out that the pressure drop due to solids across each in the stage has been obtained from the difference between the pressure drop with and without solids and rendered that the pressure drop due to solids decreases with an increase in the gas flow rate and increases with increment in the solids flow rate. The justification can be presumed that an increment in gas-flow rate escalates the porosity of the bed in the system, resulting in reduction in the solids concentration and therefore the pressure drop across the stage, as the height of the fluidized bed in the system corresponds to downcomer weir height. Another reason is that the pressure drop due to solids decreases with an increase in the gas-flow rate and increases with increment in the solids flow rate may be due to less frictional force, inertia and impact forces. [12]

Thus summing up, the maximum pressure drop occurred in the stage at low gas flow rate corresponding to maximum solid flow rate. [12]

According to Botterill [13], beds pressure drop is considered as an essential factor, which influences the uniformity and stability fluidization. For shallow bed, it is recommended to have a minimum distributor pressure drop of 350 mm of water [7]. Saxana [14] noticed that the pressure drop increased with fluidizing velocity and decreased with open area of the distributor plate. It was also reported that a distributor with greater pressure drop across it gives rise to smaller bubbles for the same excess fluidizing velocity than a distributor with smaller pressure drop. However, in the case of a swirling fluidized bed, these prescriptions do not hold and the pressure drop across the distributor is considerably less than 350 mm. This is achieved because the swirling particles suppress bubble formation at the distributor. Any jets of gas that may be formed are dissipated by the regularly ordered swirling particles. The limitation of a single-stage fluidized bed is wide distribution of residence time of solids and low efficiency of operation both with respect to gas and solid phase besides the chance of slugging in deep beds. The alternative way to obtain a narrow residence time distribution along with high efficiency of operation with respect to gas and solid phase is to use multi-staged fluidized bed systems. These multistage fluidized beds can be classified based on the transfer of the solids from one stage to next stage below namely (a) solids passing through perforated plates (b) solids passing through downcomers which are simply empty tubes allowing the transfer of solids from upper fluidized bed to lower one. In perforated plates multi-staged fluidized bed systems, the diameter of the perforated plate holes must be 5-30 times the particle diameter [15]. According to [15], the pressure drops of the gas circulating upwards through the standpipe and of the gas circulating upwards outside the standpipe are equal.

2.4 Design Specific Research and Recent Findings

In accordance to [11], multistage contacting of gas and solids can be obtained by simple multiple contacting system; cross-flow contacting system; counter-current contacting system. The counter-current multistage system is an improvement over the cross-flow system.

Important aspects considered on multi-staged SFB could be summarized into five parts, namely:

- Operating velocity
- Aspect ratio
- Distributors
- Downcomers
- Valves

2.4.1 Operating Velocity

In gas-fluidization the operating velocity is based on the hydrodynamics, heat transfer and reaction conditions. The ideal velocity in reaction or heat transfer processes can differ vastly from that of a cold bed. In order for fluidization one needs to first attain minimum fluidization velocity and that is the fundamental velocity to base calculations on. The hydrodynamics of the operating velocity plays a role in the stability and success of the operation. To reach stability the range of the velocity should make good gas-solid contact with optimum energy consumption. The safe operating velocity is usually theoretically applied as three to five times the minimum fluidization velocity.

2.4.2 Aspect Ratio

The aspect ratio refers to the ratio of the bed height *(H)* to bed diameter *(D)*. A fluidized bed is termed as ‘deep’ when the ratio is above one, and ‘shallow’ when is it below. Generally, a deep bed is better as the bubbling takes longer time to travel and chances of reacting are more than a shallow bed, where short-circuiting would prevail.

According to [14], the distributor has major impact on the bed height in terms of complete fluidization. The distributor pressure drop must be changed if the bed height or aspect ration is changed. If the bed height is increased by rising the operating velocity or reducing cross-sectional area.

Studies show that as the aspect ratio increases, the distributor to bed pressure drops ratio *(R)* decreases indicating improvement in quality of fluidization and approaching a steady

state and as R increases with an increase in operating velocity indicating gas channeling to some extent. Thus R-value steeply increases with a decrease in aspect ratio revealing its influence on the uniformity of fluidization. [11]

2.4.3 Distributor

A distributor is basically a flow restrictor and a bed-supporting device. The roles it plays are:

- Initiation of fluidization (swirling; inclined-blade spiral distributor)
- Maintaining stable operation
- Preventing dead or de-fluidized zones of particles
- Preserving the distributor surface and preventing solids from flowing into the plenum chamber during downtime
- Minimizing the attrition of solid particles (wearing down by friction) and erosion of bed internals

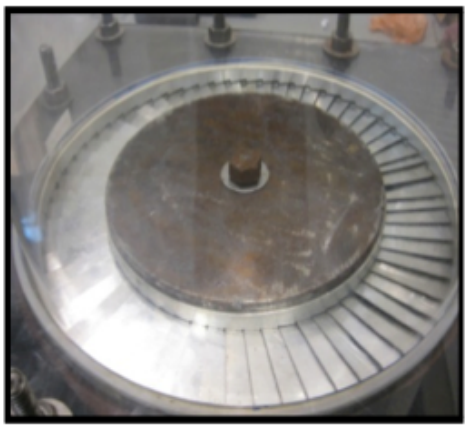

Figure 2.2 Annular Spiral Distributor [Reproduced from 15, p. 2]

It is important to consider the design of the distributor as it affects the hydrodynamics of a fluidized bed. The grid zone is affected by the design of the distributor plate. Since this is the base zone, it has large influence over the characteristics other two zones (dead and de-fluidized zones).

The type of distributor also affects the interfacial area of the bed. The distributor controls bubbles and airstreams. Thus, it is of high emphasis that the distributor defines the

fluidized bed. By considering the different zones in the fluidized bed one can deduce that each zone is caused by pressure drop characteristics. The distributor determines the flow and pressure drop occurrences.

2.4.4 Downcomer

Adapted from [12], a three-stage counter-current gas-solid fluidized bed reactor has been designed, constructed and investigated stable operating range for different particles and the influence of downcomer for stable operation. Further the role of aspect ratio for uniform fluidization has been critically examined. An attempt has therefore been made to acquire precise knowledge on the dynamics of the distributor and downcomer used in the system and stable operating range of the two-phase flow.

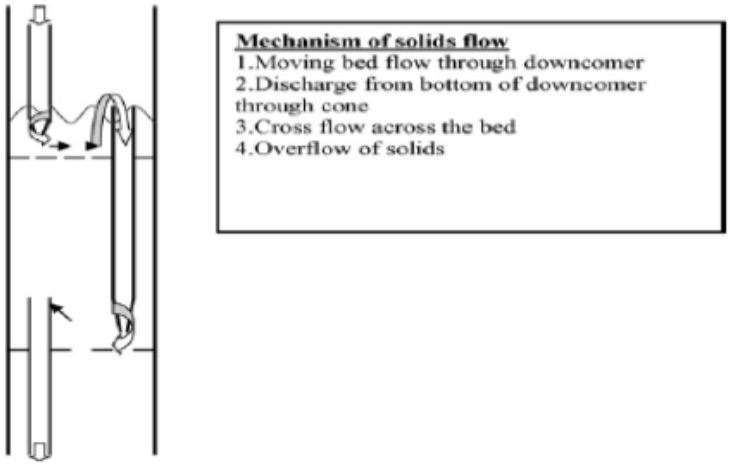

Figure 2.3 Downcomers of A Multi-Staged Fluidized Bed [Reproduced from 11, p. 2]

2.4.5 Valves

In the valve mode of operation, the solids flow rate through the non-mechanical device is controlled by the amount of aeration gas added to it. The aeration gas is to aid the downward flow of particles by the injection of a small stream of gas in the direction of desired flow of solids. These devices are shown schematically in Figure 2.4. The primary differences between these devices are their shapes and the directions in which they discharge solids. Both devices operate on the same principle. It is harder to fabricate a

smooth 180-degree bend for a typical J-valve. The most common non-mechanical valve is the L-valve, because it is easiest to construct, and also because it is slightly more efficient than the J-valve. Solids flow through a non- mechanical valve because of drag forces on the particles produced by the aeration gas. Furthermore, the actual gas flow that causes the solids to flow around the L-valve is not just the amount of aeration gas added to the valve. When aeration is added to a non- mechanical valve, solids do not begin to flow immediately. The initial aeration gas added is not enough to produce the frictional force required to start solids flow. Apart from the gas-flow an angle of declination would enhance flow due to gravitational forces. An experimental study was done to determine the best angle for valves. [16]

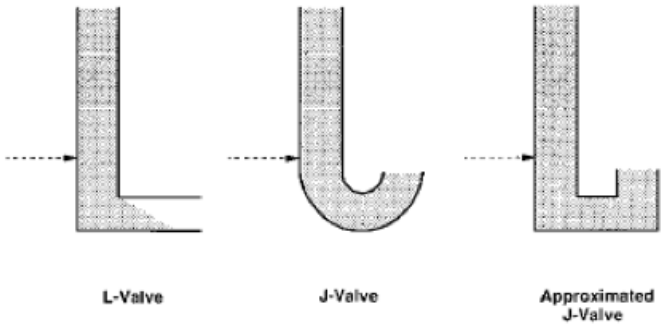

Figure 2.4 Schematic Diagram of Non-Mechanical Valves [Reproduced from 16]

2.5 Residence Time Distribution

The calculation and the precise analysis of residence time distribution (RTD) has turned out to be an essential tool in the study, analysis and design of continuous flow systems, for investigating the performance of a continuous fluidized bed and to get a deep understanding of the fluidization process. The concept of residence time concerns with the particles entrance, flow inside and leaving from the system. It is naturally expected that the fluidized particles will not have identical residence times inside the system [17].

Danckwerts was the first researcher to propose the idea of using the residence time distribution in the analysis of chemical reactors in an innovative paper by in 1953 in which he utilized the internal and external age distributions to describe the residence time distributions in a given system [17].

RTD can be calculated directly by a commonly used method of investigation, the tracers' response experiment, in which some tracers of distinct color are injected within the flow stream and then the residence time of the particles in this batch is measured at the outlet. There are several techniques for tracer injection that can be implemented such as pulse injection, step injection, periodic concentration fluctuation injection and random concentration change. The pulse and step injection techniques of tracers are easier to implement. Hence, they have been very widely and commonly applied in most of the studies and experiments [17].

As for pulse injection technique, the residence time distribution density function developed by Danckwerts represented by *E(t)dt* is defined as the portion of the particles that spend a given period of time, *t* inside the fluidized bed.

$$\int_0^\infty E(t)\, dt = 1$$

Another very useful function in the field of RTD is *F* curve. The *F* curve is the integral of exit age distribution density function *E(t)*.

$$F(t) = \int_0^t E(t)\, dt$$

In many cases a dimensionless time θ is a better time parameter than *t*. The dimensionless time θ is defined as $\theta = \frac{t}{\bar{t}}$ where $\bar{t}$ is a mean residence time or mean holding time. A great deal of literature attention has been devoted to determine $\bar{t}$ from physical considerations. For a constant density system, Levenspiel [18] showed that $\bar{t} = \frac{V}{Q}$ where *V* is the volume of the system and *Q* is the volumetric flow rate. This result of $\bar{t}$ was part of a more general theorem that relates $\bar{t}$ to the ratio of total particle inventory (or hold up of particles in the system) to total throughput (total outflow of particle). The mean residence time $\bar{t}$ and the variance of RTD can also be obtained from the relations;

$$\bar{t} = \int_0^\infty tE(t)dt$$

It becomes standard practice to discuss RTD and its models in their dimensionless or normalized forms so that *t* is not considered an adjustable parameter in the models.
Another important property of the RTD function is the convolution integral theorem discussed in detailed by Levenspiel [18] and being used by Mann et al. [22] and Fu et al. [21]. The convolution integral relates the shapes of the initial tracer disturbance with the shape of the final exit age distribution curve. The simplest example of a convolution integral is obtained when two reactors are connected in series and the RTD over the two reactors is measured. The final RTD is equal to the RTD in the first reactor convoluted in the second one.

2.6 Residence Time Distribution (RTD) Measurement Method

According to [13], superficial air velocity in circular fluidized bed normally range from 2.0 to 6.0 m/s and single pass RTD recorded by the majority of observers is of the order of 10 to 20 seconds. Since the usual span of a single pass RTD is tens of seconds the resolution needed for a good exit age distribution curve is less than 1 second. Therefore, if one does not employ an extremely fast, automated, online sampling system for detection of tracer, one cannot obtain the "fraction of a second" resolution required. Thus, to achieve fast, online concentration capabilities, one needed to employ a suitable tracer measuring method. The author suggested that it would be best to measure the concentration through the wall of vessel. The fastest and most successful "through the wall" concentration measuring methods were reported as the ones employing radioactive tracers [17]. However, due to safety reasons, many authors chose not to employ this kind of method.

CHAPTER 3
METHODOLOGY

3.1 Flow Chart

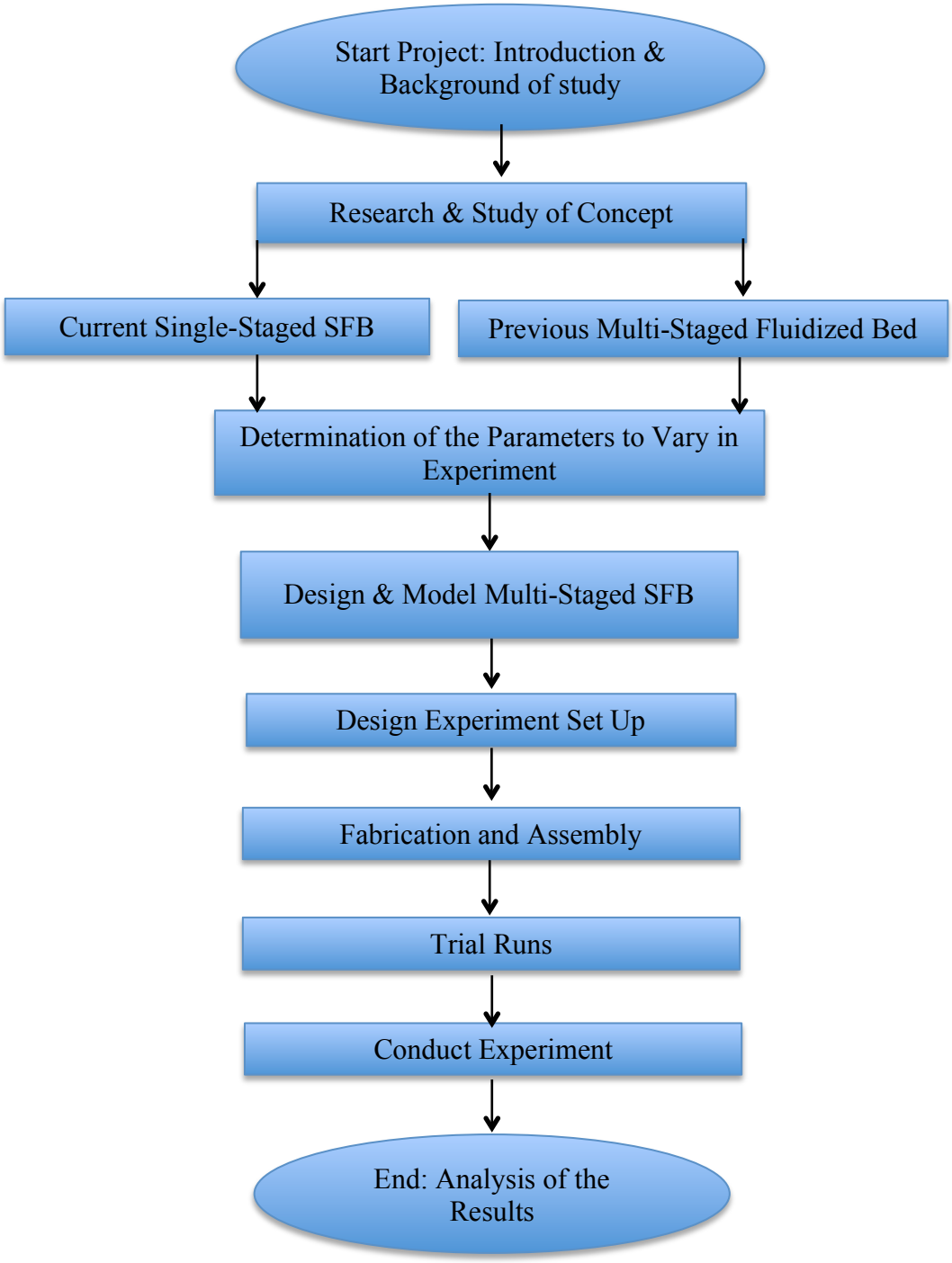

3.2 Project Work

The tasks based on the flow chart are as follows:

1. Research and studying concept.
   Research was done by reading different journals to have a better understanding about the concept of fluidization; single-stage SFB and multi-stage conventional fluidized beds. This relates to the study on the hydrodynamics and residence time distribution.
2. Determination of the parameters to vary in experiment.
   Parameter of the amount of particles inside the fluidized bed with a given period of time has been chosen to measure the RTD in the experiment. On the other hand, pressure drop needs to be measured so that the efficiency could be evaluated. The pressure drop was measured by using piezometric ring.
3. Design and model multi-staged SFB.
   Using the parameters and constraints of the previous design and analysis of draft design sketches a full 3D design is modeled in CATIA.
4. Design experiment set up.
   The experiment set up was designed with the help of PhD student.
5. Fabrication and assembly.
   Equipment parts such as downcomer and blades were fabricated by fabricator and assembly of the set up was done by the author with a help of PhD student.
6. Trial runs.
   Trial runs were conducted in order to test the experiment set up.
7. Conduct experiments.
   The experiments will be conducted with one particle and with four different weights (500g, 1000g, 1500g and 2000g) and three-distributor blade overlap angles (9°, 12° and 15°).
8. Analysis of the results.
   The results which will be obtained and shall be tabulated and analyzed using graphs.

The schematic diagram of the set-up is shown in the Figure 3.4. This existing test set-up consists of two sets of Perspex cylinder, which forms the bed wall. The cylinder is

mounted on the distributor. The type of distributor used in this test is flexible version of annular spiral distributor. The blades are arranged on stepped rings, an outer and inner, with steps machined at an angle of 10° with respect to the horizontal. The blades are made of 1 mm Aluminum sheet and there are sixty blades. The blades are held intact by two other rings, an outer and inner, on the top. The inclined overlapping blades direct the fluidizing air as desired. The annular spiral distributor and blades used in this experiment is shown in the Figure 3.16 and Figure 3.17 respectively. Whereas, the detailed blade drawings are shown in the Figures 3.19, 3.20 and 3.21.

Both perspex cylinder and distributor are mounted on the plenum chamber by using bolts and nuts. Utilization of permanent joint was avoided due to the needs of changes in the distributor blades. The plenum chamber is a hollow cylinder with a hole at one of its side for the air entry. A flange is welded to the plenum chamber at the hole in order to connect the chamber to the pipes. The chamber is connected to the blower with polyvinyl chloride (PVC) pipes. There are two paths for the air to flow, which are larger flow and lower flow. Two valves control this flow. If the air flows from the blower through the first valve, the second valve should be closed and vice versa. Two orifice plates are mounted in the middle of the pipe connecting the blower and plenum chamber to measure the air flow rate.

A hollow metal cone is centrally located at the base of the beds. These cones cause the superficial velocity of the air decreases continuously from the distributor to the free surface of the bed. It also eliminates the ‘dead zone’ at the centre of the bed. [7]
The pictorial experimental set up is shown in the Figure 3.5.

3.2.1 Physical Representation of the Bed Behavior

During the operation of multi-stage SFB, the bed shows several flow regimes with respect to the superficial velocity *(U)* that has been injected to the bed column. The faster *U* generated the more it will be to exhibit elutriation. The suggestion of the physical model shows that only a fraction of the feed particles will leave the bed after one trip in a circular path from the feed position to the discharge position and the rest of the particles continue to travel across the circular path both in the second stage and the first stage of

the bed column. This can be seen from the visual observation as shown in Figure 3.1(a) and Figure 3.1(b).

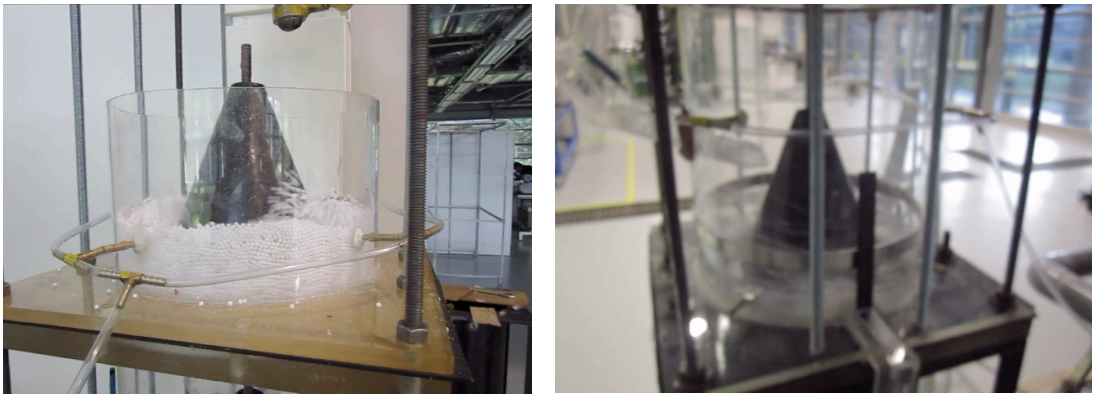

(a) (b)

Figure 3.1 Physical Observations for the Operation of Multi-Stage SFB (a) Second Stage (b) First Stage

3.2.2 Residence Time Distribution Density Function

According to Shukrie [17], RTD density function *E(t)* is defined as:

$$E(t) = \frac{M_{ti}}{\Sigma M_{ti}}.$$

3.2.3 Mean Residence Time

In accordance to Levenspiel [18], the definition of mean residence time is given by:

$$\bar{t} = \frac{\Sigma t_i M_{ti} \Delta t_i}{\Sigma M_{ti} \Delta t_i}.$$

3.2.4 Dimensionless Residence Time Distribution Density Function

It is better to utilize the dimensionless residence time θ, in which it is defined by $\theta = \frac{t}{\bar{t}}$.

The derivation of the dimensionless form of RTD density function is elaborated in [17].

3.3 The Construction of Multi-Stage SFB

There are a few essential requirements to scientifically explore the RTD of particles in Multi-Stage SFB, which are:

1. Sufficiently long horizontal section of pipe arrangement for an air-flow.
2. Interchangeable distributor blades to allow future experiments.
3. Visible acrylic cylinder to enable visualization of studies.
4. Pressure and flow measurement.
5. Solid feeder and sample collector.
6. To keep cost to minimum.

The photographs and schematic diagram of experimental set up are exhibited in Figures 3.2, 3.3, and 3.4 respectively. There were two passages of PVC pipe developed for the air-flow. The first was for high flow rates and the second was for low flow rates, in which the entrance to the respective flow is controlled by two butterfly valves. Two Venturi meters were located in the mid-section of the air passages to allow air-flow rate measurements. The 5 m horizontal pipe then lead into a 0.32 m diameter plenum chamber that pre-distributed the flowing air without misdistribution before it enters the swirling bed distributor. To achieve a flexible layout, ten adjustable height car jacks were modified to accommodate the weight of the pipes.

The bed unit consists of two transparent perspex cylinders, the second stage and the first stage. The inner diameter for both stages is 300 mm and the height for the first stage is 350 mm and the second stage is 300 mm. The cylinder columns are provided with pressure taps. In the first stage of bed column, there are two pressure taps, one located at 15 mm above the distributor blades of the first stage and the other is located at 200 mm from the bottom of the cylinder in order to measure the bed pressure drop in the first stage. Whereas in the second stage, the pressure tap is located 70 mm above the distributor blade of the second stage. Four strips of scale tape are located at four cardinal points on the outside of the cylinder to measure the bed height. A hollow metal cone of base diameter 200 mm and height of 150 mm is installed pointing upwards at each bed centre above the distributor flange. The motionless cone has two functions, first is to cover the idle portion of the distributor and to avoid a dead zone and second, it is also

increasing the effectiveness regime of swirling bed caused by the upward gas velocity to decrease by means of an increase in bed cross sectional area.

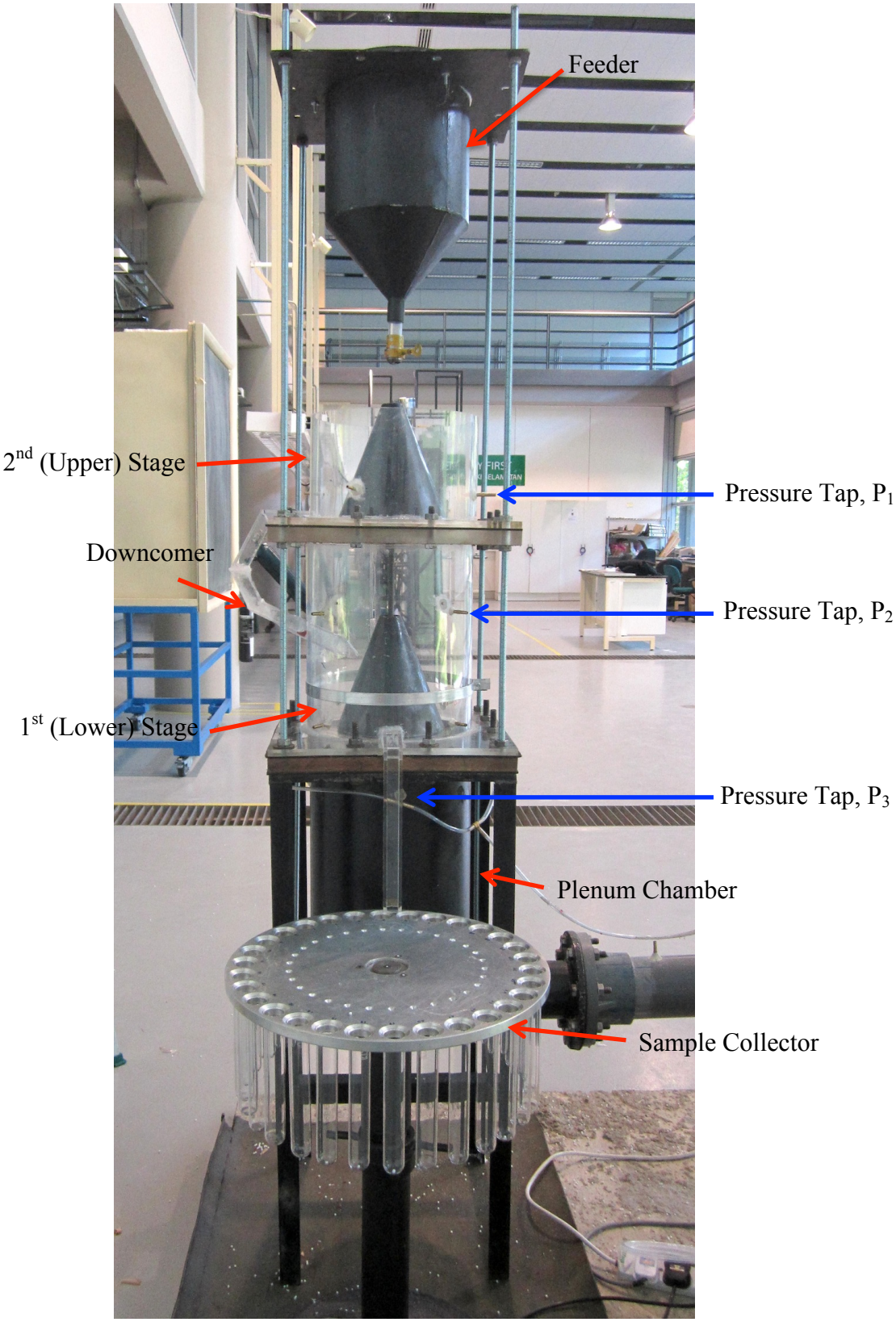

Figure 3.2. Close-Up View of Experimental Apparatus of SFB

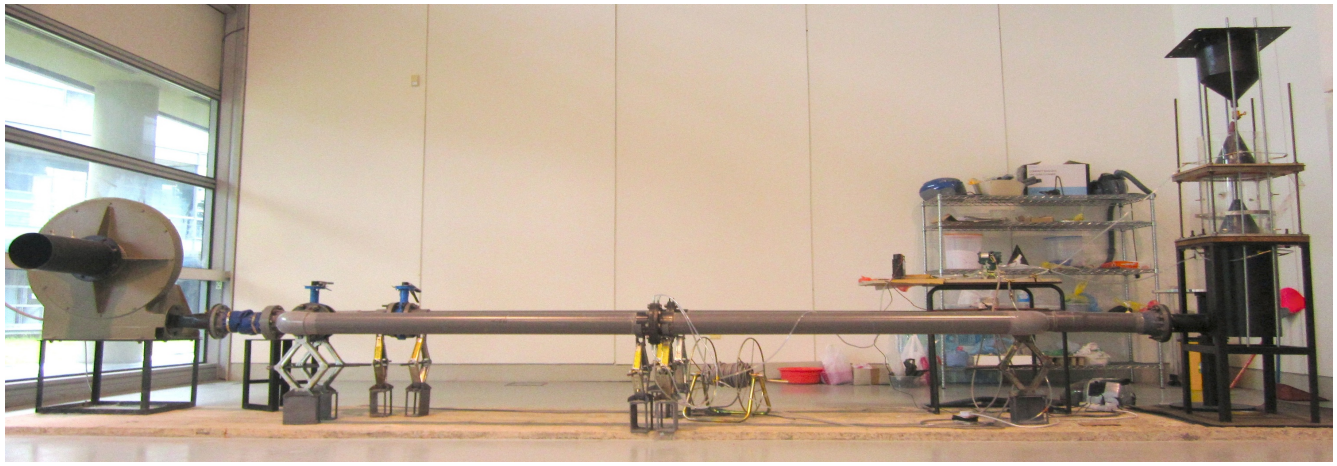

Figure 3.3 Photograph of Multi-Stage SFB Experimental Set Up

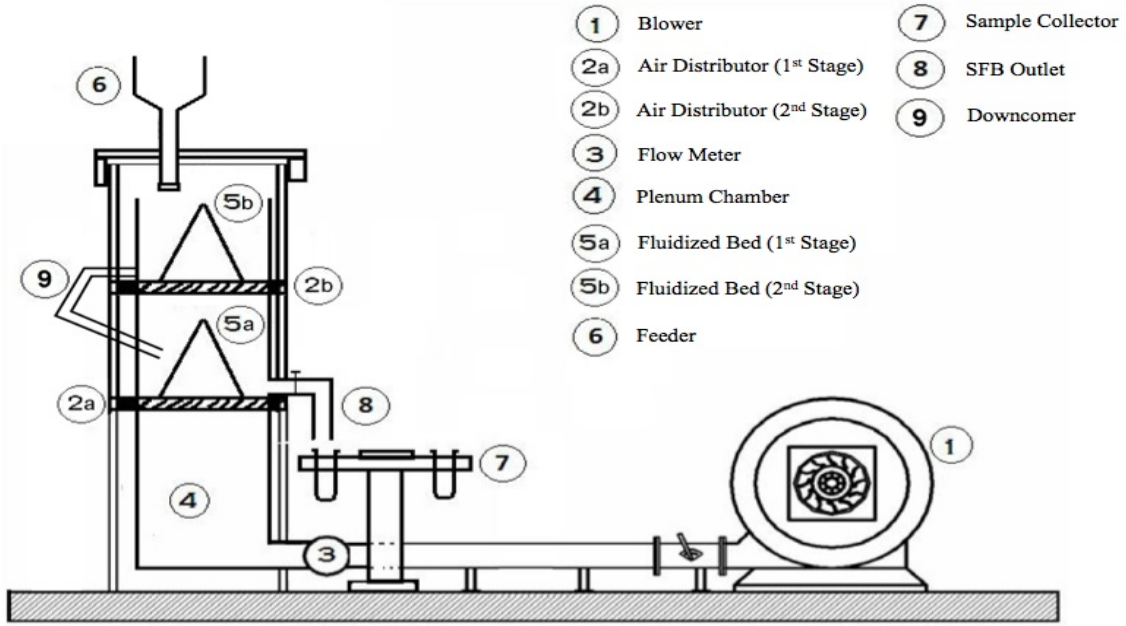

Figure 3.4 Schematic Diagram of the Experimental Set Up

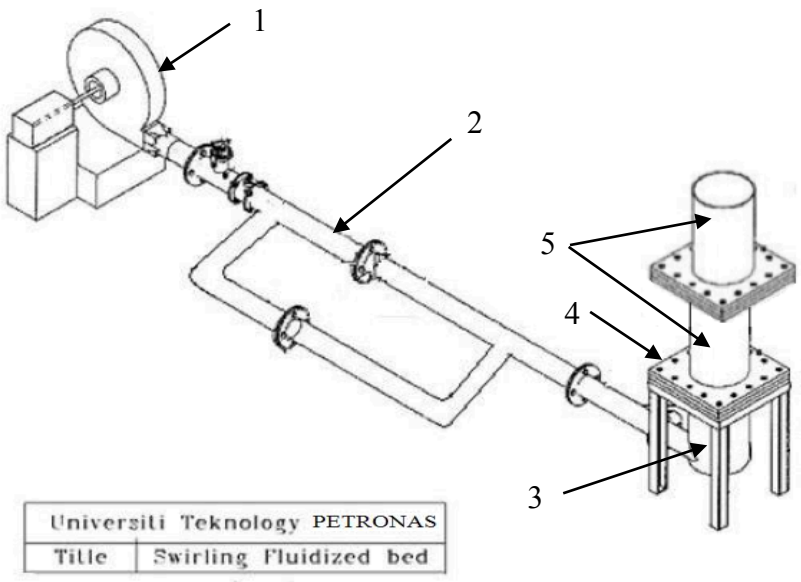

Figure 3.5 Simple Schematic Diagram of Experimental Set Up

Table 3.1 Major Equipment for Experiments

Blower (1)	***Pipes (2)***	***Plenum Chamber (3)***
Brand: Massive Fan Group	Material: PVC	Material: Mild Steel
CFM: 1000 cmh	Inner Diameter: 100 mm	Height: 1100 mm
5.5 kW	Outer Diameter: 115 mm	Inner Diameter: 320 mm
7.5 HP	Length: 5000 mm (straight) 600 mm + 3200 mm + 600 mm (n junction)	Depth: 490 mm
Column Flange (4)	***Bed Column (5)***	***Piezometric Ring***
Material: Perspex	Material: Perspex	Will be installed in the plenum chamber and in the bed columns. The function is to measure the pressure at the chamber and the column.
Size: 425 mm x 425 mm	Height: 1st bed 350 mm and 2nd bed 300 mm	Material: Hose and Metal Pluck
Thickness: 20 mm	Inner Diameter: 300 mm	Hose diameter: 5 mm
	Outer Diameter: 310 mm	

3.3.1 Pressure Monitoring

The experimental set up was instrumented to monitor the pressure drop along each of the major sections i.e. distributor and bed in each stage. This was achieved by drilling four tappings, equally spaced at four quadrants around the circumference of the plenum chamber and perspex cylinder and connected to a pressure transmitter. The four tappings were then linked together by means of rubber tubing and bronze T-shape connectors. The resulting tappings are shown in Figure 3.6.

The distributor pressure drop is measured by measuring the pressure difference between the two pressure taps below (P_3) and above the distributor plate of the first (P_2) and second stage (P_1) without any particles in the bed. The total pressure drop, i.e. the sum of the bed and the distributor pressure drops, is obtained from the pressure difference between the pressure tap below the distributor plate (plenum chamber) and that at the top of the perspex cylinder section on both stages. The bed pressure drop at a particular air velocity is determined by subtracting the distributor pressure drop from the total pressure drop.

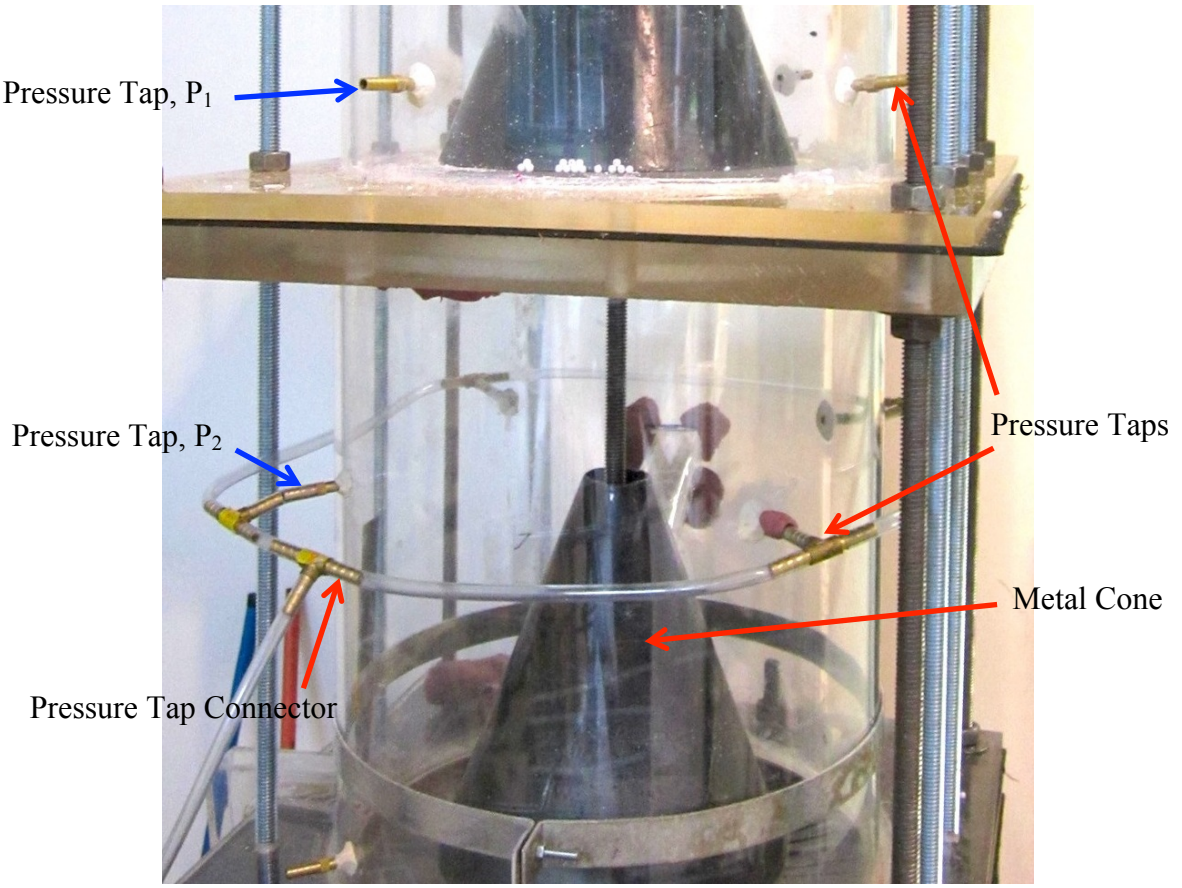

Figure 3.6 Experimental Test

3.3.2 Solid Feed and Solid Discharge

Selection of the particle feeding mechanism, there were two main criteria: the delivery of a stable feed with time and the delivery of uniform feed across the cross section of a bed. The particle feeder system should have the potential to deliver the particles in a controlled manner and allow for adjustment of the material feed rate. There are number of mechanisms available to feed particles including simple gravity hoppers fitted with a gate valve, screw feeders, vibratory feeders and rotary feeders.

A simple feeding mechanism is determined, in which it is a supply hopper feeding under gravity, but with some improvements with the gate to have a better control on the material flow rate. A salt-and-pepper type of dispenser is chosen for the gate where the opening is regulated by a ball bearing. Pictures of the feeding system along with the salt-and-pepper feeding mechanism are shown in Figures 3.7, 3.8, 3.9(a), and 3.9(b), in which the top of the column is a solids feed hopper with an annular section (260 mm diameter) and a converging section (250 mm long). It ends in a transparent acrylic tube of 25 mm diameter with the regulated gate attached together.

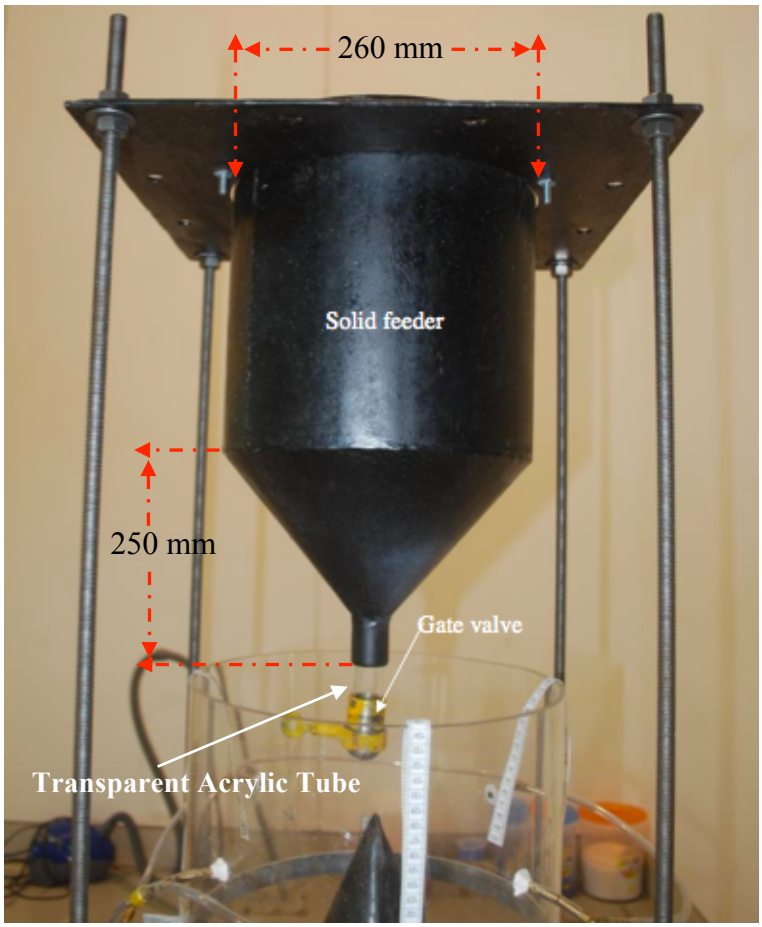

Figure 3.7 Feeder Hopper

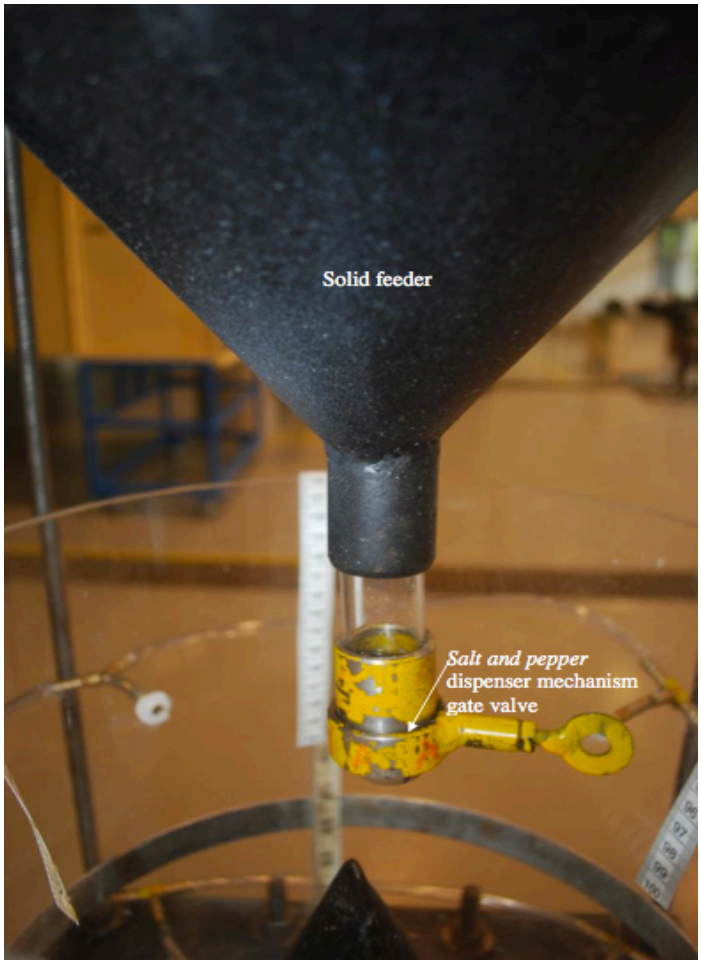

Figure 3.8 Close-Up View of Feeder Hopper

Figure 3.9 (a)-(b) Close-Up View of Salt-And-Pepper Dispenser Mechanism

The performance results for calibration of the feeding system are in Table 3.2 for 50 grams of particles being fed at four different openings and it is found to be smooth flow.

Table 3.2 Solid Feed Calibration Data

Sector Opening Area (mm^2)	***% of Sector Opening***	***Feed Rate (g/s)***
0	0	0
13.26	25	0.43
26.51	50	1.1
39.77	75	2.6
53.02	100	4.8

3.3.3 Sample Collector

The rotatable disk is 400 mm diameter and made of aluminum plate of 14 mm thickness. 30 holes of 32 mm inner diameter are located at the periphery of the disk to hold the test tubes while sampling of the material is taken place. The samples are collected in Pyrex test tubes of diameter 30 mm and 200 mm height. The outlet of the bed (20 mm x 20 mm) is mounted to the sample collector and the gate valve is inserted at the outlet to control the sampling period. The rotatable disk is designed with adjustable shaft so that the desired height can be controlled accordingly. After admission of the tracer, disk will be rotated to align the first test tube under the sampling point by using ball-bearing slot turning mechanism. Then the gate valve will be opened to collect the sample for a specified sampling interval. The samples are collected in sequence in one tube after another. Figure 3.10 to Figure 3.13 show the details of the sample collector.

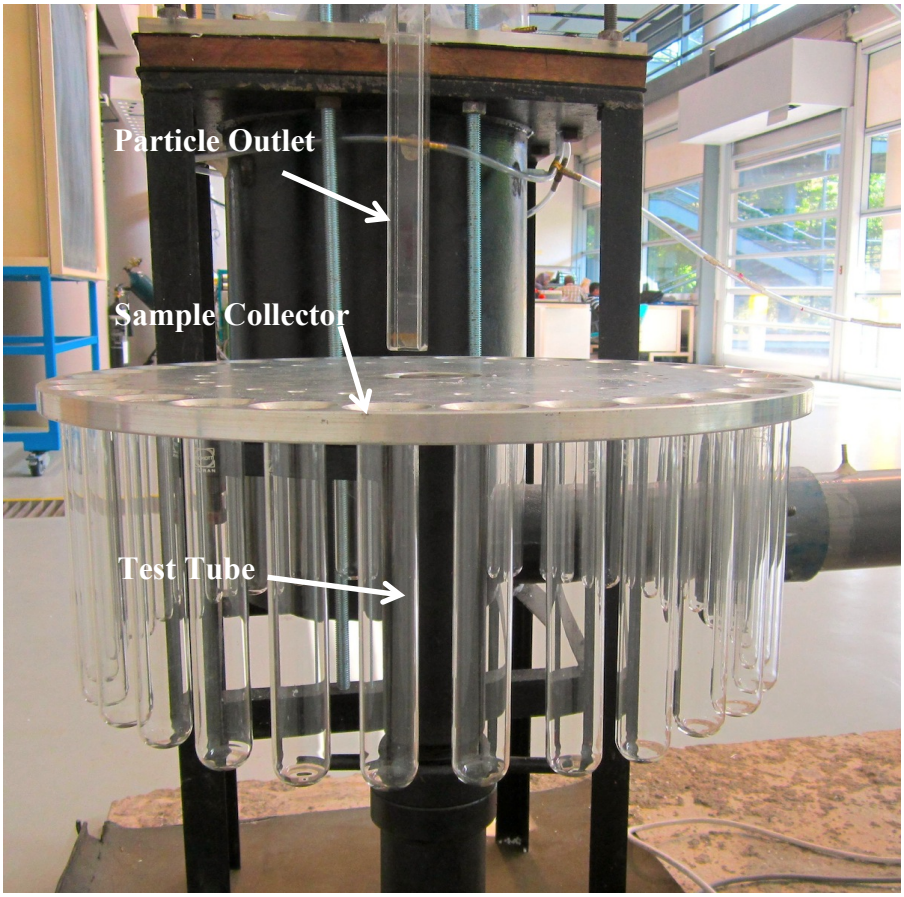

Figure 3.10 Sample Collector With Tubes

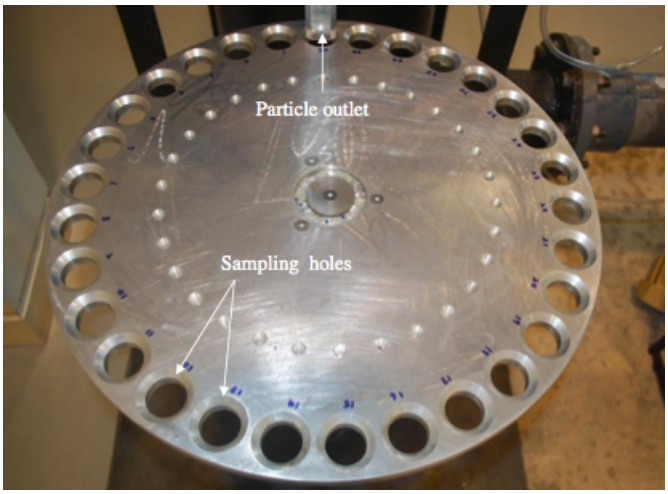

Figure 3.11 Top View of Sample Collector

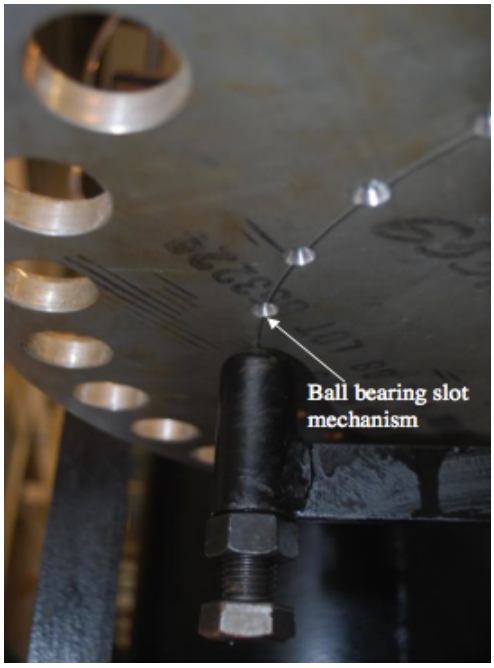

Figure 3.12. Ball Bearings And Slot Mechanism of Sample Collector

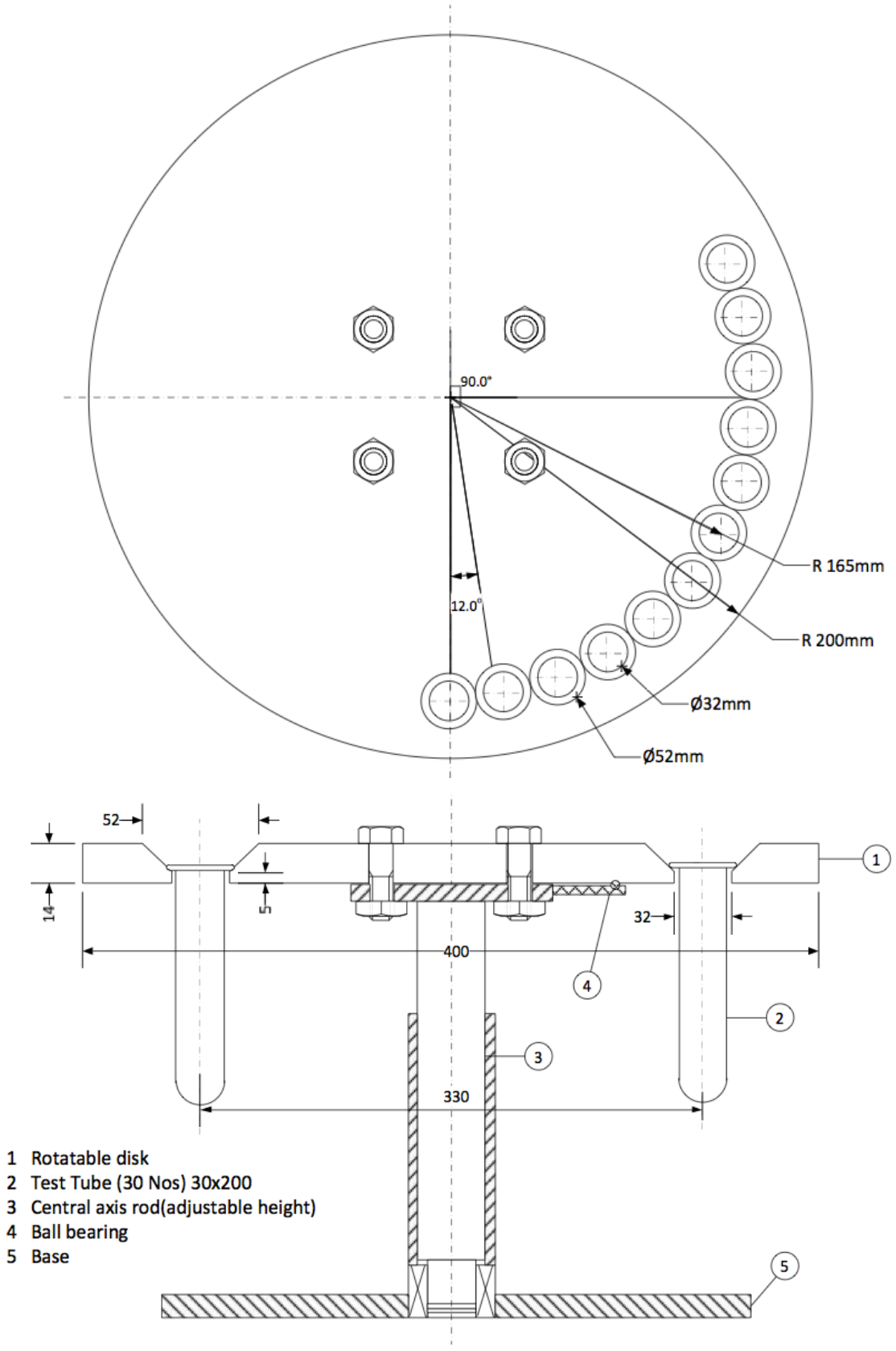

Figure 3.13. Schematic Drawing of Sample Collector (In Unit of mm)

3.3.4 Bed and Tracer Material

The bed material used in the experimental work is colored spherical plastic beads made by molding. Since the beads are molded, they have a nearly a uniform spherical shape with a central through hole and it can be seen in Figure 3.14 and Figure 3.15. One size of spherical particle size was used for the experiments. Samples of 30 particles were taken from each size and the diameter of each particle was measured accurately by using a vernier caliper, and the average weight was taken accurately by a digital balance of resolution 0.01 mg. The mean particle diameter (d_p), weight and their standard deviation (*SD*) were calculated. The result of the size estimation is shown in a Table 3.3.

Table 3.3 Properties of Bed and Tracer Particles Used in the Experiments

	Bed Particle	***Tracer Particle***
Color	White	Dark Blue
Mean Particle Diameter *(d_p)*	2.99 mm (SD ± 0.08272)	2.98 mm (SD ± 0.07232)
Mean Particle Weight	0.011 gram (SD ± 0.00254)	0.013 (SD ± 0.004987)
Particle Density	1381.43 kg/m^3	1519.81 kg/m^3

Figure 3.14 White Bed Particles of 2.99 mm

Figure 3.15 Dark Blue Tracer of 2.98 mm

3.3.5 Residence Time Distribution Experimental Conditions

The details of the experimental conditions are shown in Table 3.4.

Table 3.4 Experimental Conditions

Bed Weight (M_b), g	500, 1000, 1500, 2000
Particle diameter (d_p), mm	2.99
Number of Distributor Blades	60
Blade Overlap Angle	9°, 12°, 15°

Experiment activities for measuring solids RTD in the swirling fluidized bed will be carried out to study the effect of the system variables i.e. bed weight, in which it is carried out to utilize four different bed weights (500, 1000, 1500, and 2000 g) and particle size of 2.99 mm diameter with three different blade overlap angles. Details of experimental procedures are explained in Appendix B.

Experiments will be conducted under identical conditions and RTD data are collected during fluidization state, in which in this case superficial velocity *(U)* is greater than minimum swirling velocity *(U_s)*. Several experiments will be repeated under identical conditions to check the replicated results. The measured clock time, t_i and tracer weight collected in each sample, M_{ti} will be shown in the raw data. The clock time is the duration that elapsed from the time the tracer is introduced into the bed to that at which the collection of this sample is completed. The clock time t_i of sample number i is equal to $\Delta T \times i$, where ΔT is the sampling period.

RTD experiments will be conducted at different air-flow rate, solid flow rate and bed weight for one particle size.

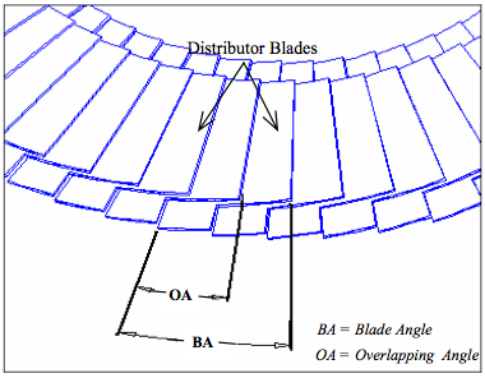

Figure 3.16 Distributor [Reproduced from 2, p. 4]

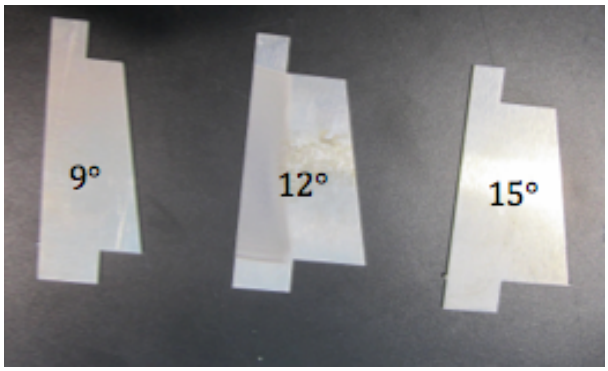

Figure 3.17 Shape of Blades Used In This Experiment

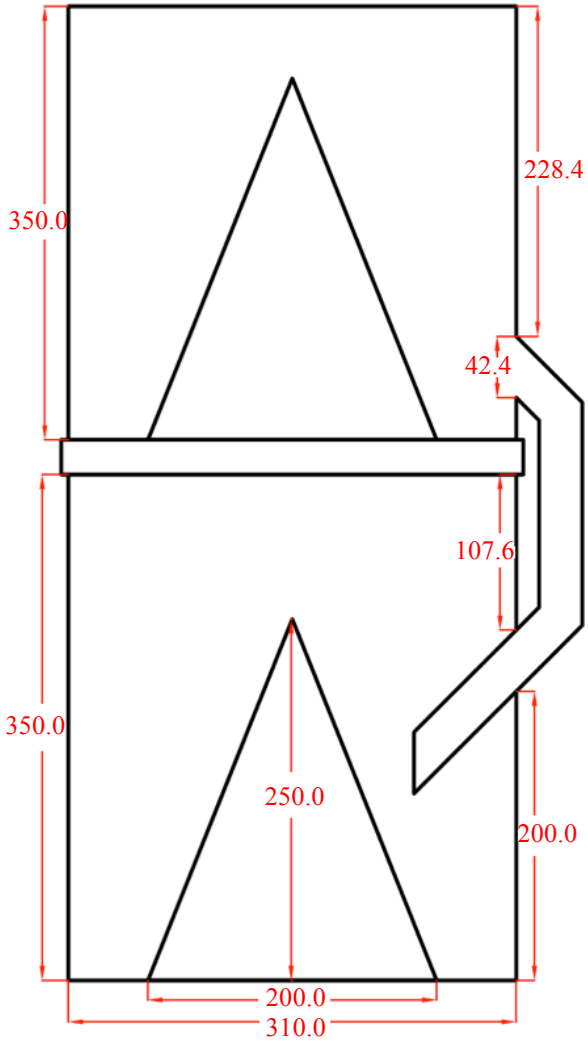

Figure 3.18 Multi-Staged SFB Detailed Design (In Unit of mm)

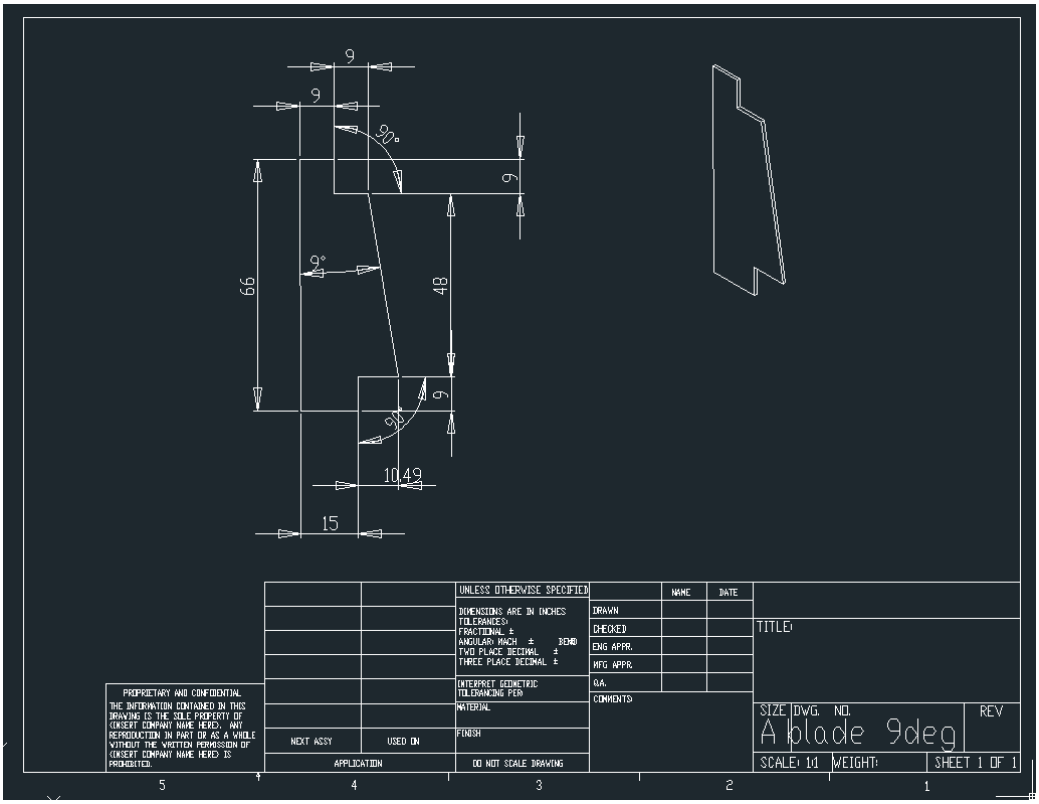

Figure 3.19 Detailed Blade Drawing of 9°

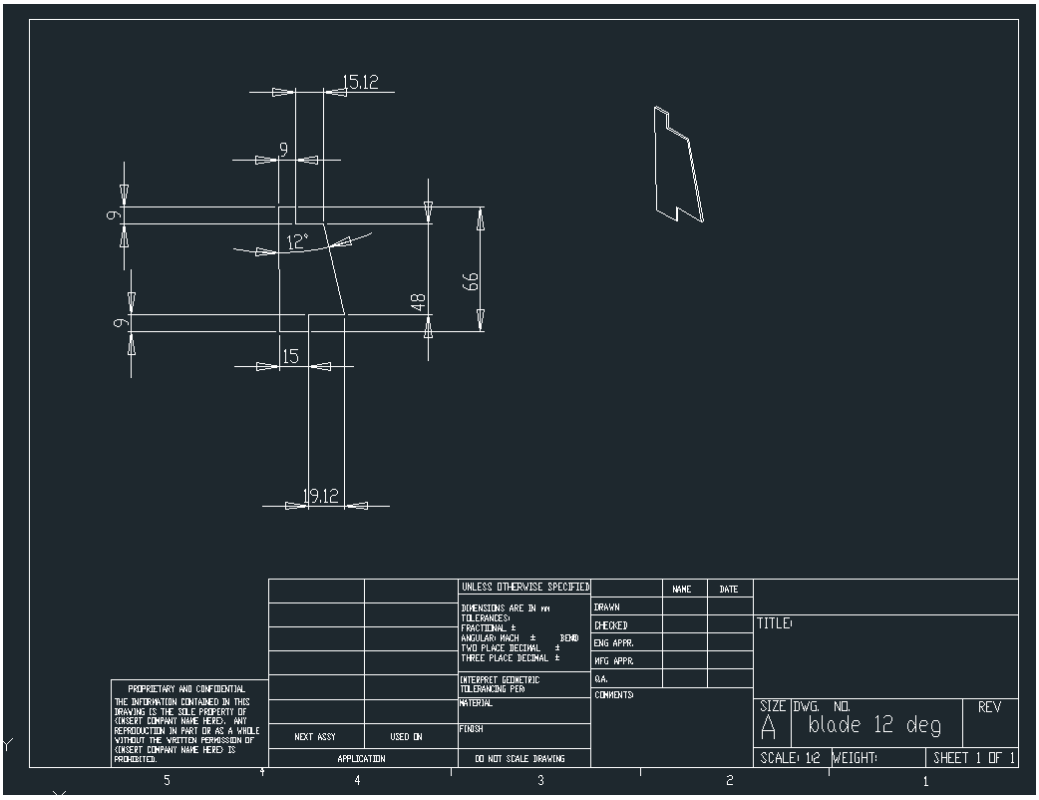

Figure 3.20 Detailed Blade Drawing of 12°

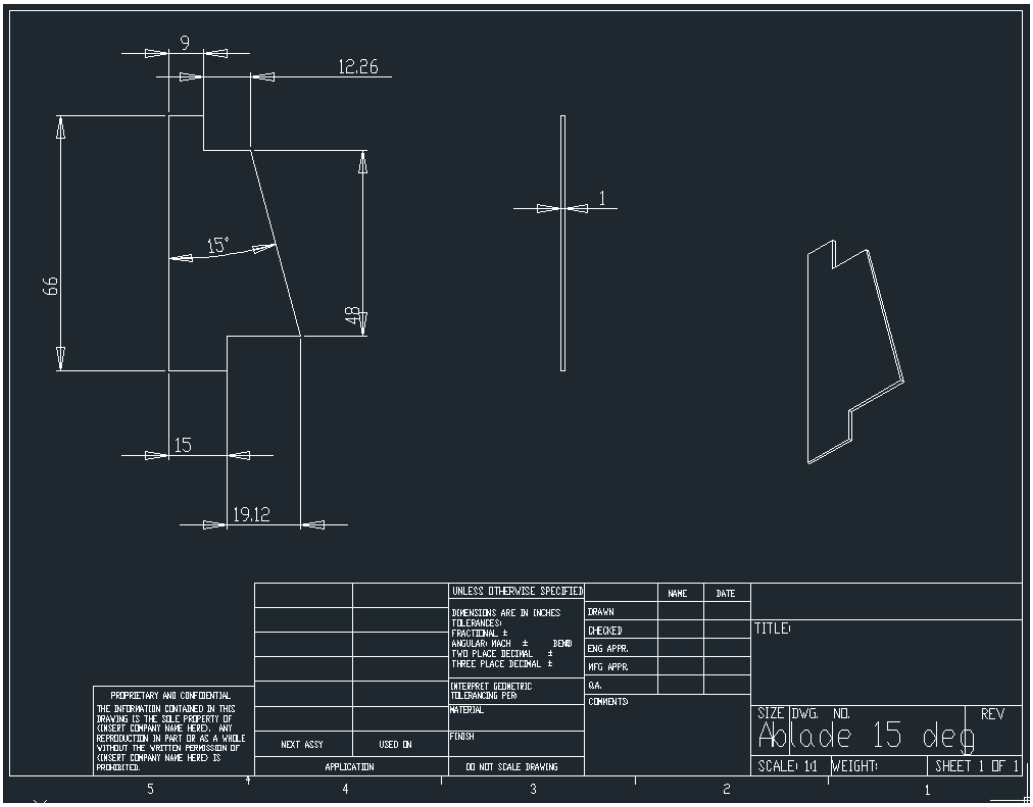

Figure 3.21 Detailed Blade Drawing of 15°

CHAPTER 4
RESULTS AND DISCUSSION

4.1 Introduction

The results of experimental investigations on the multi-stage SFB are presented in this chapter. The following aspects are covered in this chapter:

1. Pressure Drop of multi-stage SFB.
2. Residence time distribution (RTD) of solids in the bed.

4.2 Experiment Results

Experiments had been done by utilizing three different blade overlap angles, which are 9°, 12° and 15° blade overlap angle. The experimental investigations for pressure drop and residence time distribution (RTD) on multi-stage SFB are shown in the next section.

4.2.1 Pressure Drop

The pressure drop across the bed (ΔP_b) at a particular at a particular value of the superficial air velocity is determined by subtracting the distributor pressure drop from the total pressure drop. The bed pressure drop for each stage is then deducted from the operation of the bed pressure drop with particles minus the bed pressure drop without particles in particular stage of fluidized bed. Figures 4.1, .4.2 and 4.3 show the results of ΔP_b for 1st stage and Figures 4.4, 4.5 and 4.6 show the results of ΔP_b for 2nd stage both with particle diameter of 2.99 mm at different bed weights.

From Figure 4.1 to Figure 4.3, it can be seen that ΔP_b for the 1st stage increases with superficial velocity and bed weight. The same phenomenon occurs for the 2nd stage. This occurrence happens due to an increment in particle swirling speed. As the swirling speed of the particles gets faster with an increasing of air velocity, the friction losses between particle-particle, particle-wall and particle-air are also increased. It leads to degradation of

energy in terms of pressure drop across the bed. Moreover, the results show that for a given superficial velocity, as the area of blade opening increase (from 9° to 15°), the pressure drop across the bed is reduced. It is due to the air passing through a single opening will have higher velocity. This velocity gives rise to pressure loss through the openings. For any distributor, the difference in pressure (pressure drop) is mainly due to the fluidizing gas velocity after passing through the distributor. The variation of blade overlap angle from 9° to 15° of the distributor has determined to generate lower gas velocity at the distributor exit. The results have also shown that the distributor with 15° blade overlap angle is superior to the other two distributor with 12° and 9° blade overlap angles. Figure 4.7 is the experimental result for single-stage SFB [17]. It can be observed that bed pressure drop for multi-stage SFB is better than single-stage one.

In operation of swirling fluidized bed, different regimes of operation can be distinguished such as packed regimes, minimum swirling regime, two-layer regime and finally reaching elutriation [2].

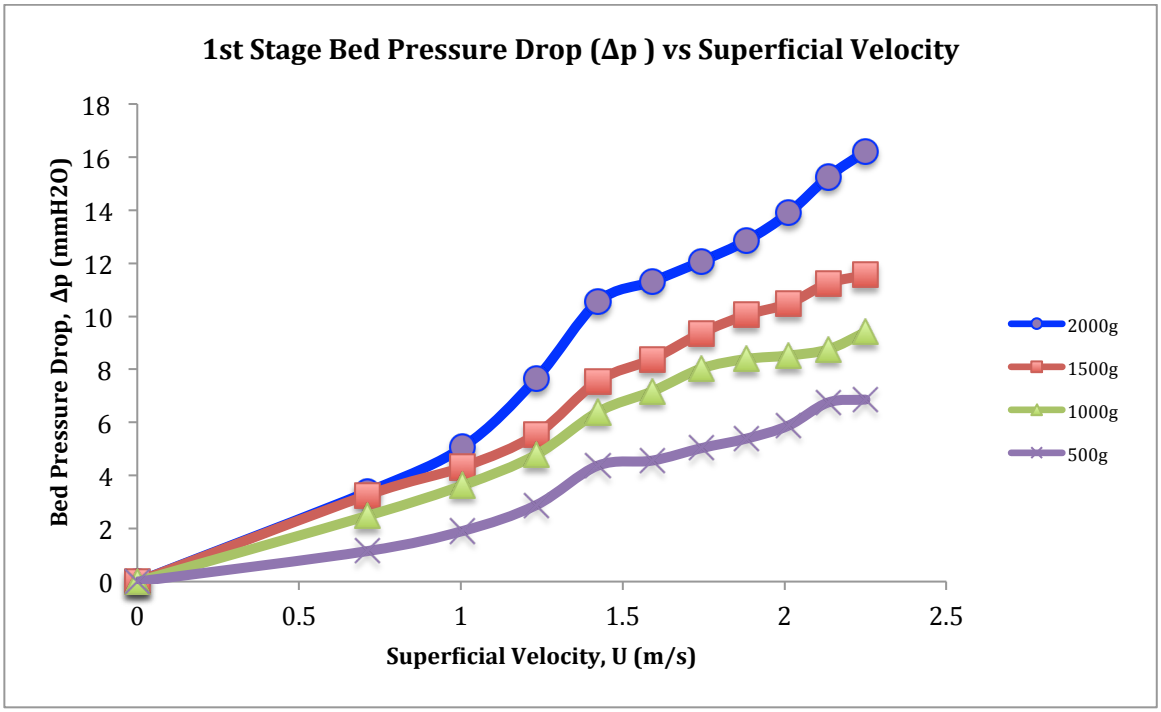

Figure 4.1 Bed Pressure Drop vs Superficial Velocity In The 1st Stage For 2.99 mm Spherical Particles With 9° Blade Overlap

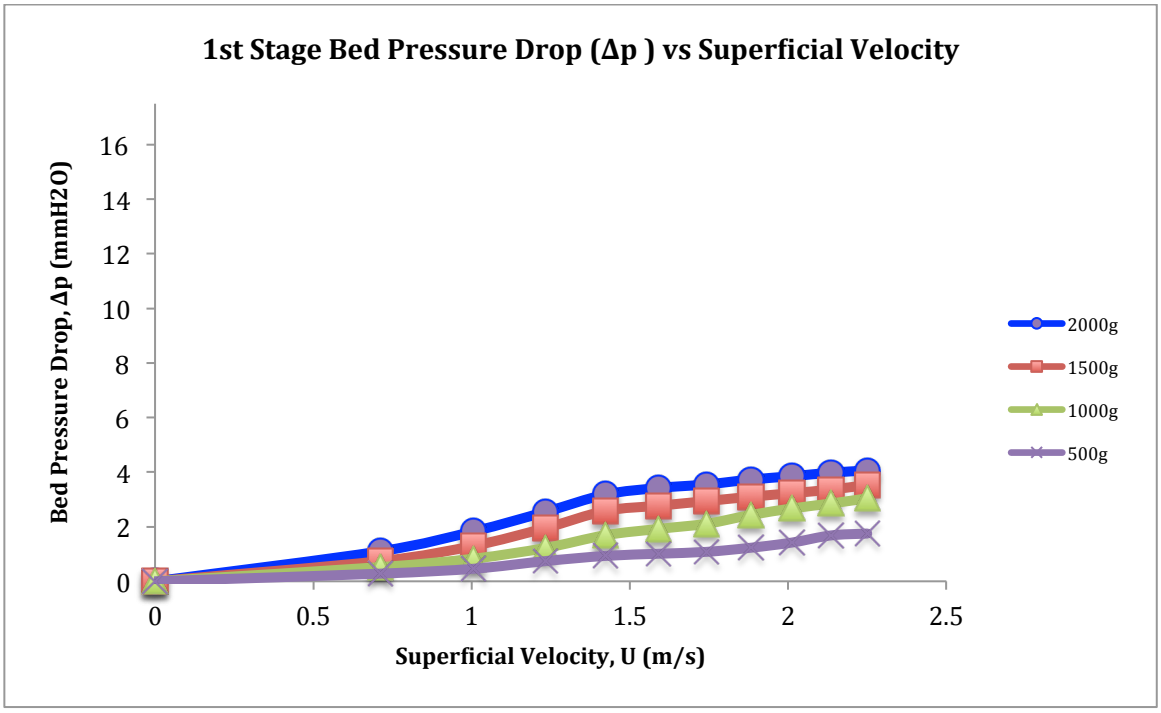

Figure 4.2 Bed Pressure Drop vs Superficial Velocity In The 1st Stage For 2.99 mm Spherical Particles With 12° Blade Overlap

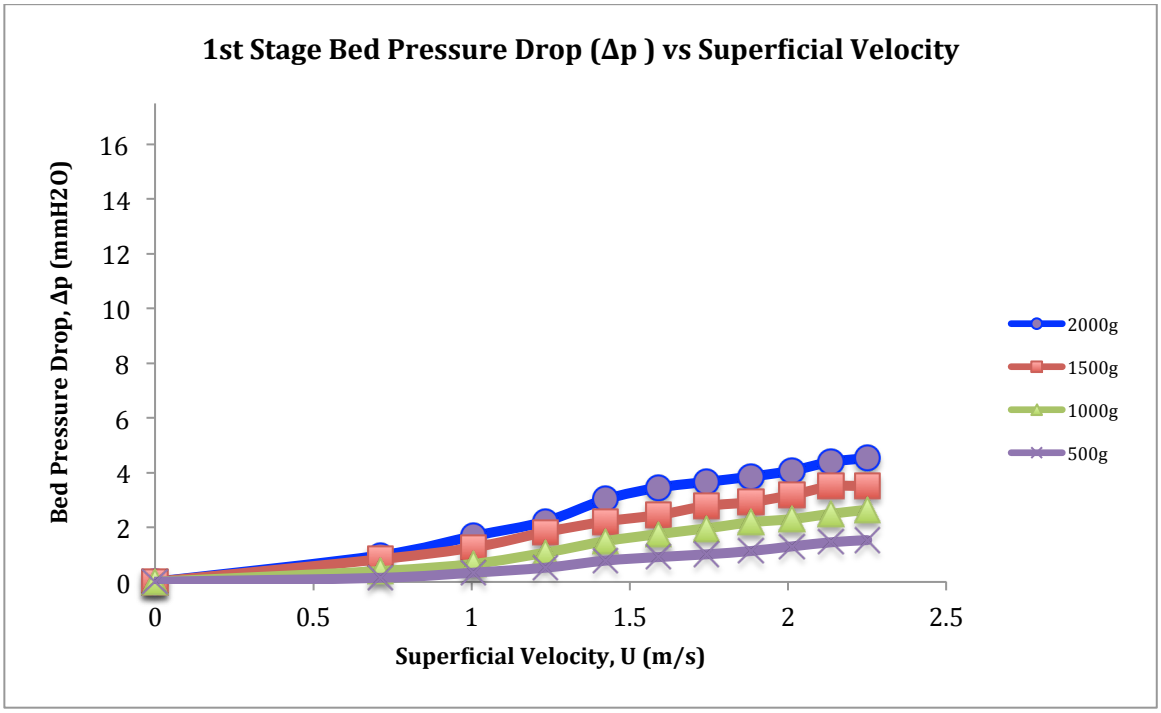

Figure 4.3 Bed Pressure Drop vs Superficial Velocity In The 1st Stage For 2.99 mm Spherical Particles with 15° Blade Overlap

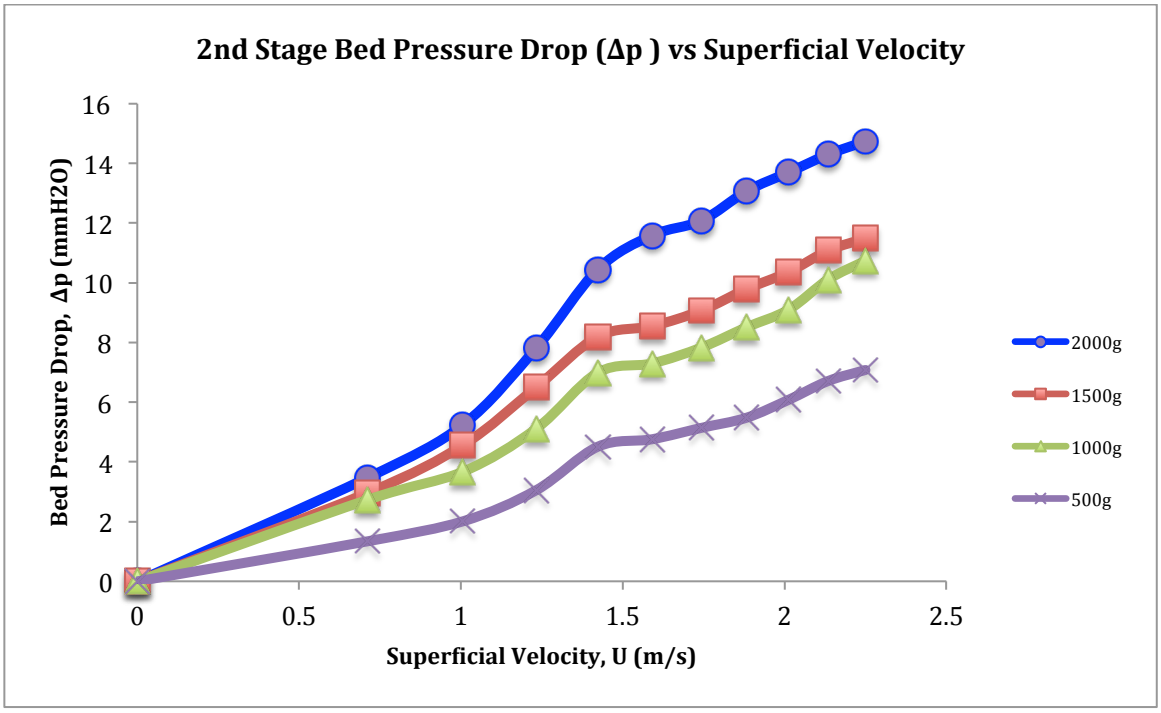

Figure 4.4 Bed Pressure Drop vs Superficial Velocity In The 2nd Stage For 2.99 mm Spherical Particles with 9° Blade Overlap

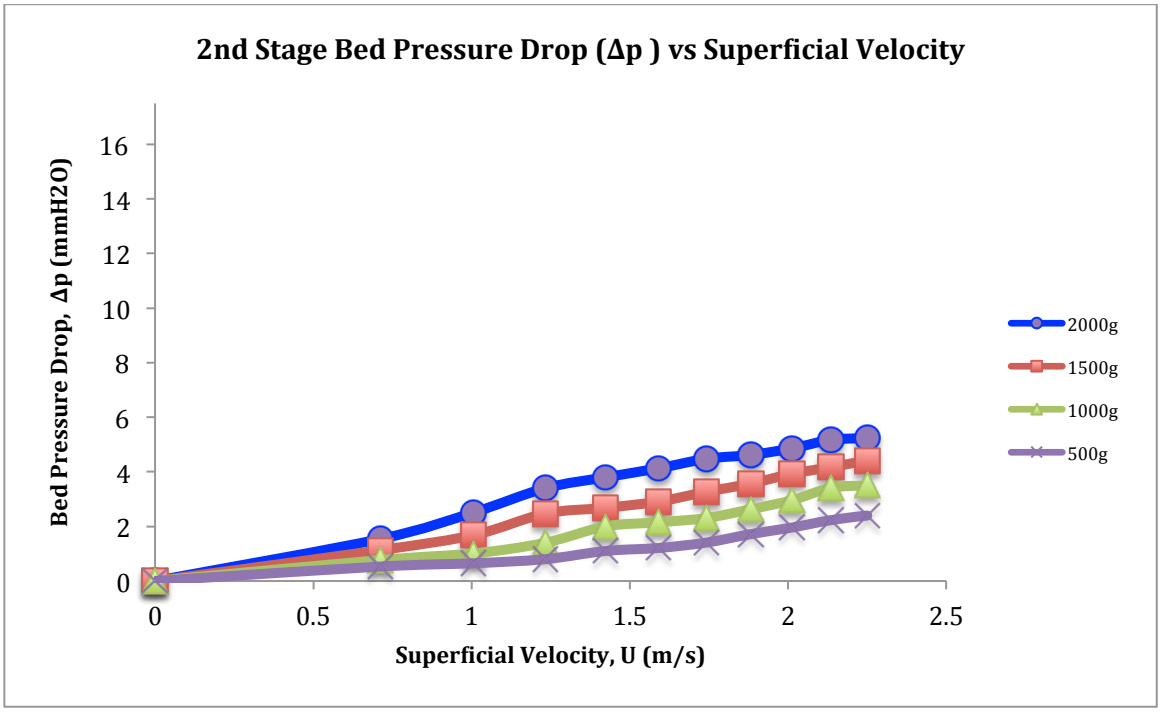

Figure 4.5 Bed Pressure Drop vs Superficial Velocity In The 2nd Stage For 2.99 mm Spherical Particles with 12° Blade Overlap

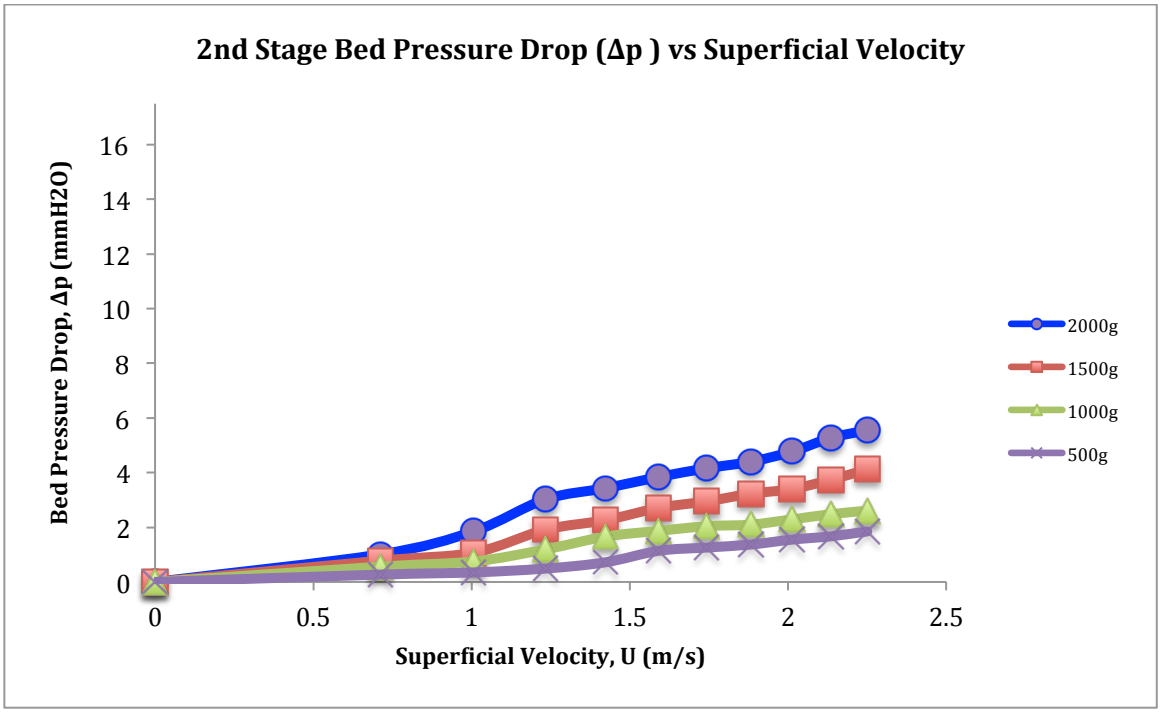

Figure 4.6 Bed Pressure Drop vs Superficial Velocity In The 2nd Stage For 2.99 mm Spherical Particles with 15° Blade Overlap

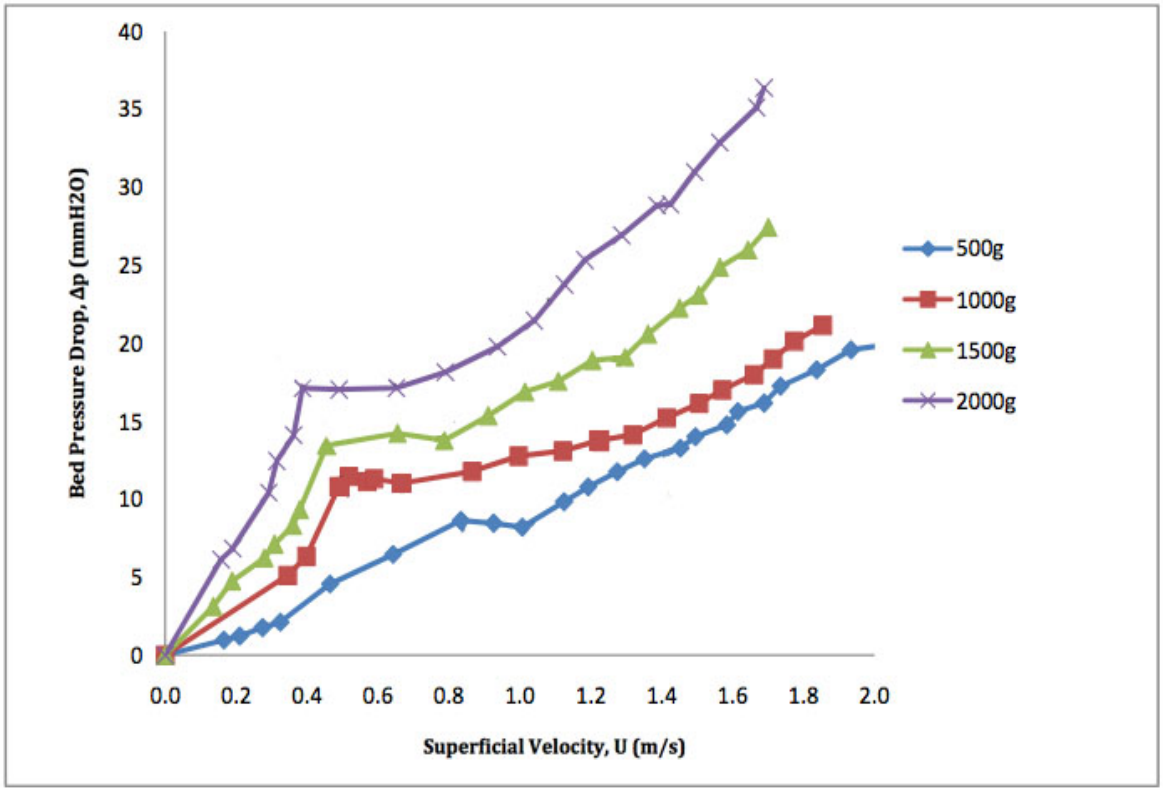

Figure 4.7 Bed Pressure Drop vs Superficial Velocity of Single-Staged SFB for 2.99 mm Spherical Particles with 12° Blade Overlap [Reproduced from 17]

4.2.2 Residence Time Distribution of Solids in the Bed

Figures 4.8, 4.9 and 4.10 exhibit the results of the RTD of solids and the observations have been drawn in accordance to two parameters, which are bed weight and blade overlap angle. The data of $E(\theta)$ are based on the effect of bed weight and effect of blade overlap angle.

It is shown that increasing the bed weight will increase the area under the tail of curve and shifts the peak of the distribution towards the higher value of θ (moving to the right) with the value of $E(\theta)$ reduced [17]. This occurrence happens due to an increase in resistance to swirling motion ascribed to a greater bed weight and escalation to the amount of time in which the particles reside inside the bed. On the other hand, the improvement of RTD of solids in multi-stage SFB is because of the numerous contacting and the solid product consequently is more uniform. This also leads the RTD to have a precise improvement over the single stage SFB. According to [9], the gas required is less than in a cross flow unit, therefore the unit gives better thermal and conversion efficiency for both gas and solid phase. Meanwhile, the effects of blade overlap angle (9°, 12° and 15°) can be seen on the value of $E(\theta)$. As the blade overlap angle increase (from 9° to 12° and 15°), the value of $E(\theta)$ shifts to the lower value. On the other hand, the value of θ remains constant or there is no significant change on the θ value with respect to the peak of distribution. On the other hand, Figure 4.11 (a)-(d) show the results of RTD of solids for single-stage SFB with 12° blade overlap angle.

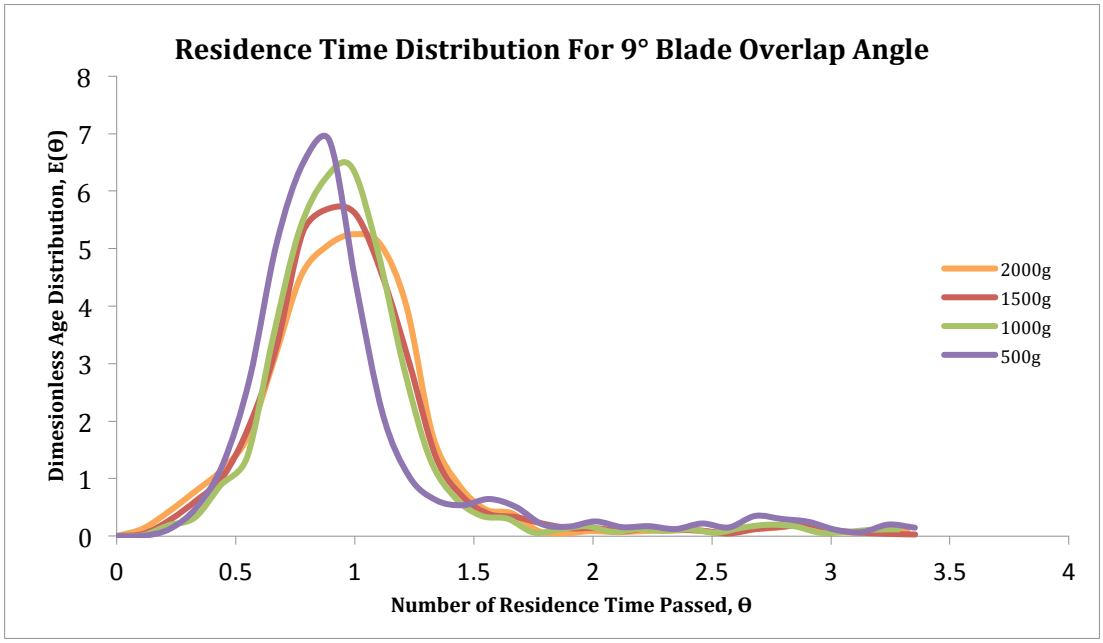

Figure 4.8. RTD Density Function for 2.99 mm Spherical Particles with 9° Blade Overlap

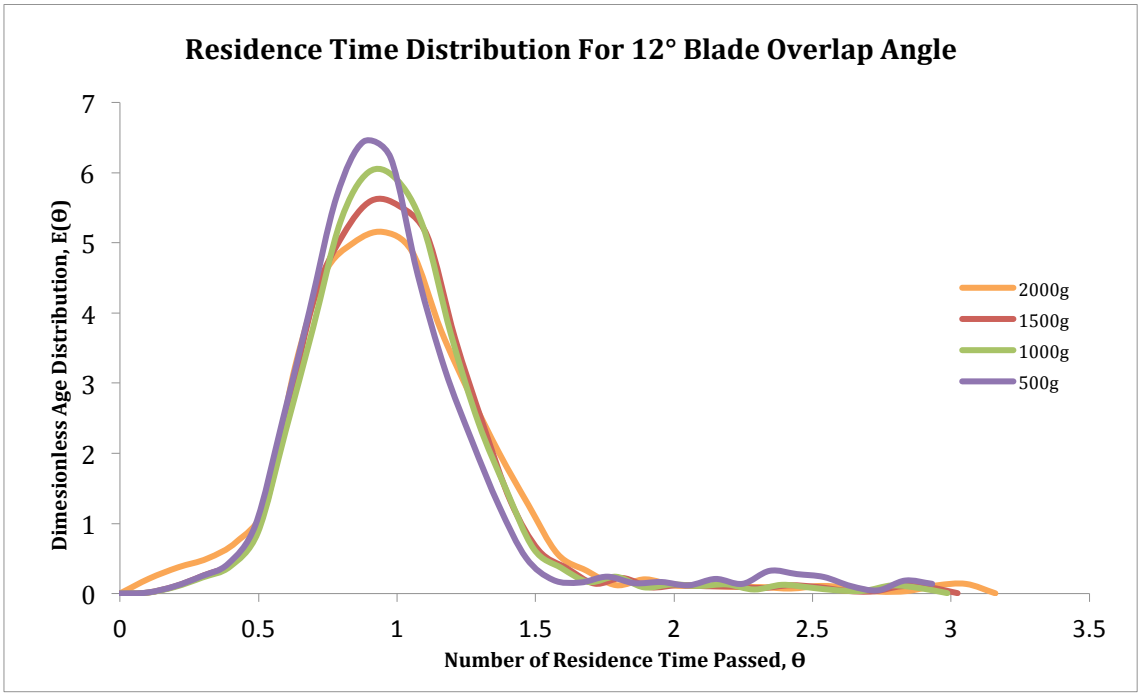

Figure 4.9 RTD Density Function for 2.99 mm Spherical Particles with 12° Blade Overlap

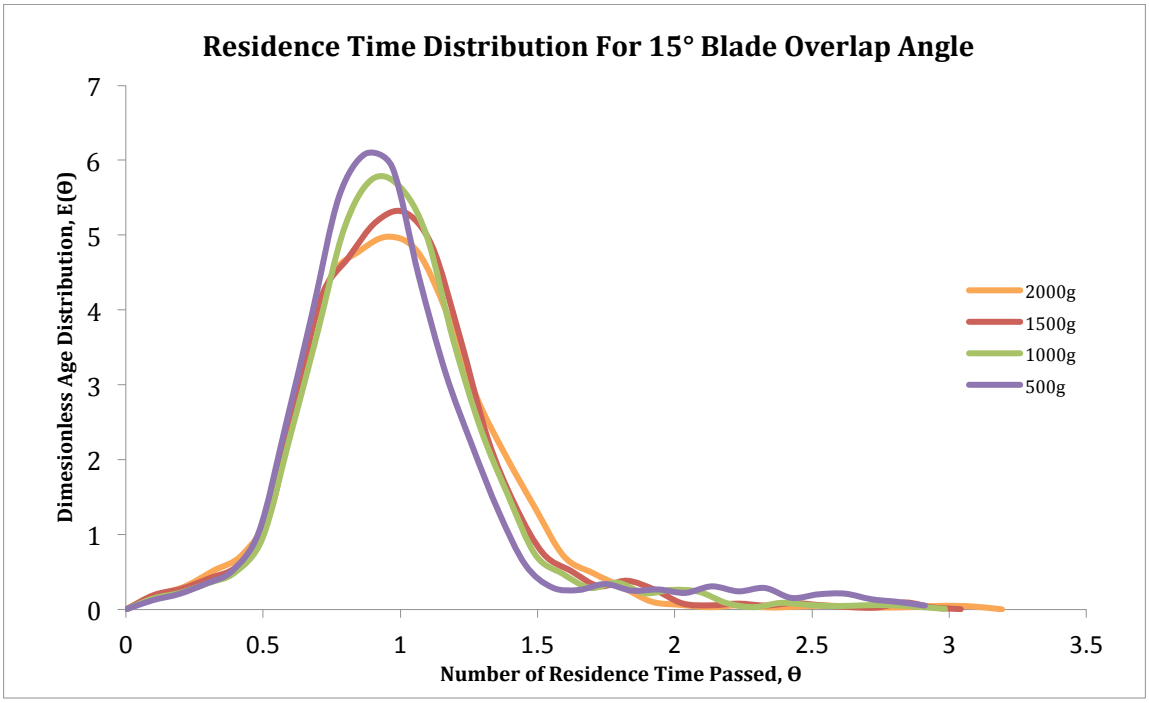

Figure 4.10 RTD Density Function for 2.99 mm Spherical Particles with 15° Blade Overlap

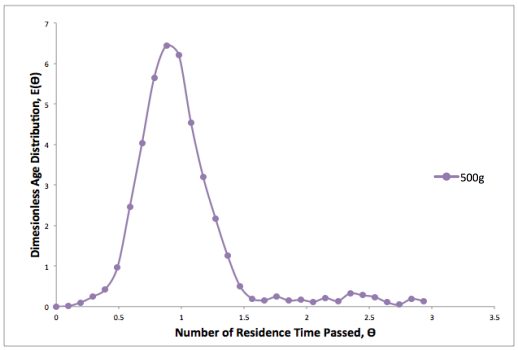

(a)

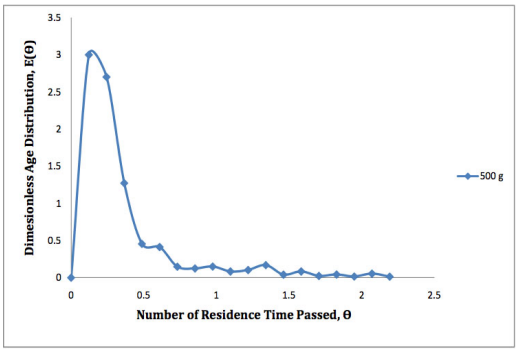

(e)

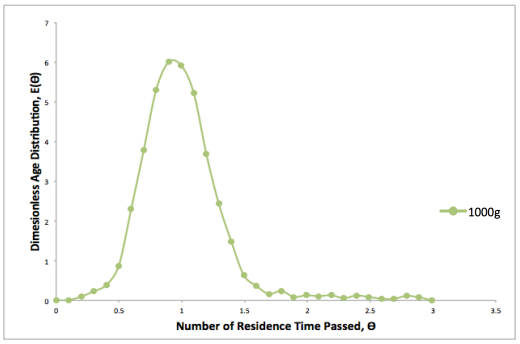

(b)

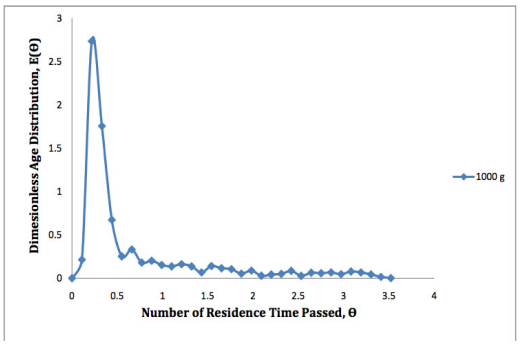

(f)

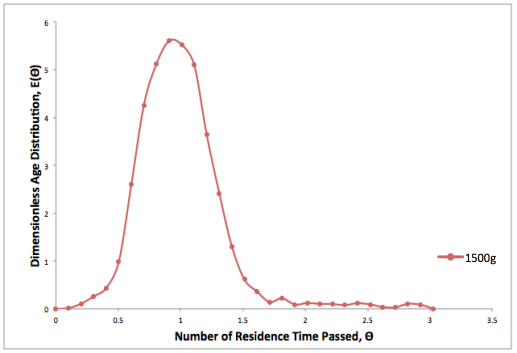

(c)

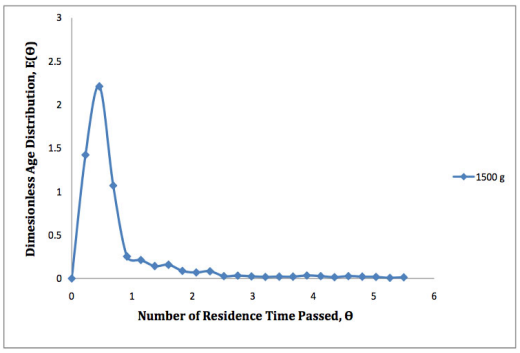

(g)

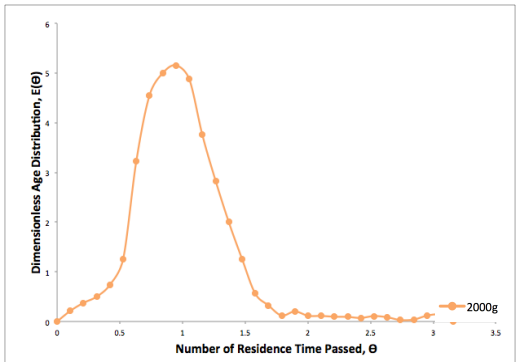

(d)

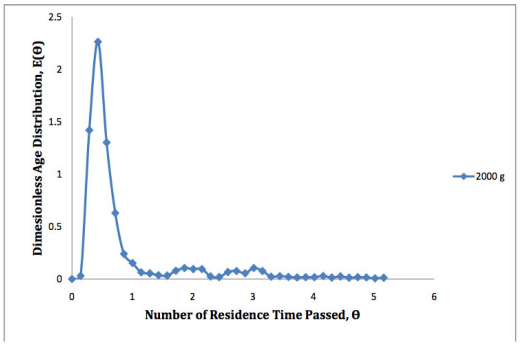

(h)

Figure 4.11 (a)-(h) Comparison of RTD Density Function between Multi-Staged SFB (Left) and Single-Staged SFB (Right) for 2.99 mm Spherical Particles with 12° Blade Overlap [Reproduced from 17]

There are many advantages to SFB more specifically in a multi-staged mode of operation. Apart from reviews that pressure drop across the various stages does not vary that much, swirling fluidization boasts that large open area fractions and low pressure drops at the distributor can be employed without ill-effects. [6]

Each component of the multi-staged SFB Prototype is carefully selected to suit best requirements. Based on previous literature and design parameters of multi-staged fluidized beds one can see that the new swirling regime requires a new approach. The encompassment of downcomers and annular spiral distributor has rendered a promising multi-staged mode of operation. Downcomers are made to fit outside the bed wall to prevent air resistances and particle flooding. However, there was a major alteration in downcomer physical design since the earlier design did not work properly as in the particles did not flow down from the second stage upper stage to the first stage (lower stage). Therefore, the downcomer was cut and being lifted up 80 mm from the original centre of the hole to reduce the incoming air to downcomer from the 1st stage. By lifting up the position of the outlet pipe, it would decrease the intensity of the air coming in through the outlet of downcomer. The plastic paper (elastic duct) was used to extend and modify the shape of the downcomer outlet and it is installed at the bottom tip of downcomer so that the particle could flow down and exit from upper stage to the below stage.

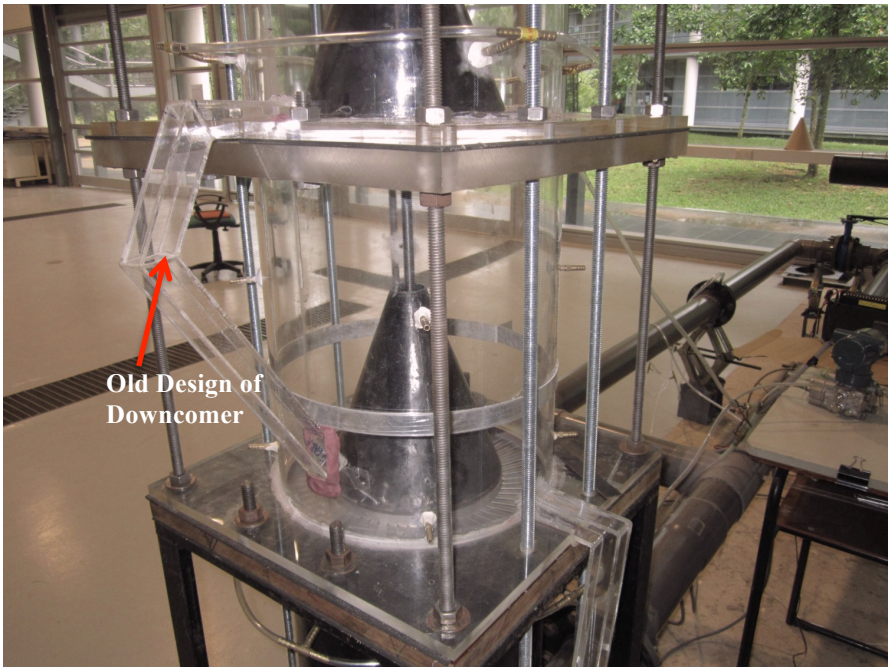

Figure 4.12 The Original Design of Downcomer

Figure 4.13 The Modified Design of Downcomer

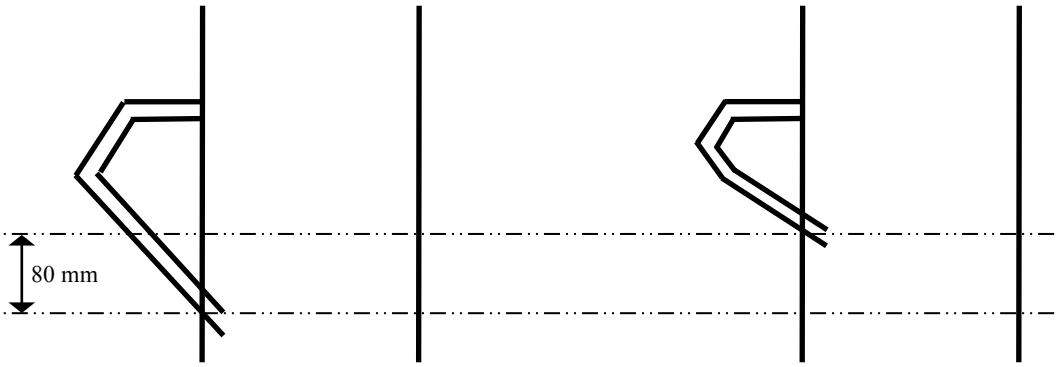

Figure 4.14 Schematic Diagram of Modification on the Downcomer Height

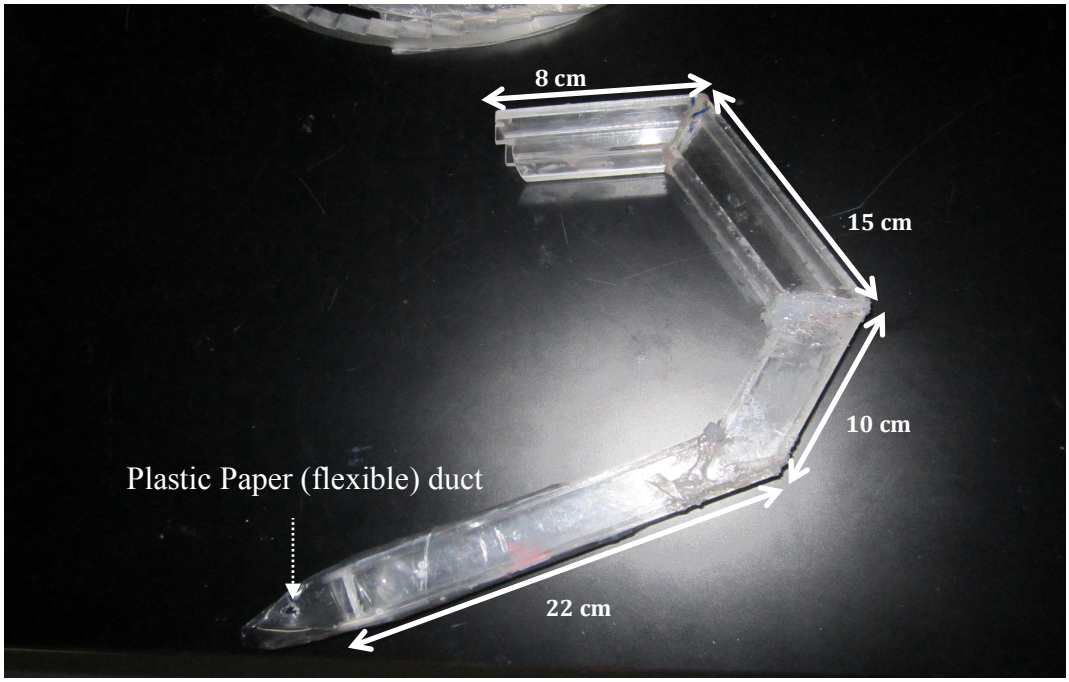

Figure 4.15 Dimension of the Modified Downcomer Design

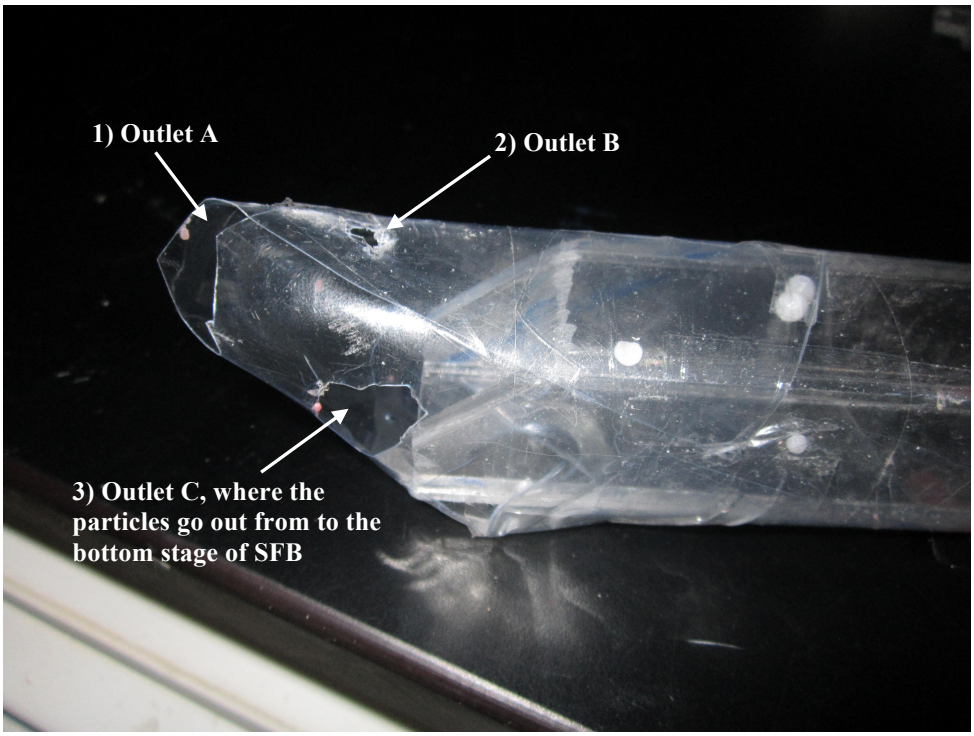

Figure 4.16 Details of the Modified Downcomer

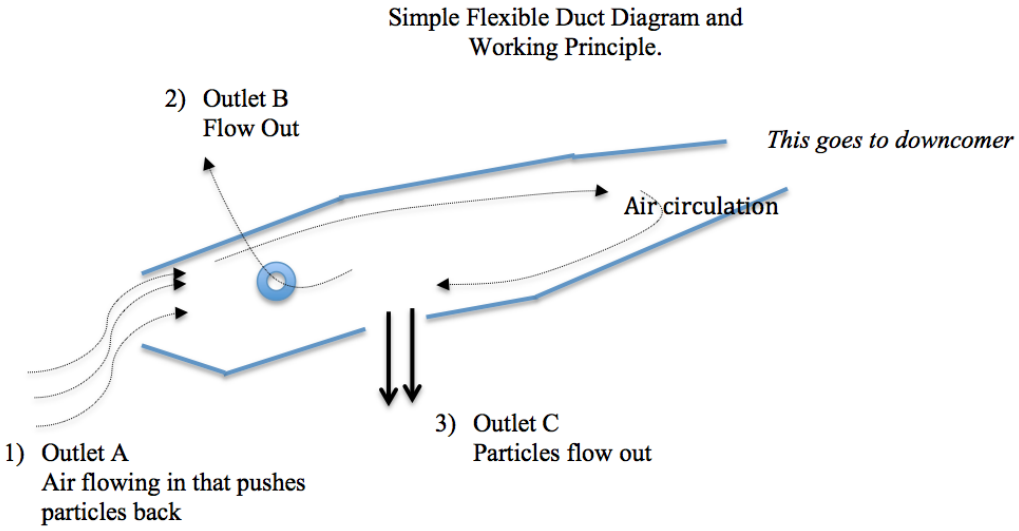

Figure 4.17 Simple Working Principle of Flexible Duct

Figure 4.14 shows plastic paper (the one used report cover page) is attached as an elastic duct at the end of the outlet of downcomer. The selection of flexible duct's shape and size are based on trial and error method. Initially, particles did not flow down with original shape and after minimizing the tip of flexible duct outlet (resemblance of cone shape), particles flow down through outlet C but it was stuck and jammed at the tip of flexible duct (outlet A). Third outlet was made in order to compensate an air-flow (outlet B). The particles eventually go down and flow seamlessly through outlet C.

CHAPTER 5
CONCLUSION AND RECOMMENDATION

5.1 Conclusion

Multi-staged SFB are considered a new field to be researched. The characteristics of multi-stage SFB are very interesting to be explored as they may be applied in many industrial and research applications. The project investigates the RTD and pressure drop via multi-stage SFB to measure its effectiveness. Experimental activities for investigating RTD of solids and pressure drop in SFB were conducted to study the effect of the two parameters, which are the effects of bed weight and the effects of blade overlap angle. The experiment condition was to utilizing four different bed weights (500g, 1000g, 1500g and 2000g) and three different blade overlap angle (9°, 12° and 15°) with one spherical particle size (2.99 mm).

Based on the study on the variation of the bed pressure drop with respect to three different distributor blades and four bed weights, the pressure drop for 15° blade is proven to be superior to 12° and 9° blade overlaps. It is due the smaller opening area of 9° blade overlap than the 15° blade overlap. The pressure drop is much smaller compared to the distributor with 9° blade overlap and it surely delivers higher efficiency in terms of energy usage. This indicates that lower potential energy is required to achieve same level of fluidization, complying superiority of 15° blades overlap to 12° and 9° blade overlap. Faizal Mohideen et al. [2] has justified that the higher the pressure drop means higher potential energy required for fluidization process. The pressure drop reading for different bed weights has shown to have slight deviation between one bed weight to the other. This means that the distributor with straight blade in multi-staged SFB is equally effective to be used and it is also important for scale-up.

The experimental result of solid RTD shows that increasing the bed weight will increase the area under the tail of curve and shifts the peak of the distribution towards the higher value of θ (moving to the right) with the value of $E(\theta)$ reduced. Meanwhile, the effects of blade overlap angle (9°, 12° and 15°) can be seen on the value of $E(\theta)$. As the blade

overlap angle increase (from 9° to 12° and 15°), the value of $E(\theta)$ shifts to the lower value. On the other hand, the value of θ remains constant or there is no significant change on the θ value with respect to the peak of distribution. Thus, the experiment set up is shown to be highly versatile and capable of representing widely different conditions depending on the variables from the parameters.

5.2 Recommendation for Future Work

In time ahead, there are some recommendations that can be used to improve the solids RTD and bed pressure drop via multi-stage SFB that utilizes annular distributor blade. They are pointed out as follows:

1. Increase the bed weight in the experiment and also use another particle shapes to study the effectiveness of multi-stage SFB.
2. Utilize the distributor with twisted blades into a multi-stage SFB to study its efficiency in terms of energy consumption.
3. Utilize three-stage SFB instead of two-stage SFB to investigate the solids RTD and bed pressure drop.
4. Change the design of downcomer to study the behavior of multi-stage SFB.
5. Vary the bed particles in terms of its density and size.

REFERENCES

[1] J. Shu, V.I. Lakshmanan, C.E. Dodson *"Hydrodynamic study of a toroidal fluidized bed reactor"* in *Elsevier Journal: Chemical Engineering and Processing*, Vol. 39, Issue 6, 1 November 2000, Pages 499–506.

[2] M. Faizal, V.Vinod Kumar and V. R. Raghavan, *"Experimental Studies on a Swirling Fluidized Bed with Annular Distributor"* in *Int. Conference on Plant, Equipment and Reliability*, Kuala Lumpur, Malaysia, June 15-17, 2010.

[3] R. Holdich, *"Fundamentals of Particle Technology"*, Loughborough University, Midland Information Technology and Publishing, 2002.

[4] L.G Gibilaro. (2001). *Fluidization-Dynamics* [Online]. Available: http://training.nigc.ir/files/files/chemist%20book/Fluidization_Dynamics.pdf [June 29, 2012].

[5] Green Field Research Encorporated. (2012, Jul. 20). *"What is Fluidization"* [Online]. Available: http://greenfieldresearch.ca/products/fluidized-bed-boiler-designs [June 30, 2012].

[6] Dr. K. Sasi, R. K. Niven, H. Chiorean, & A. Chatterjee, *"Physical Insight into the Ergun and Wen & Yu Equations for Fluid Flow in Packed and Fluidized Beds"*, ACT 2600, Australia, 2001.

[7] B. Sreenivasan, & V.R. Raghavan, "Hydrodynamics of a Swirling Fluidised Bed" in *Chemical Engineering and Processing*, Vol. 41, p. 99-106, 2002.

[8] C. Yang, & Y. Lin, "A Study in the Swirling Fluidizing Pattern" in *Journal of Chemical Engineering of Japan,* Vol. 35, Issue 6, 12 August 2002, Pages 503-512.

[9] V.V. Kumar, M. Faizal and V.R. Raghavan, "*Study of the Fluid Dynamic Performance of Distributor Type in Torbed Type Reactors*" in *Engineering e-Transaction* (ISSN 1823-6379), Vol. 6, No.1, June 2011, pp 70-75.

[10] Sascha R.A. Kersten, Wolter Prins, Bram van der Drift, Wim P.M. van Swaaij, *"Principles of a novel multistage circulating fluidized bed reactor for biomass gasifcation"*, Netherlands (ECN), 2009.

[11] C.R. Mohanty, B. Rajmohan, B.C. Meikap, *"Identification of stable operating ranges of a counter-current multi-stage fluidized bed reactor with downcomer"*, India & South-Africa, 2009.

[12] C.R. Mohanty and B.C. Meikap, *"Pressure drop characteristics of a multi-stage counter-current fluidized bed reactor for control of gaseous pollutants"*, India & South-Africa, 2008.

[13] J. S. M. Botterill, Y. Teoman, and K. R. Yuregir, *"The Effect of Operating Temperature on the V elocity of Minimum Fluidization. Bed Voidage and General Behaviour"* in *Powder Technology*, Vol. 31, pp. 101-110, 1982.

[14] S. C. Saxena, A. Chatterjee, and S. J. Zhou, *"Effect of Distributor on Gas-Solid Fluidization"* in *Powder Technology*, Vol. 22, pp. 191-198, 1979.

[15] I. Martin-Gullon, A. Marcilla, R. Font, M. Asensio, *"Stable operating velocity range for multistage fluidized bed reactors with downcomers"* in *Powder Technology*., Vol. 85, 193-201, 1995.

[16] W. Yang, *"Handbook of Fluidization and Fluid-Particle Systems"* in Siemens Westinghouse Power Corporation, Pennsylvania, USA 2003. – *"Standpipes and Non-mechanical Valves";* T. M. Knowlton.

[17] A.S.M. Yudin, *"Studies on Residence Time Distribution in Swrling Fluidized Beds"* MSc Thesis (2011), Department of Mechanical Engineering, Universiti Teknologi Petronas, Perak, Malaysia, July, 2011.

[18] O. Levenspiel, *"Chemical Reaction Engineering"*. New York: John Wiley and Sons 1965, 1972.

[19] U. Mann and E. J. Crosky, "*Cycle Time Distribution in Circulating Systems*" in *Chem. Engg. Sci.*, Vol. 28, 1973, pp 623.

[20] B. Fu, H. Weinstein, B. Bernstein, A.B. Shaffer, "*Residence Time Distributions of Recycle Systems – Integral Equation Formulation*" in *Ind. Eng. Chem. Process. Des. Dev.*, Vol. 10, pp 501, 1971.

[21] A. Didwania and L.S. Tsimring. (2002, Dec 24). *"Swirling Air Fluidized Beds for Microgravity Applications"* [Online]. Available: http://inls.ucsd.edu/~volfson/cur_research/node5.html [June 30, 2012].

[22] R. Siegel, *"Effect of Distributor Plate to Bed Resistance Ratio on Onset of Fluidized Bed Channeling"* in *AIChE J.*, 22, 590, 1976.

[23] M. Jeevaneswary, V.Vinod Kumar, and V.R. Raghavan, *"Experimental Studies on the Effect of Blade Overlap Angle on Bed Pressure Drop in a Swirling Fluidized Bed"* Department of Mechanical Engineering, Universiti Teknologi Petronas, Perak, Malaysia, June, 2011.

[24] D. Wolf and W. Resnick, *"Experimental study of residence time distribution in a multistage fluidized bed"*, Technion-Israel Institute of Technology, Haifa, 1965.

[25] IEEE Computer Society. (2007, Nov.). *"IEEE Computer Society Style Guide – References"* [Online]. Available: tinyurl.com/ypdfts [April 25, 2012].

[26] H. Chiorean, "*Retention Time Distribution in a Circulating Fluidized Bed*" MSc Thesis (1998), Chemical Engineering, 1998.

[27] P. V. Dackwerts, "*Continuous Flow System. Distribution of Residence Time*", *Chem. Eng. Sci.*, 2, 1-13, 1953.

APPENDICES

Appendix A - Project Gantt Chart and Project Milestones

Appendix B - Residence Time Distribution Experimental Procedure

Appendix C - 1st (Lower) Stage Pressure Drop Data Collection

Appendix D - 2nd (Upper) Stage Pressure Drop Data Collection

Appendix E - Residence Time Distribution of Solids Data Collection

Appendix F - Project Recognition

Appendix G - Calculation of Superficial Velocity

Appendix A - Project Gantt Chart and Project Milestones

i. **FYP I**

No	Detail/Week	1	2	3	4	5	6	7		8	9	10	11	12	13	14	Key Milestone (•)
1	Topic Selection & Discussion		•														Topic Selection (Week 2)
2	Preliminary Research Study						•										Extended Proposal Submission (Week 6)
3	Design The Multi - Stage SFB																
4	Proposal Defence										•						Proposal Defense Presentation (Week 9)
5	Fabrication of the blades & Downcomers													•			Collection of Blades from EDM's Lab
6	Submission of Interim Draft Report														•		Interim Draft Report Submission (Week 14)
7	Submission of Interim Report															•	Interim Report Submission (Week 14)

ii. **FYP II**

No	Detail/Week	1	2	3	4	5	6	7		8	9	10	11	12	13	14	15	Key Milestone (•)
1	Prepare Experimental Set Up																	
2	Experiment							•										Finish Experiment (Week 7)
3	Result and Analysis									•								Progress Report Submission (Week 8)
4	Reporting													•				Draft of Final Report Submission (Week 12)
																•		Oral Presentation (Week 14)
																	•	Hard Bound Final Report Submission (Week 15)

■ Suggested Milestone

Process

Appendix B - Residence Time Distribution Experimental Procedure

i. PROCEDURE FOR SOLIDS RTD MEASUREMENT

1. The feed hopper is filled with bed and tracer particle with particles of required diameter and weight.

2. The bed particles are fed continuously from the feed hopper to the bed at the desired rate. Air is allowed to flow into the bed at the required flow rate.

3. Under steady-state operation which will be observed by constancy of total pressure drop and pressure differential across the venture flow meter and by uniform discharge rate of solids as checked by an accurate balance-a known weight of tracer is admitted as a pulse to the bed at the position of solids feed.

4. Simultaneously with the admission of the tracer, a stop watch was started and all the discharged solids were collected is samples at constant known time intervals.

5. The collection continues until there is no tracer detected at the exit. All material in the bed is collected and accurately weighed to obtain the total bed weight (holdup).

6. The collected samples are carefully separated manually. The concentrations of the tracer were measured by weighing the separated tracer particle by using digital electronic balance.

The amount of tracer particles admitted to the bed was about 5% of the bed weight. In the separation of the colored tracer particle from the bed particle in each sample, it was confirmed that all the tracer material is separated by the clear difference in color between them.

The concentration data is now mathematically analyzed. To illustrate the analysis, consider the following experimental data of 2.99 mm particle weight of 1500 grams.

t_i	M_{ti}
0	0
4	0.00525
8	0.0385
12	0.09275
16	0.15575
20	0.3500
24	0.9275
28	1.5225
32	1.83
36	2.001
40	1.9745
44	1.824
48	1.3005
52	0.864
56	0.4674

where t_i is measured clock time and M_{ti} is tracer weight collected in each sample. The sampling period is 4 seconds. Firstly the total weight of tracer collected in the end of the sampling period is calculated.

$$\Sigma M_{ti} = 14.18331 \ grams$$

The RTD density function *E(t)* is defined by

$$E(t) = \frac{M_{ti}}{\Sigma M_{ti}}$$

t_i	M_{ti}	E(t)
0	0	0
4	0.00525	0.000370153
8	0.0385	0.002714458
12	0.09275	0.006539376
16	0.15575	0.010981217
20	0.3500	0.024676891
24	0.9275	0.065393762
28	1.5225	0.107344477
32	1.83	0.129024889
36	2.001	0.141081313
40	1.9745	0.13921292
44	1.824	0.128601857
48	1.3005	0.091692278
52	0.864	0.060916669
56	0.4674	0.032954226

According to [20] in his book of Chemical Reaction Engineering, the definition of mean residence time is given by

$$\bar{t} = \frac{\Sigma t_i M_{ti} \Delta t_i}{\Sigma M_{ti} \Delta t_i}$$

$$\bar{t} = 39.6871647 \ s$$

A particle of fluid will stay in process for 31 seconds averagely. The time data is now scaled by dividing the real time by mean residence time in order to obtain θ, the number of residence time that have passed. The unit pulse response *E(t)* is now scaled by multiplying by mean residence time in order to obtain the dimensionless age distribution $E(\theta)$.

$$\theta = \frac{t}{\bar{t}}$$

$$E(\theta) = \bar{t}E(t)$$

t_i	M_{ti}	E(t)	$\Sigma t_i M_{ti} \Delta t$	$\Sigma M_{ti} \Delta t$	θ	$E(\theta)$
0	0	0	0	0	0	0
4	0.00525	0.000370153	0.084	0.021	0.100788253	0.014690338
8	0.0385	0.002714458	1.232	0.154	0.201576506	0.107729144
12	0.09275	0.006539376	4.452	0.371	0.302364759	0.259529301
16	0.15575	0.010981217	9.968	0.623	0.403153012	0.435813354
20	0.3500	0.024676891	28	1.4	0.503941265	0.979355852
24	0.9275	0.065393762	89.04	3.71	0.604729518	2.595293007
28	1.5225	0.107344477	170.52	6.09	0.705517772	4.260197955
32	1.83	0.129024889	234.24	7.32	0.806306025	5.120632025
36	2.001	0.141081313	288.144	8.004	0.907094278	5.599117313
40	1.9745	0.13921292	315.92	7.898	1.007882531	5.524966084
44	1.824	0.128601857	321.024	7.296	1.108670784	5.103843068
48	1.3005	0.091692278	249.696	5.202	1.209459037	3.639006529
52	0.864	0.060916669	179.712	3.456	1.31024729	2.417609874

Figure B represents these data. The area under the curve is unity. This is a true probability function, with a mean of $\theta = \frac{t}{\bar{t}} = 1.0$. The area under the curve between any numbers of residence times, θ_1 and θ_2 represent the probability (percentage) of material that will reside in the process between θ_1 and θ_2.

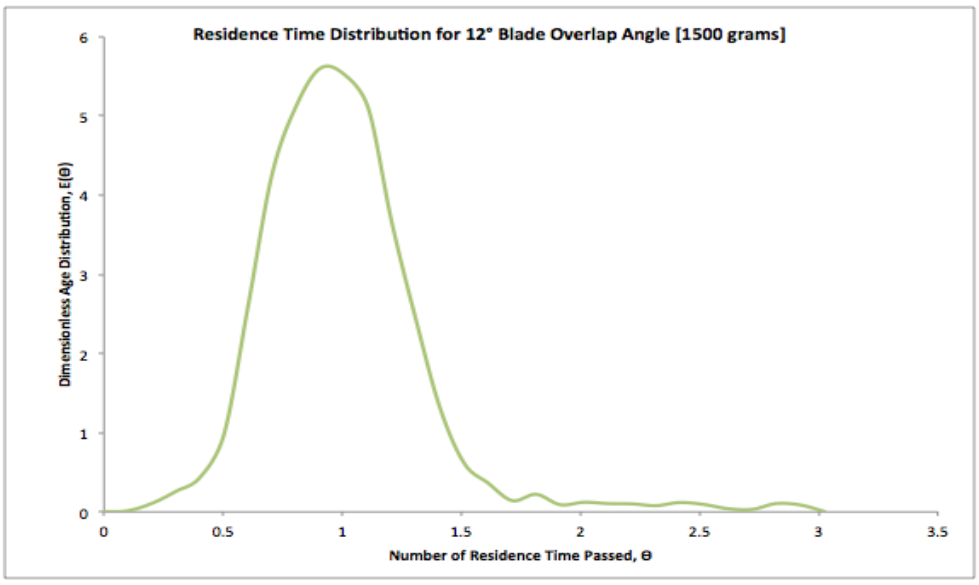

Figure B Normalized Pulse Response (Age Distribution Function)

Appendix C - 1st (Lower) Stage Pressure Drop Data Collection

i. 9° Blade Overlap Angle

			Blade Overlap Angle = 9°						
			1st With Particles			1st Without Particles			500 grams
Reading No	Δp in orifice (mmH2O)	U (m/s)	P2	P3	P2 - P3	P2a	P3	P2a - P3	(P2 - P3) - (P2a - P3)
0	0	0	0	0	0	0	0	0	0
1	10	0.711512474	15.42	3.91	11.51	14.3	3.94	10.36	1.15
2	20	1.00623059	30.52	7.95	22.57	28.11	7.45	20.66	1.91
3	30	1.232375754	44.45	11.47	32.98	41.52	11.42	30.1	2.88
4	40	1.423024947	58.32	15.01	43.31	54.43	15.49	38.94	4.37
5	50	1.590990258	72.61	18.98	53.63	66.91	17.84	49.07	4.56
6	60	1.742842506	85.51	22.32	63.19	79.87	21.71	58.16	5.03
7	70	1.88248506	98.75	25.89	72.86	92.81	25.34	67.47	5.39
8	80	2.01246118	111.47	29.32	82.15	105.7	29.43	76.27	5.88
9	90	2.134537421	125.57	32.91	92.66	118.83	32.92	85.91	6.75
10	100	2.25	139.79	36.67	103.12	131.79	35.53	96.26	6.86

			Blade Overlap Angle = 9°						
			1st With Particles			1st Without Particles			1000 grams
Reading No	Δp in orifice (mmH2O)	U (m/s)	P2	P3	P2 - P3	P2a	P3	P2a - P3	(P2 - P3) - (P2a - P3)
0	0	0	0	0	0	0	0	0	0
1	10	0.711512474	16.75	3.91	12.84	14.3	3.94	10.36	2.48
2	20	1.00623059	31.87	7.58	24.29	28.11	7.45	20.66	3.63
3	30	1.232375754	45.95	11.07	34.88	41.52	11.42	30.1	4.78
4	40	1.423024947	60.34	15.01	45.33	54.43	15.49	38.94	6.39
5	50	1.590990258	74.81	18.57	56.24	66.91	17.84	49.07	7.17
6	60	1.742842506	87.51	21.32	66.19	79.87	21.71	58.16	8.03
7	70	1.88248506	100.75	24.89	75.86	92.81	25.34	67.47	8.39
8	80	2.01246118	113.67	28.88	84.79	105.7	29.43	76.27	8.52
9	90	2.134537421	127.57	32.91	94.66	118.83	32.92	85.91	8.75
10	100	2.25	142.33	36.67	105.66	131.79	35.53	96.26	9.4

			Blade Overlap Angle = 9°						
			1st With Particles			1st Without Particles			1500 grams
Reading No	Δp in orifice (mmH2O)	U (m/s)	P2	P3	P2 - P3	P2a	P3	P2a - P3	(P2 - P3) - (P2a - P3)
0	0	0	0	0	0	0	0	0	0.00
1	10	0.711512474	17.8	4.18	13.62	14.3	3.94	10.36	3.26
2	20	1.00623059	32.47	7.49	24.98	28.11	7.45	20.66	4.32
3	30	1.232375754	46.89	11.24	35.65	41.52	11.42	30.1	5.55
4	40	1.423024947	61.31	14.81	46.5	54.43	15.49	38.94	7.56
5	50	1.590990258	75.67	18.22	57.45	66.91	17.84	49.07	8.38
6	60	1.742842506	89.56	22.03	67.53	79.87	21.71	58.16	9.37
7	70	1.88248506	102.39	24.87	77.52	92.81	25.34	67.47	10.05
8	80	2.01246118	114.32	27.57	86.75	105.7	29.43	76.27	10.48
9	90	2.134537421	128.36	31.21	97.15	118.83	32.92	85.91	11.24
10	100	2.25	142.52	34.71	107.81	131.79	35.53	96.26	11.55

			Blade Overlap Angle = 9°						
			1st With Particles			1st Without Particles			2000 grams
Reading No	Δp in orifice (mmH2O)	U (m/s)	P2	P3	P2 - P3	P2a	P3	P2a - P3	(P2 - P3) - (P2a - P3)
0	0	0	0	0	0	0	0	0	0
1	10	0.711512474	16.88	3.14	13.74	14.3	3.94	10.36	3.38
2	20	1.00623059	32.84	7.11	25.73	28.11	7.45	20.66	5.07
3	30	1.232375754	48.25	10.51	37.74	41.52	11.42	30.1	7.64
4	40	1.423024947	63.18	13.7	49.48	54.43	15.49	38.94	10.54
5	50	1.590990258	77.64	17.26	60.38	66.91	17.84	49.07	11.31
6	60	1.742842506	91.36	21.13	70.23	79.87	21.71	58.16	12.07
7	70	1.88248506	104.73	24.41	80.32	92.81	25.34	67.47	12.85
8	80	2.01246118	118.52	28.36	90.16	105.7	29.43	76.27	13.89
9	90	2.134537421	133.34	32.18	101.16	118.83	32.92	85.91	15.25
10	100	2.25	147.56	35.09	112.47	131.79	35.53	96.26	16.21

ii. 12° Blade Overlap Angle

			Blade Overlap Angle = 12°						
			1st With Particles			1st Without Particles			500 grams
Reading No	Δp in orifice (mmH2O)	U (m/s)	P2	P3	P2 - P3	P2a	P3	P2a - P3	(P2 - P3) - (P2a - P3)
0	0	0	0	0	0	0	0	0	0
1	10	0.711512474	15.49	3.94	11.55	15.16	3.89	11.27	0.28
2	20	1.00623059	29.39	7.57	21.82	29.92	8.56	21.36	0.46
3	30	1.232375754	42.96	11.23	31.73	43.88	12.89	30.99	0.74
4	40	1.423024947	57.72	15.05	42.67	58.62	16.88	41.74	0.93
5	50	1.590990258	72.59	18.8	53.79	73.62	20.84	52.78	1.01
6	60	1.742842506	86.72	22.36	64.36	85.64	22.36	63.28	1.08
7	70	1.88248506	101.15	26.04	75.11	98.79	24.91	73.88	1.23
8	80	2.01246118	114.77	29.82	84.95	112.87	29.34	83.53	1.42
9	90	2.134537421	128.73	32.67	96.06	126.95	32.57	94.38	1.68
10	100	2.25	142.93	36.24	106.69	140.97	36.03	104.94	1.75

			Blade Overlap Angle = 12°						
			1st With Particles			1st Without Particles			1000 grams
Reading No	Δp in orifice (mmH2O)	U (m/s)	P2	P3	P2 - P3	P2a	P3	P2a - P3	(P2 - P3) - (P2a - P3)
0	0	0	0	0	0	0	0	0	0
1	10	0.711512474	16.04	4.25	11.79	15.16	3.89	11.27	0.52
2	20	1.00623059	31.71	9.52	22.19	29.92	8.56	21.36	0.83
3	30	1.232375754	45.63	13.42	32.21	43.88	12.89	30.99	1.22
4	40	1.423024947	59.89	16.46	43.43	58.62	16.88	41.74	1.69
5	50	1.590990258	74.38	19.68	54.7	73.62	20.84	52.78	1.92
6	60	1.742842506	89.37	23.98	65.39	85.64	22.36	63.28	2.11
7	70	1.88248506	103.56	27.25	76.31	98.79	24.91	73.88	2.43
8	80	2.01246118	116.73	30.53	86.2	112.87	29.34	83.53	2.67
9	90	2.134537421	130.97	33.74	97.23	126.95	32.57	94.38	2.85
10	100	2.25	144.91	36.93	107.98	140.97	36.03	104.94	3.04

			Blade Overlap Angle = 12°						
			1st With Particles			1st Without Particles			1500 grams
Reading No	Δp in orifice (mmH2O)	U (m/s)	P2	P3	P2 - P3	P2a	P3	P2a - P3	(P2 - P3) - (P2a - P3)
0	0	0	0	0	0	0	0	0	0.00
1	10	0.711512474	16.29	4.28	12.01	15.16	3.89	11.27	0.74
2	20	1.00623059	30.68	8.02	22.66	29.92	8.56	21.36	1.30
3	30	1.232375754	45.22	12.28	32.94	43.88	12.89	30.99	1.95
4	40	1.423024947	59.88	15.56	44.32	58.62	16.88	41.74	2.58
5	50	1.590990258	75.37	19.82	55.55	73.62	20.84	52.78	2.77
6	60	1.742842506	89.33	23.11	66.22	85.64	22.36	63.28	2.94
7	70	1.88248506	103.1	26.12	76.98	98.79	24.91	73.88	3.10
8	80	2.01246118	116.78	30.02	86.76	112.87	29.34	83.53	3.23
9	90	2.134537421	130.84	33.1	97.74	126.95	32.57	94.38	3.36
10	100	2.25	144.85	36.38	108.47	140.97	36.03	104.94	3.53

			Blade Overlap Angle = 12°						
			1st With Particles			1st Without Particles			2000 grams
Reading No	Δp in orifice (mmH2O)	U (m/s)	P2	P3	P2 - P3	P2a	P3	P2a - P3	(P2 - P3) - (P2a - P3)
0	0	0	0	0	0	0	0	0	0
1	10	0.711512474	16.65	4.28	12.37	15.16	3.89	11.27	1.1
2	20	1.00623059	32.03	8.84	23.19	29.92	8.56	21.36	1.83
3	30	1.232375754	46.08	12.55	33.53	43.88	12.89	30.99	2.54
4	40	1.423024947	60.79	15.87	44.92	58.62	16.88	41.74	3.18
5	50	1.590990258	75.33	19.13	56.2	73.62	20.84	52.78	3.42
6	60	1.742842506	89.36	22.53	66.83	85.64	22.36	63.28	3.55
7	70	1.88248506	103.73	26.12	77.61	98.79	24.91	73.88	3.73
8	80	2.01246118	116.81	29.43	87.38	112.87	29.34	83.53	3.85
9	90	2.134537421	130.95	32.59	98.36	126.95	32.57	94.38	3.98
10	100	2.25	145.25	36.25	109	140.97	36.03	104.94	4.06

iii. 15° Blade Overlap Angle

			Blade Overlap Angle = 15°						
			1st With Particles			1st Without Particles			500 grams
Reading No	Δp in orifice (mmH2O)	U (m/s)	P2	P3	P2 - P3	P2a	P3	P2a - P3	(P2 - P3) - (P2a - P3)
0	0	0	0	0	0	0	0	0	0
1	10	0.711512474	15.21	4.05	11.16	14.64	3.63	11.01	0.15
2	20	1.00623059	29.11	8.14	20.97	27.86	7.23	20.63	0.34
3	30	1.232375754	43.34	12.51	30.83	41.2	10.89	30.31	0.52
4	40	1.423024947	55.6	15.2	40.4	54.13	14.51	39.62	0.78
5	50	1.590990258	71.55	18.62	52.93	69.8	17.78	52.02	0.91
6	60	1.742842506	85.91	22.83	63.08	84.12	22.05	62.07	1.01
7	70	1.88248506	100.27	26.65	73.62	98.23	25.74	72.49	1.13
8	80	2.01246118	114.74	31.05	83.69	112.17	29.78	82.39	1.3
9	90	2.134537421	128.73	34.7	94.03	125.23	32.65	92.58	1.45
10	100	2.25	142.39	37.79	104.6	139.04	35.97	103.07	1.53

			Blade Overlap Angle = 15°						
			1st With Particles			1st Without Particles			1000 grams
Reading No	Δp in orifice (mmH2O)	U (m/s)	P2	P3	P2 - P3	P2a	P3	P2a - P3	(P2 - P3) - (P2a - P3)
0	0	0	0	0	0	0	0	0	0
1	10	0.711512474	15.51	4.1	11.41	14.64	3.63	11.01	0.4
2	20	1.00623059	30.15	8.86	21.29	27.86	7.23	20.63	0.66
3	30	1.232375754	44.2	12.82	31.38	41.2	10.89	30.31	1.07
4	40	1.423024947	58.02	16.91	41.11	54.13	14.51	39.62	1.49
5	50	1.590990258	73.82	20.05	53.77	69.8	17.78	52.02	1.75
6	60	1.742842506	88.17	24.14	64.03	84.12	22.05	62.07	1.96
7	70	1.88248506	102.9	28.23	74.67	98.23	25.74	72.49	2.18
8	80	2.01246118	116.84	32.15	84.69	112.17	29.78	82.39	2.3
9	90	2.134537421	130.4	35.33	95.07	125.23	32.65	92.58	2.49
10	100	2.25	143.24	37.53	105.71	139.04	35.97	103.07	2.64

			Blade Overlap Angle = 15°						
			1st With Particles			1st Without Particles			1500 grams
Reading No	Δp in orifice (mmH2O)	U (m/s)	P2	P3	P2 - P3	P2a	P3	P2a - P3	(P2 - P3) - (P2a - P3)
0	0	0	0	0	0	0	0	0	0.00
1	10	0.711512474	15.87	4.03	11.84	14.64	3.63	11.01	0.83
2	20	1.00623059	30.36	8.47	21.89	27.86	7.23	20.63	1.26
3	30	1.232375754	44.66	12.53	32.13	41.2	10.89	30.31	1.82
4	40	1.423024947	58.43	16.6	41.83	54.13	14.51	39.62	2.21
5	50	1.590990258	73.57	19.1	54.47	69.8	17.78	52.02	2.45
6	60	1.742842506	87.4	22.55	64.85	84.12	22.05	62.07	2.78
7	70	1.88248506	101.45	26.04	75.41	98.23	25.74	72.49	2.92
8	80	2.01246118	116.38	30.81	85.57	112.17	29.78	82.39	3.18
9	90	2.134537421	130.27	34.2	96.07	125.23	32.65	92.58	3.49
10	100	2.25	143.34	36.76	106.58	139.04	35.97	103.07	3.51

			Blade Overlap Angle = 15°						
			1st With Particles			1st Without Particles			2000 grams
Reading No	Δp in orifice (mmH2O)	U (m/s)	P2	P3	P2 - P3	P2a	P3	P2a - P3	(P2 - P3) - (P2a - P3)
0	0	0	0	0	0	0	0	0	0
1	10	0.711512474	16.1	4.12	11.98	14.64	3.63	11.01	0.97
2	20	1.00623059	31.02	8.71	22.31	27.86	7.23	20.63	1.68
3	30	1.232375754	45.21	12.69	32.52	41.2	10.89	30.31	2.21
4	40	1.423024947	59.34	16.7	42.64	54.13	14.51	39.62	3.02
5	50	1.590990258	74.53	19.06	55.47	69.8	17.78	52.02	3.45
6	60	1.742842506	89.6	23.87	65.73	84.12	22.05	62.07	3.66
7	70	1.88248506	102.52	26.18	76.34	98.23	25.74	72.49	3.85
8	80	2.01246118	117.02	30.56	86.46	112.17	29.78	82.39	4.07
9	90	2.134537421	131.2	34.23	96.97	125.23	32.65	92.58	4.39
10	100	2.25	146.1	38.5	107.6	139.04	35.97	103.07	4.53

Appendix D - 2nd (Upper) Stage Pressure Drop Data Collection

i. 9° Blade Overlap Angle

			Blade Overlap Angle = 9°						
			2nd With Particles			2nd Without Particles			500 grams
Reading No	Δp in orifice (mmH2O)	U (m/s)	P1	P3	P1 - P3	P1a	P3	P1a - P3	(P1 - P3) - (P1a - P3)
0	0	0	0	0	0	0	0	0	0
1	10	0.711512474	18.62	5.51	13.11	15.5	3.73	11.77	1.34
2	20	1.00623059	35.86	9.65	26.21	31.78	7.58	24.2	2.01
3	30	1.232375754	53.75	14.77	38.98	47.28	11.35	35.93	3.05
4	40	1.423024947	71.32	19.21	52.11	62.37	14.77	47.6	4.51
5	50	1.590990258	88.51	24.58	63.93	77.31	18.14	59.17	4.76
6	60	1.742842506	104.32	28.58	75.74	91.94	21.34	70.6	5.14
7	70	1.88248506	120.15	32.79	87.36	107.09	25.21	81.88	5.48
8	80	2.01246118	136.57	36.14	100.43	122.67	28.32	94.35	6.08
9	90	2.134537421	154.53	41.26	113.27	137.88	31.32	106.56	6.71
10	100	2.25	170.79	45.67	125.12	152.27	34.23	118.04	7.08

			Blade Overlap Angle = 9°						
			2nd With Particles			2nd Without Particles			1000 grams
Reading No	Δp in orifice (mmH2O)	U (m/s)	P1	P3	P1 - P3	P1a	P3	P1a - P3	(P1 - P3) - (P1a - P3)
0	0	0	0	0	0	0	0	0	0
1	10	0.711512474	18.62	4.12	14.5	15.5	3.73	11.77	2.73
2	20	1.00623059	35.89	8.02	27.87	31.78	7.58	24.2	3.67
3	30	1.232375754	53.75	12.71	41.04	47.28	11.35	35.93	5.11
4	40	1.423024947	70.62	16.03	54.59	62.37	14.77	47.6	6.99
5	50	1.590990258	87.11	20.64	66.47	77.31	18.14	59.17	7.3
6	60	1.742842506	102.21	23.78	78.43	91.94	21.34	70.6	7.83
7	70	1.88248506	117.45	27.06	90.39	107.09	25.21	81.88	8.51
8	80	2.01246118	134.27	30.82	103.45	122.67	28.32	94.35	9.1
9	90	2.134537421	150.56	33.89	116.67	137.88	31.32	106.56	10.11
10	100	2.25	165.49	36.71	128.78	152.27	34.23	118.04	10.74

			Blade Overlap Angle = 9°						
			2nd With Particles			2nd Without Particles			1500 grams
Reading No	Δp in orifice (mmH2O)	U (m/s)	P1	P3	P1 - P3	P1a	P3	P1a - P3	(P1 - P3) - (P1a - P3)
0	0	0	0	0	0	0	0	0	0
1	10	0.711512474	19.22	3.49	14.73	15.5	3.73	11.77	2.96
2	20	1.00623059	37.19	7.43	28.76	31.78	7.58	24.2	4.56
3	30	1.232375754	55.24	11.81	42.43	47.28	11.35	35.93	6.5
4	40	1.423024947	72.42	15.62	55.8	62.37	14.77	47.6	8.2
5	50	1.590990258	87.78	19.06	67.72	77.31	18.14	59.17	8.55
6	60	1.742842506	104.63	23.96	79.67	91.94	21.34	70.6	9.07
7	70	1.88248506	119.35	27.68	91.67	107.09	25.21	81.88	9.79
8	80	2.01246118	133.64	28.93	104.71	122.67	28.32	94.35	10.36
9	90	2.134537421	149.42	31.78	117.64	137.88	31.32	106.56	11.08
10	100	2.25	164.39	34.86	129.53	152.27	34.23	118.04	11.49

			Blade Overlap Angle = 9°						
			2nd With Particles			2nd Without Particles			2000 grams
Reading No	Δp in orifice (mmH2O)	U (m/s)	P1	P3	P1 - P3	P1a	P3	P1a - P3	(P1 - P3) - (P1a - P3)
0	0	0	0	0	0	0	0	0	0
1	10	0.711512474	19.97	3.23	15.24	15.5	3.73	11.77	3.47
2	20	1.00623059	38.44	7.5	29.44	31.78	7.58	24.2	5.24
3	30	1.232375754	56.65	11.41	43.74	47.28	11.35	35.93	7.81
4	40	1.423024947	75.18	15.63	58.05	62.37	14.77	47.6	10.45
5	50	1.590990258	92.15	19.89	70.76	77.31	18.14	59.17	11.59
6	60	1.742842506	107.26	23.08	82.68	91.94	21.34	70.6	12.08
7	70	1.88248506	121.73	25.28	94.95	107.09	25.21	81.88	13.07
8	80	2.01246118	138.92	29.37	108.05	122.67	28.32	94.35	13.7
9	90	2.134537421	155.87	33.51	120.86	137.88	31.32	106.56	14.3
10	100	2.25	171.6	37.32	132.78	152.27	34.23	118.04	14.74

ii. 12° Blade Overlap Angle

			Blade Overlap Angle = 12°						
			2nd With Particles			2nd Without Particles			500 grams
Reading No	Δp in orifice (mmH2O)	U (m/s)	P1	P3	P1 - P3	P1a	P3	P1a - P3	(P1 - P3) - (P1a - P3)
0	0	0	0	0	0	0	0	0	0
1	10	0.711512474	16.66	4.01	12.65	16.13	4.01	12.12	0.53
2	20	1.00623059	32.17	7.22	24.95	32.24	7.94	24.3	0.65
3	30	1.232375754	48.68	11.75	36.93	47.91	11.78	36.13	0.8
4	40	1.423024947	65.13	15.63	49.5	63.56	15.16	48.4	1.1
5	50	1.590990258	81.17	19.84	61.33	79.59	19.47	60.12	1.21
6	60	1.742842506	96.21	23.4	72.81	94.74	23.34	71.4	1.41
7	70	1.88248506	111.28	26.55	84.73	109.83	26.82	83.01	1.72
8	80	2.01246118	127.21	30.2	97.01	125.16	30.11	95.05	1.96
9	90	2.134537421	141.46	33.85	107.61	139.27	33.89	105.38	2.23
10	100	2.25	159.65	37.71	121.94	155.67	36.13	119.54	2.4

			Blade Overlap Angle = 12°						
			2nd With Particles			2nd Without Particles			1000 grams
Reading No	Δp in orifice (mmH2O)	U (m/s)	P1	P3	P1 - P3	P1a	P3	P1a - P3	(P1 - P3) - (P1a - P3)
0	0	0	0	0	0	0	0	0	0
1	10	0.711512474	17.2	4.31	12.89	16.13	4.01	12.12	0.77
2	20	1.00623059	34.53	9.22	25.31	32.24	7.94	24.3	1.01
3	30	1.232375754	50.28	12.75	37.53	47.91	11.78	36.13	1.4
4	40	1.423024947	66.53	16.13	50.4	63.56	15.16	48.4	2
5	50	1.590990258	82.11	19.84	62.27	79.59	19.47	60.12	2.15
6	60	1.742842506	97.11	23.4	73.71	94.74	23.34	71.4	2.31
7	70	1.88248506	113.19	27.55	85.64	109.83	26.82	83.01	2.63
8	80	2.01246118	129.63	31.62	98.01	125.16	30.11	95.05	2.96
9	90	2.134537421	144.64	35.85	108.79	139.27	33.89	105.38	3.41
10	100	2.25	161.76	38.71	123.05	155.67	36.13	119.54	3.51

			Blade Overlap Angle = 12°						
			2nd With Particles			2nd Without Particles			1500 grams
Reading No	Δp in orifice (mmH2O)	U (m/s)	P1	P3	P1 - P3	P1a	P3	P1a - P3	(P1 - P3) - (P1a - P3)
0	0	0	0	0	0	0	0	0	0
1	10	0.711512474	18.12	3.87	13.25	16.13	4.01	12.12	1.13
2	20	1.00623059	35.95	8.97	25.98	32.24	7.94	24.3	1.68
3	30	1.232375754	52.42	12.82	38.6	47.91	11.78	36.13	2.47
4	40	1.423024947	68.41	16.33	51.08	63.56	15.16	48.4	2.68
5	50	1.590990258	84.24	20.21	63.03	79.59	19.47	60.12	2.91
6	60	1.742842506	99.81	24.14	74.67	94.74	23.34	71.4	3.27
7	70	1.88248506	114.53	27.95	86.58	109.83	26.82	83.01	3.57
8	80	2.01246118	130.15	31.17	98.98	125.16	30.11	95.05	3.93
9	90	2.134537421	144.63	35.08	109.55	139.27	33.89	105.38	4.17
10	100	2.25	162.49	38.53	123.96	155.67	36.13	119.54	4.42

			Blade Overlap Angle = 12°						
			2nd With Particles			2nd Without Particles			2000 grams
Reading No	Δp in orifice (mmH2O)	U (m/s)	P1	P3	P1 - P3	P1a	P3	P1a - P3	(P1 - P3) - (P1a - P3)
0	0	0	0	0	0	0	0	0	0
1	10	0.711512474	19.24	4.08	13.66	16.13	4.01	12.12	1.54
2	20	1.00623059	36.43	8.12	26.81	32.24	7.94	24.3	2.51
3	30	1.232375754	53.81	12.78	39.53	47.91	11.78	36.13	3.4
4	40	1.423024947	70.54	16.84	52.2	63.56	15.16	48.4	3.8
5	50	1.590990258	86.32	20.57	64.25	79.59	19.47	60.12	4.13
6	60	1.742842506	102.21	24.83	75.88	94.74	23.34	71.4	4.48
7	70	1.88248506	117.54	28.41	87.63	109.83	26.82	83.01	4.62
8	80	2.01246118	132.8	31.39	99.91	125.16	30.11	95.05	4.86
9	90	2.134537421	147.78	35.73	110.55	139.27	33.89	105.38	5.17
10	100	2.25	165.21	38.93	124.78	155.67	36.13	119.54	5.24

iii. 15° Blade Overlap Angle

			Blade Overlap Angle = 15°						
			2nd With Particles			2nd Without Particles			500 grams
Reading No	Δp in orifice (mmH2O)	U (m/s)	P1	P3	P1 - P3	P1a	P3	P1a - P3	(P1 - P3) - (P1a - P3)
0	0	0	0	0	0	0	0	0	0
1	10	0.711512474	16.96	4.39	12.57	16.25	3.95	12.3	0.27
2	20	1.00623059	33.25	7.31	25.94	32.87	7.28	25.59	0.35
3	30	1.232375754	48.76	11.5	37.26	48.11	11.34	36.77	0.49
4	40	1.423024947	65.64	16.11	49.53	64.26	15.45	48.81	0.72
5	50	1.590990258	80.3	19.94	60.36	78.15	18.93	59.22	1.14
6	60	1.742842506	95.42	23.12	72.3	93.92	22.88	71.04	1.26
7	70	1.88248506	110.61	26.44	84.17	108.71	25.91	82.8	1.37
8	80	2.01246118	126.21	30.65	95.56	123.86	29.85	94.01	1.55
9	90	2.134537421	140.6	34.05	106.55	138.22	33.34	104.88	1.67
10	100	2.25	159.22	37.89	121.33	154.8	35.32	119.48	1.85

			Blade Overlap Angle = 15°						
			2nd With Particles			2nd Without Particles			1000 grams
Reading No	Δp in orifice (mmH2O)	U (m/s)	P1	P3	P1 - P3	P1a	P3	P1a - P3	(P1 - P3) - (P1a - P3)
0	0	0	0	0	0	0	0	0	0
1	10	0.711512474	17.11	4.25	12.86	16.25	3.95	12.3	0.56
2	20	1.00623059	35.37	9.03	26.34	32.87	7.28	25.59	0.75
3	30	1.232375754	51.57	13.61	37.96	48.11	11.34	36.77	1.19
4	40	1.423024947	67.98	17.51	50.47	64.26	15.45	48.81	1.66
5	50	1.590990258	83.02	21.93	61.09	78.15	18.93	59.22	1.87
6	60	1.742842506	98.45	25.37	73.08	93.92	22.88	71.04	2.04
7	70	1.88248506	112.78	27.88	84.9	108.71	25.91	82.8	2.1
8	80	2.01246118	128.2	31.9	96.3	123.86	29.85	94.01	2.29
9	90	2.134537421	142.8	35.44	107.36	138.22	33.34	104.88	2.48
10	100	2.25	161.5	39.41	122.09	154.8	35.32	119.48	2.61

			Blade Overlap Angle = 15°						
			2nd With Particles			2nd Without Particles			1500 grams
Reading No	Δp in orifice (mmH2O)	U (m/s)	P1	P3	P1 - P3	P1a	P3	P1a - P3	(P1 - P3) - (P1a - P3)
0	0	0	0	0	0	0	0	0	0
1	10	0.711512474	17.31	3.23	13.08	16.25	3.95	12.3	0.78
2	20	1.00623059	34.78	7.12	26.66	32.87	7.28	25.59	1.07
3	30	1.232375754	51.45	11.77	38.68	48.11	11.34	36.77	1.91
4	40	1.423024947	67.9	15.83	51.07	64.26	15.45	48.81	2.26
5	50	1.590990258	82.89	19.96	61.93	78.15	18.93	59.22	2.71
6	60	1.742842506	99.17	24.18	73.99	93.92	22.88	71.04	2.95
7	70	1.88248506	113.79	27.76	86.03	108.71	25.91	82.8	3.23
8	80	2.01246118	128.84	31.43	97.41	123.86	29.85	94.01	3.4
9	90	2.134537421	143.4	34.78	108.62	138.22	33.34	104.88	3.74
10	100	2.25	161.43	37.83	123.6	154.8	35.32	119.48	4.12

			Blade Overlap Angle = 15°						
			2nd With Particles			2nd Without Particles			2000 grams
Reading No	Δp in orifice (mmH2O)	U (m/s)	P1	P3	P1 - P3	P1a	P3	P1a - P3	(P1 - P3) - (P1a - P3)
0	0	0	0	0	0	0	0	0	0
1	10	0.711512474	18.86	4.05	13.31	16.25	3.95	12.3	1.01
2	20	1.00623059	36.9	7.96	27.44	32.87	7.28	25.59	1.85
3	30	1.232375754	53.17	11.88	39.79	48.11	11.34	36.77	3.02
4	40	1.423024947	69.5	15.76	52.24	64.26	15.45	48.81	3.43
5	50	1.590990258	84.53	19.97	63.06	78.15	18.93	59.22	3.84
6	60	1.742842506	100.41	23.71	75.2	93.92	22.88	71.04	4.16
7	70	1.88248506	115.83	27.13	87.2	108.71	25.91	82.8	4.4
8	80	2.01246118	131.73	31.45	98.78	123.86	29.85	94.01	4.77
9	90	2.134537421	147.34	35.69	110.15	138.22	33.34	104.88	5.27
10	100	2.25	165.3	38.77	125.03	154.8	35.32	119.48	5.55

Appendix E - Residence Time Distribution of Solids Data Collection

i. 9° Blade Overlap Angle

			500 grams				
			Blade Overlap Angle = 9°				
Sample No	Time Interval, *ti*	Tracer Weight, *Mti*	*ti.Mti.Δt*	*Mti.Δt*	*θ*	*E(t)*	*E(θ)*
0	0	0	0	0	0	0	0
1	4	0.0012	0.0192	0.0048	0.111773219	0.000164251	0.005878002
2	8	0.026	0.832	0.104	0.223546439	0.003558768	0.127356717
3	12	0.102	4.896	0.408	0.335319658	0.013961319	0.499630198
4	16	0.2579	16.5056	1.0316	0.447092877	0.035300237	1.263280668
5	20	0.56	44.8	2.24	0.558866097	0.076650378	2.743067755
6	24	1.035	99.36	4.14	0.670639316	0.141666324	5.069777011
7	28	1.323	148.176	5.292	0.782412535	0.181086519	6.480497571
8	32	1.403	179.584	5.612	0.894185755	0.192036573	6.872364393
9	36	0.89	128.16	3.56	1.005958974	0.121819351	4.359518396
10	40	0.433	69.28	1.732	1.117732193	0.059267168	2.120979175
11	44	0.211	37.136	0.844	1.229505413	0.028880768	1.033548743
12	48	0.128	24.576	0.512	1.341278632	0.017520087	0.626986915
13	52	0.11	22.88	0.44	1.453051851	0.015056324	0.53881688
14	56	0.132	29.568	0.528	1.564825071	0.018067589	0.646580257
15	60	0.104	24.96	0.416	1.67659829	0.01423507	0.509426869
16	64	0.042	10.752	0.168	1.78837151	0.005748778	0.205730082
17	68	0.0341	9.2752	0.1364	1.900144729	0.004667461	0.167033233
18	72	0.0523	15.0624	0.2092	2.011917948	0.007158598	0.256182935
19	76	0.032	9.728	0.128	2.123691168	0.004380022	0.156746729
20	80	0.0356	11.392	0.1424	2.235464387	0.004872774	0.174380736
21	84	0.0253	8.5008	0.1012	2.347237606	0.003462955	0.123927882
22	88	0.045	15.84	0.18	2.459010826	0.006159405	0.220425087
23	92	0.031	11.408	0.124	2.570784045	0.004243146	0.151848394
24	96	0.072	27.648	0.288	2.682557264	0.009855049	0.35268014
25	100	0.061	24.4	0.244	2.794330484	0.008349416	0.298798452
26	104	0.051	21.216	0.204	2.906103703	0.006980659	0.249815099
27	108	0.023	9.936	0.092	3.017876922	0.003148141	0.112661711
28	112	0.0142	6.3616	0.0568	3.129650142	0.001943635	0.069556361
29	116	0.0412	19.1168	0.1648	3.241423361	0.005639278	0.201811413
30	120	0.0301	14.448	0.1204	3.35319658	0.004119958	0.147439892
		ΣMti =	*Σti.Mti.Δti =*	*ΣMti.Δt =*	tbar =		
		7.3059	1045.8176	29.2236	35.7867477		

			1000 grams				
			Blade Overlap Angle = 9°				
Sample No	Time Interval, *ti*	Tracer Weight, *Mti*	*ti.Mti.Δt*	*Mti.Δt*	*Θ*	*E(t)*	*E(Θ)*
0	0	0	0	0	0	0	0
1	4	0.00504	0.08064	0.02016	0.109510272	0.000391942	0.014316179
2	8	0.0672	2.1504	0.2688	0.219020544	0.005225896	0.190882388
3	12	0.114	5.472	0.456	0.328530816	0.008865359	0.323818337
4	16	0.314	20.096	1.256	0.438041088	0.024418619	0.891920682
5	20	0.482	38.56	1.928	0.54755136	0.037483358	1.369126652
6	24	1.218	116.928	4.872	0.657061632	0.094719357	3.459743282
7	28	1.8676	209.1712	7.4704	0.766571904	0.145236347	5.304939699
8	32	2.1876	280.0128	8.7504	0.876082176	0.170121564	6.213903452
9	36	2.262	325.728	9.048	0.985592448	0.175907377	6.425237524
10	40	1.754	280.64	7.016	1.09510272	0.136402095	4.982257567
11	44	1.042	183.392	4.168	1.204612992	0.081032488	2.959813218
12	48	0.481	92.352	1.924	1.314123264	0.037405592	1.36628614
13	52	0.232	48.256	0.928	1.423633536	0.018041782	0.65899872
14	56	0.124	27.776	0.496	1.533143808	0.009643022	0.352223454
15	60	0.1065	25.56	0.426	1.64265408	0.008282111	0.302514499
16	64	0.0221	5.6576	0.0884	1.752164352	0.001718635	0.062775309
17	68	0.0421	11.4512	0.1684	1.861674624	0.003273961	0.119585544
18	72	0.0612	17.6256	0.2448	1.971184896	0.004759298	0.173839318
19	76	0.0273	8.2992	0.1092	2.080695168	0.00212302	0.07754597
20	80	0.0421	13.472	0.1684	2.19020544	0.003273961	0.119585544
21	84	0.033	11.088	0.132	2.299715712	0.002566288	0.093736887
22	88	0.0415	14.608	0.166	2.409225984	0.003227302	0.117881237
23	92	0.0211	7.7648	0.0844	2.518736256	0.001640869	0.059934797
24	96	0.0523	20.0832	0.2092	2.628246528	0.004067178	0.148558763
25	100	0.0701	28.04	0.2804	2.7377568	0.005451418	0.199119872
26	104	0.0607	25.2512	0.2428	2.847267072	0.004720415	0.172419062
27	108	0.0209	9.0288	0.0836	2.956777344	0.001625316	0.059366695
28	112	0.0262	11.7376	0.1048	3.066287616	0.002037477	0.074421407
29	116	0.0395	18.328	0.158	3.175797888	0.003071769	0.112200213
30	120	0.042	20.16	0.168	3.28530816	0.003266185	0.119301492
		ΣMti =	*Σti.Mti.Δti =*	*ΣMti.Δt =*	tbar =		
		12.85904	1878.77024	51.43616	36.5262539		

			1500 grams				
			Blade Overlap Angle = 9°				
Sample No	Time Interval, *ti*	Tracer Weight, *Mti*	*ti.Mti.Δt*	*Mti.Δt*	*Θ*	*E(t)*	*E(Θ)*
0	0	0	0	0	0	0	0
1	4	0.015	0.24	0.06	0.111802745	0.001122948	0.040176037
2	8	0.1056	3.3792	0.4224	0.223605489	0.007905553	0.282839303
3	12	0.2328	11.1744	0.9312	0.335408234	0.01742815	0.623532101
4	16	0.388	24.832	1.552	0.447210979	0.029046917	1.039220168
5	20	0.725	58	2.9	0.559013723	0.054275811	1.941841808
6	24	1.228	117.888	4.912	0.670816468	0.091931994	3.289078262
7	28	1.976	221.312	7.904	0.782619213	0.147929659	5.292523328
8	32	2.128	272.384	8.512	0.894421957	0.159308863	5.699640507
9	36	2.086	300.384	8.344	1.006224702	0.156164609	5.587147602
10	40	1.682	269.12	6.728	1.118027447	0.125919881	4.505072994
11	44	1.122	197.472	4.488	1.229830191	0.083996496	3.005167598
12	48	0.511	98.112	2.044	1.341632936	0.038255089	1.368663674
13	52	0.256	53.248	1.024	1.453435681	0.019164976	0.685671038
14	56	0.143	32.032	0.572	1.565238425	0.010705436	0.383011557
15	60	0.124	29.76	0.496	1.67704117	0.009283035	0.332121909
16	64	0.082	20.992	0.328	1.788843915	0.006138781	0.219629004
17	68	0.052	14.144	0.208	1.900646659	0.003892886	0.13927693
18	72	0.0521	15.0048	0.2084	2.012449404	0.003900372	0.13954477
19	76	0.0321	9.7584	0.1284	2.124252149	0.002403108	0.08597672
20	80	0.0514	16.448	0.2056	2.236054893	0.003847968	0.137669888
21	84	0.0423	14.2128	0.1692	2.347857638	0.003166713	0.113296425
22	88	0.0354	12.4608	0.1416	2.459660383	0.002650157	0.094815448
23	92	0.0179	6.5872	0.0716	2.571463127	0.001340051	0.047943405
24	96	0.0457	17.5488	0.1828	2.683265872	0.003421248	0.122402994
25	100	0.0613	24.52	0.2452	2.795068617	0.004589113	0.164186073
26	104	0.0772	32.1152	0.3088	2.906871361	0.005779438	0.206772673
27	108	0.0371	16.0272	0.1484	3.018674106	0.002777424	0.099368733
28	112	0.0229	10.2592	0.0916	3.130476851	0.001714367	0.061335417
29	116	0.0149	6.9136	0.0596	3.242279595	0.001115461	0.039908197
30	120	0.011	5.28	0.044	3.35408234	0.000823495	0.029462427
		ΣMti =	*Σti.Mti.Δti =*	*ΣMti.Δt =*	tbar =		
		13.3577	1911.6096	53.4308	35.77729699		

			2000 grams				
			Blade Overlap Angle = 9°				
Sample No	Time Interval, *ti*	Tracer Weight, *Mti*	*ti.Mti.Δt*	*Mti.Δt*	*Θ*	*E(t)*	*E(Θ)*
0	0	0	0	0	0	0	0
1	4	0.0476	0.7616	0.1904	0.110686674	0.0036742	0.132778416
2	8	0.156	4.992	0.624	0.221373348	0.012041497	0.435156155
3	12	0.282	13.536	1.128	0.332060022	0.021767321	0.786628433
4	16	0.415	26.56	1.66	0.442746696	0.032033469	1.15762695
5	20	0.627	50.16	2.508	0.55343337	0.048397555	1.748993006
6	24	1.113	106.848	4.452	0.664120044	0.085911449	3.104671795
7	28	1.623	181.776	6.492	0.774806718	0.125277881	4.527297684
8	32	1.811	231.808	7.244	0.885493392	0.139789428	5.05171664
9	36	1.882	271.008	7.528	0.996180066	0.145269853	5.249768479
10	40	1.82	291.2	7.28	1.10686674	0.14048413	5.076821803
11	44	1.431	251.856	5.724	1.217553414	0.110457577	3.991720879
12	48	0.624	119.808	2.496	1.328240088	0.048165987	1.740624618
13	52	0.317	65.936	1.268	1.438926762	0.024468939	0.884259622
14	56	0.167	37.408	0.668	1.549613436	0.012890577	0.465840242
15	60	0.143	34.32	0.572	1.66030011	0.011038039	0.398893142
16	64	0.033	8.448	0.132	1.770986784	0.00254724	0.092052263
17	68	0.017	4.624	0.068	1.881673458	0.001312214	0.047420863
18	72	0.032	9.216	0.128	1.992360132	0.002470051	0.089262801
19	76	0.025	7.6	0.1	2.103046806	0.001929727	0.069736563
20	80	0.0321	10.272	0.1284	2.213733479	0.00247777	0.089541747
21	84	0.035	11.76	0.14	2.324420153	0.002701618	0.097631189
22	88	0.0371	13.0592	0.1484	2.435106827	0.002863715	0.10348906
23	92	0.0182	6.6976	0.0728	2.545793501	0.001404841	0.050768218
24	96	0.043	16.512	0.172	2.656480175	0.003319131	0.119946889
25	100	0.0521	20.84	0.2084	2.767166849	0.004021551	0.145330998
26	104	0.0682	28.3712	0.2728	2.877853523	0.005264295	0.190241344
27	108	0.0323	13.9536	0.1292	2.988540197	0.002493207	0.09009964
28	112	0.0217	9.7216	0.0868	3.099226871	0.001675003	0.060531337
29	116	0.0189	8.7696	0.0756	3.209913545	0.001458874	0.052720842
30	120	0.031	14.88	0.124	3.320600219	0.002392862	0.086473338
		ΣMti =	*Σti.Mti.Δti =*	*ΣMti.Δt =*	tbar =		
		12.9552	1872.7024	51.8208	36.13804495		

ii. 12° Blade Overlap Angle

			500 grams				
			Blade Overlap Angle = 12°				
Sample No	Time Interval, *ti*	Tracer Weight, *Mti*	*ti.Mti.Δt*	*Mti.Δt*	*Θ*	*E(t)*	*E(Θ)*
0	0	0	0	0	0	0	0
1	4	0.003	0.048	0.012	0.097731778	0.000339755	0.013905598
2	8	0.022	0.704	0.088	0.195463556	0.002491534	0.101974383
3	12	0.053	2.544	0.212	0.293195334	0.006002333	0.24566556
4	16	0.092	5.888	0.368	0.390927112	0.010419144	0.42643833
5	20	0.21	16.8	0.84	0.48865889	0.023782829	0.97339184
6	24	0.53	50.88	2.12	0.586390668	0.06002333	2.456655595
7	28	0.87	97.44	3.48	0.684122446	0.098528862	4.032623335
8	32	1.22	156.16	4.88	0.781854224	0.13816691	5.654943068
9	36	1.39	200.16	5.56	0.879586002	0.157419676	6.442926938
10	40	1.34	214.4	5.36	0.97731778	0.151757098	6.211166976
11	44	0.98	172.48	3.92	1.075049558	0.110986534	4.542495251
12	48	0.69	132.48	2.76	1.172781336	0.07814358	3.198287473
13	52	0.47	97.76	1.88	1.270513114	0.053228236	2.178543641
14	56	0.27	60.48	1.08	1.368244892	0.030577923	1.251503794
15	60	0.11	26.4	0.44	1.46597667	0.012457672	0.509871916
16	64	0.042	10.752	0.168	1.563708448	0.004756566	0.194678368
17	68	0.034	9.248	0.136	1.661440226	0.003850553	0.157596774
18	72	0.052	14.976	0.208	1.759172004	0.005889081	0.24103036
19	76	0.032	9.728	0.128	1.856903782	0.00362405	0.148326376
20	80	0.0356	11.392	0.1424	1.95463556	0.004031756	0.165013093
21	84	0.0253	8.5008	0.1012	2.052367338	0.002865265	0.117270541
22	88	0.045	15.84	0.18	2.150099116	0.00509632	0.208583966
23	92	0.03	11.04	0.12	2.247830894	0.003397547	0.139055977
24	96	0.07	26.88	0.28	2.345562672	0.00792761	0.324463947
25	100	0.06	24	0.24	2.44329445	0.006795094	0.278111954
26	104	0.051	21.216	0.204	2.541026228	0.00577583	0.236395161
27	108	0.023	9.936	0.092	2.638758007	0.002604786	0.106609582
28	112	0.01	4.48	0.04	2.736489785	0.001132516	0.046351992
29	116	0.04	18.56	0.16	2.834221563	0.004530063	0.185407969
30	120	0.03	14.4	0.12	2.931953341	0.003397547	0.139055977
		ΣMti =	*Σti.Mti.Δti =*	*ΣMti.Δt =*	tbar =		
		8.8299	1445.5728	35.3196	40.92834573		

			1000 grams Blade Overlap Angle = 12°				
Sample No	Time Interval, *ti*	Tracer Weight, *Mti*	*ti.Mti.Δt*	*Mti.Δt*	*Θ*	*E(t)*	*E(Θ)*
0	0	0	0	0	0	0	0
1	4	0.0045	0.072	0.018	0.099557711	0.0003248	0.013049698
2	8	0.033	1.056	0.132	0.199115423	0.002381863	0.095697788
3	12	0.0795	3.816	0.318	0.298673134	0.005738125	0.230544672
4	16	0.1335	8.544	0.534	0.398230845	0.009635719	0.387141053
5	20	0.3	24	1.2	0.497788557	0.021653302	0.869979893
6	24	0.795	76.32	3.18	0.597346268	0.05738125	2.305446717
7	28	1.305	146.16	5.22	0.696903979	0.094191863	3.784412536
8	32	1.83	234.24	7.32	0.79646169	0.132085141	5.30687735
9	36	2.07	298.08	8.28	0.896019402	0.149407782	6.002861264
10	40	2.04	326.4	8.16	0.995577113	0.147242452	5.915863275
11	44	1.8	316.8	7.2	1.095134824	0.129919811	5.21987936
12	48	1.275	244.8	5.1	1.194692536	0.092026533	3.697414547
13	52	0.84	174.72	3.36	1.294250247	0.060629245	2.435943701
14	56	0.5125	114.8	2.05	1.393807958	0.036991057	1.486215651
15	60	0.22	52.8	0.88	1.49336567	0.015879088	0.637985255
16	64	0.1265	32.384	0.506	1.592923381	0.009130476	0.366841522
17	68	0.057	15.504	0.228	1.692481092	0.004114127	0.16529618
18	72	0.0825	23.76	0.33	1.792038804	0.005954658	0.239244471
19	76	0.031	9.424	0.124	1.891596515	0.002237508	0.089897922
20	80	0.045	14.4	0.18	1.991154226	0.003247995	0.130496984
21	84	0.0375	12.6	0.15	2.090711937	0.002706663	0.108747487
22	88	0.045	15.84	0.18	2.190269649	0.003247995	0.130496984
23	92	0.02	7.36	0.08	2.28982736	0.001443553	0.05799866
24	96	0.043	16.512	0.172	2.389385071	0.00310364	0.124697118
25	100	0.03	12	0.12	2.488942783	0.00216533	0.086997989
26	104	0.016	6.656	0.064	2.588500494	0.001154843	0.046398928
27	108	0.014	6.048	0.056	2.688058205	0.001010487	0.040599062
28	112	0.04	17.92	0.16	2.787615917	0.002887107	0.115997319
29	116	0.027	12.528	0.108	2.887173628	0.001948797	0.07829819
30	120	0.0022	1.056	0.0088	2.986731339	0.000158791	0.006379853
		ΣMti =	*Σti.Mti.Δti* =	*ΣMti.Δt* =	tbar =		
		13.8547	2226.6	55.4188	40.17770143		

			1500 grams				
			Blade Overlap Angle = 12°				
Sample No	Time Interval, *ti*	Tracer Weight, *Mti*	*ti.Mti.Δt*	*Mti.Δt*	*Θ*	*E(t)*	*E(Θ)*
0	0	0	0	0	0	0	0
1	4	0.00525	0.084	0.021	0.100788253	0.000370153	0.014690338
2	8	0.0385	1.232	0.154	0.201576506	0.002714458	0.107729144
3	12	0.09275	4.452	0.371	0.302364759	0.006539376	0.259529301
4	16	0.15575	9.968	0.623	0.403153012	0.010981217	0.435813354
5	20	0.35	28	1.4	0.503941265	0.024676891	0.979355852
6	24	0.9275	89.04	3.71	0.604729518	0.065393762	2.595293007
7	28	1.5225	170.52	6.09	0.705517772	0.107344477	4.260197955
8	32	1.83	234.24	7.32	0.806306025	0.129024889	5.120632025
9	36	2.001	288.144	8.004	0.907094278	0.141081313	5.599117313
10	40	1.9745	315.92	7.898	1.007882531	0.13921292	5.524966084
11	44	1.824	321.024	7.296	1.108670784	0.128601857	5.103843068
12	48	1.3005	249.696	5.202	1.209459037	0.091692278	3.639006529
13	52	0.864	179.712	3.456	1.31024729	0.060916669	2.417609874
14	56	0.4674	104.6976	1.8696	1.411035543	0.032954226	1.307859786
15	60	0.22	52.8	0.88	1.511823796	0.015511189	0.615595107
16	64	0.1298	33.2288	0.5192	1.612612049	0.009151601	0.363201113
17	68	0.05092	13.85024	0.20368	1.713400302	0.003590135	0.142482286
18	72	0.0792	22.8096	0.3168	1.814188555	0.005584028	0.221614238
19	76	0.0324	9.8496	0.1296	1.914976808	0.002284375	0.09066037
20	80	0.0435	13.92	0.174	2.015765062	0.003066985	0.121719942
21	84	0.0375	12.6	0.15	2.116553315	0.002643953	0.104930984
22	88	0.036	12.672	0.144	2.217341568	0.002538195	0.100733745
23	92	0.0282	10.3776	0.1128	2.318129821	0.001988252	0.0789081
24	96	0.0424	16.2816	0.1696	2.418918074	0.002989429	0.118641966
25	100	0.0331	13.24	0.1324	2.519706327	0.002333729	0.092619082
26	104	0.0143	5.9488	0.0572	2.62049458	0.001008227	0.040013682
27	108	0.0114	4.9248	0.0456	2.721282833	0.000803762	0.031899019
28	112	0.0376	16.8448	0.1504	2.822071086	0.002651003	0.1052108
29	116	0.0312	14.4768	0.1248	2.922859339	0.002199769	0.087302579
30	120	0.00214	1.0272	0.00856	3.023647592	0.000150882	0.005988061
		ΣMti =	*Σti.Mti.Δti* =	*ΣMti.Δt* =	tbar =		
		14.18331	2251.58144	56.73324	39.6871647		

			2000 grams				
			Blade Overlap Angle = 12°				
Sample No	Time Interval, *ti*	Tracer Weight, *Mti*	*ti.Mti.Δt*	*Mti.Δt*	*Θ*	*E(t)*	*E(Θ)*
0	0	0	0	0	0	0	0
1	4	0.08325	1.332	0.333	0.105336613	0.005621326	0.213461444
2	8	0.14625	4.68	0.585	0.210673227	0.009875303	0.374999834
3	12	0.19504	9.36192	0.78016	0.31600984	0.013169772	0.500102342
4	16	0.2886	18.4704	1.1544	0.421346453	0.019487265	0.739999672
5	20	0.49	39.2	1.96	0.526683066	0.033086486	1.256409699
6	24	1.26	120.96	5.04	0.63201968	0.085079535	3.230767797
7	28	1.776	198.912	7.104	0.737356293	0.11992163	4.553844133
8	32	1.95	249.6	7.8	0.842692906	0.131670708	4.999997782
9	36	2.01066	289.53504	8.04264	0.948029519	0.13576668	5.155536174
10	40	1.904	304.64	7.616	1.053366133	0.12856463	4.882049116
11	44	1.464	257.664	5.856	1.158702746	0.098854316	3.753844488
12	48	1.105	212.16	4.42	1.264039359	0.074613401	2.833332076
13	52	0.78	162.24	3.12	1.369375973	0.052668283	1.999999113
14	56	0.492	110.208	1.968	1.474712586	0.033221533	1.261537902
15	60	0.22	52.8	0.88	1.580049199	0.014855157	0.564102314
16	64	0.1265	32.384	0.506	1.685385812	0.008541715	0.32435883
17	68	0.046892	12.754624	0.187568	1.790722426	0.003166309	0.120235844
18	72	0.0792	22.8096	0.3168	1.896059039	0.005347856	0.203076833
19	76	0.045	13.68	0.18	2.001395652	0.003038555	0.115384564
20	80	0.0435	13.92	0.174	2.106732265	0.00293727	0.111538412
21	84	0.0375	12.6	0.15	2.212068879	0.002532129	0.096153803
22	88	0.036	12.672	0.144	2.317405492	0.002430844	0.092307651
23	92	0.0282	10.3776	0.1128	2.422742105	0.001904161	0.07230766
24	96	0.0424	16.2816	0.1696	2.528078718	0.002862994	0.1087179
25	100	0.0331	13.24	0.1324	2.633415332	0.002235026	0.084871757
26	104	0.0113	4.7008	0.0452	2.738751945	0.000763015	0.028974346
27	108	0.0146	6.3072	0.0584	2.844088558	0.000985842	0.037435881
28	112	0.0456	20.4288	0.1824	2.949425172	0.003079069	0.116923025
29	116	0.0536	24.8704	0.2144	3.054761785	0.003619256	0.137435836
30	120	0.00148	0.7104	0.00592	3.160098398	9.99347E-05	0.00379487
		ΣMti =	*Σti.Mti.Δti* =	*ΣMti.Δt* =	tbar =		
		14.809672	2249.500384	59.238688	37.9735011		

iii. 15° Blade Overlap Angle

			500 grams				
			Blade Overlap Angle = 15°				
Sample No	Time Interval, *ti*	Tracer Weight, *Mti*	*ti.Mti.Δt*	*Mti.Δt*	*θ*	*E(t)*	*E(θ)*
0	0	0	0	0	0	0	0
1	4	0.028	0.448	0.112	0.097045859	0.003007228	0.123950805
2	8	0.047	1.504	0.188	0.194091719	0.005047847	0.208060279
3	12	0.078	3.744	0.312	0.291137578	0.008377278	0.345291527
4	16	0.117	7.488	0.468	0.388183438	0.012565917	0.517937291
5	20	0.235	18.8	0.94	0.485229297	0.025239236	1.040301396
6	24	0.555	53.28	2.22	0.582275156	0.059607557	2.456882019
7	28	0.895	100.24	3.58	0.679321016	0.096123898	3.961998932
8	32	1.245	159.36	4.98	0.776366875	0.133714249	5.511383989
9	36	1.375	198	5.5	0.873412734	0.147676379	6.086869867
10	40	1.335	213.6	5.34	0.970458594	0.143380339	5.909797289
11	44	1.005	176.88	4.02	1.067504453	0.107938008	4.448948521
12	48	0.715	137.28	2.86	1.164550313	0.076791717	3.165172331
13	52	0.495	102.96	1.98	1.261596172	0.053163497	2.191273152
14	56	0.295	66.08	1.18	1.358642031	0.031683296	1.305910262
15	60	0.135	32.4	0.54	1.455687891	0.014499135	0.597619951
16	64	0.067	17.152	0.268	1.55273375	0.007195867	0.296596568
17	68	0.059	16.048	0.236	1.649779609	0.006336659	0.261182052
18	72	0.077	22.176	0.308	1.746825469	0.008269877	0.340864713
19	76	0.057	17.328	0.228	1.843871328	0.006121857	0.252328424
20	80	0.0606	19.392	0.2424	1.940917188	0.006508501	0.268264956
21	84	0.0503	16.9008	0.2012	2.037963047	0.00540227	0.222668767
22	88	0.07	24.64	0.28	2.135008906	0.00751807	0.309877011
23	92	0.055	20.24	0.22	2.232054766	0.005907055	0.243474795
24	96	0.065	24.96	0.26	2.329100625	0.006981065	0.287742939
25	100	0.035	14	0.14	2.426146484	0.003759035	0.154938506
26	104	0.046	19.136	0.184	2.523192344	0.004940446	0.203633465
27	108	0.048	20.736	0.192	2.620238203	0.005155248	0.212487094
28	112	0.031	13.888	0.124	2.717284063	0.003329431	0.137231248
29	116	0.023	10.672	0.092	2.814329922	0.002470223	0.101816732
30	120	0.012	5.76	0.048	2.911375781	0.001288812	0.053121773
		ΣMti =	*Σti.Mti.Δti =*	*ΣMti.Δt =*	tbar =		
		9.3109	1535.0928	37.2436	41.21762665		

			1000 grams				
			Blade Overlap Angle = 15°				
Sample No	Time Interval, *ti*	Tracer Weight, *Mti*	*ti.Mti.Δt*	*Mti.Δt*	*Θ*	*E(t)*	*E(Θ)*
0	0	0	0	0	0	0	0
1	4	0.0545	0.872	0.218	0.099487709	0.003670849	0.147590068
2	8	0.083	2.656	0.332	0.198975417	0.005590468	0.224770195
3	12	0.1295	6.216	0.518	0.298463126	0.008722477	0.350695665
4	16	0.1835	11.744	0.734	0.397950835	0.012359649	0.496931696
5	20	0.35	28	1.4	0.497438543	0.023574262	0.947826123
6	24	0.845	81.12	3.38	0.596926252	0.056915005	2.288323067
7	28	1.355	151.76	5.42	0.696413961	0.091266073	3.669441132
8	32	1.88	240.64	7.52	0.79590167	0.126627466	5.091180316
9	36	2.12	305.28	8.48	0.895389378	0.142792674	5.741118228
10	40	2.09	334.4	8.36	0.994877087	0.140772023	5.659875989
11	44	1.85	325.6	7.4	1.094364796	0.124606815	5.009938076
12	48	1.325	254.4	5.3	1.193852504	0.089245422	3.588198893
13	52	0.89	185.12	3.56	1.293340213	0.059945981	2.410186426
14	56	0.5625	126	2.25	1.392827922	0.037887207	1.523291983
15	60	0.27	64.8	1.08	1.49231563	0.018185859	0.731180152
16	64	0.1765	45.184	0.706	1.591803339	0.011888164	0.477975173
17	68	0.107	29.104	0.428	1.691291048	0.007206989	0.289763986
18	72	0.1325	38.16	0.53	1.790778756	0.008924542	0.358819889
19	76	0.081	24.624	0.324	1.890266465	0.005455758	0.219354046
20	80	0.097	31.04	0.388	1.989754174	0.006533438	0.26268324
21	84	0.0875	29.4	0.35	2.089241883	0.005893566	0.236956531
22	88	0.032	11.264	0.128	2.188729591	0.002155361	0.086658388
23	92	0.012	4.416	0.048	2.2882173	0.00080826	0.032496896
24	96	0.033	12.672	0.132	2.387705009	0.002222716	0.089366463
25	100	0.023	9.2	0.092	2.487192717	0.001549166	0.062285717
26	104	0.017	7.072	0.068	2.586680426	0.001145036	0.046037269
27	108	0.021	9.072	0.084	2.686168135	0.001414456	0.056869567
28	112	0.022	9.856	0.088	2.785655843	0.001481811	0.059577642
29	116	0.014	6.496	0.056	2.885143552	0.00094297	0.037913045
30	120	0.0032	1.536	0.0128	2.984631261	0.000215536	0.008665839
		ΣMti =	*Σti.Mti.Δti =*	*ΣMti.Δt =*	tbar =		
		14.8467	2387.704	59.3868	40.2059717		

			1500 grams				
			Blade Overlap Angle = 15°				
Sample No	Time Interval, *ti*	Tracer Weight, *Mti*	*ti.Mti.Δt*	*Mti.Δt*	*Θ*	*E(t)*	*E(Θ)*
0	0	0	0	0	0	0	0
1	4	0.0752	1.2032	0.3008	0.101412012	0.004889302	0.192849009
2	8	0.1085	3.472	0.434	0.202824025	0.007054378	0.278246244
3	12	0.16275	7.812	0.651	0.304236037	0.010581567	0.417369366
4	16	0.22575	14.448	0.903	0.405648049	0.014677657	0.578931701
5	20	0.42	33.6	1.68	0.507060062	0.027307269	1.077082234
6	24	0.9975	95.76	3.99	0.608472074	0.064854764	2.558070305
7	28	1.62	181.44	6.48	0.709884086	0.105328038	4.154460045
8	32	1.833	234.624	7.332	0.811296099	0.119176725	4.700694606
9	36	2.02	290.88	8.08	0.912708111	0.131334961	5.180252649
10	40	2.07	331.2	8.28	1.014120123	0.134585827	5.308476724
11	44	1.894	333.344	7.576	1.115532136	0.123142781	4.857127978
12	48	1.421	272.832	5.684	1.216944148	0.092389594	3.644128225
13	52	0.891	185.328	3.564	1.31835616	0.057930421	2.284953025
14	56	0.5384	120.6016	2.1536	1.419768173	0.035005318	1.380716845
15	60	0.291	69.84	1.164	1.521180185	0.018920037	0.746264119
16	64	0.2008	51.4048	0.8032	1.622592197	0.013055475	0.514947887
17	68	0.12192	33.16224	0.48768	1.72400421	0.00792691	0.312661586
18	72	0.1502	43.2576	0.6008	1.825416222	0.0097656	0.385185123
19	76	0.1034	31.4336	0.4136	1.926828234	0.00672279	0.265167388
20	80	0.032	10.24	0.128	2.028240247	0.002080554	0.082063408
21	84	0.022	7.392	0.088	2.129652259	0.001430381	0.056418593
22	88	0.031	10.912	0.124	2.231064271	0.002015537	0.079498927
23	92	0.021	7.728	0.084	2.332476284	0.001365363	0.053854112
24	96	0.034	13.056	0.136	2.433888296	0.002210588	0.087192371
25	100	0.022	8.8	0.088	2.535300308	0.001430381	0.056418593
26	104	0.013	5.408	0.052	2.636712321	0.000845225	0.03333826
27	108	0.011	4.752	0.044	2.738124333	0.00071519	0.028209297
28	112	0.037	16.576	0.148	2.839536345	0.00240564	0.094885816
29	116	0.011	5.104	0.044	2.940948358	0.00071519	0.028209297
30	120	0.0021	1.008	0.0084	3.04236037	0.000136536	0.005385411
		ΣMti =	*Σti.Mti.Δti* =	*ΣMti.Δt* =	tbar =		
		15.38052	2426.61904	61.52208	39.44305914		

			2000 grams				
			Blade Overlap Angle = 15°				
Sample No	Time Interval, *ti*	Tracer Weight, *Mti*	*ti.Mti.Δt*	*Mti.Δt*	*Θ*	*E(t)*	*E(Θ)*
0	0	0	0	0	0	0	0
1	4	0.07825	1.252	0.313	0.106408471	0.005020183	0.188713674
2	8	0.12625	4.04	0.505	0.212816943	0.008099657	0.304474138
3	12	0.2154	10.3392	0.8616	0.319225414	0.013819137	0.519475083
4	16	0.306	19.584	1.224	0.425633886	0.019631644	0.73797296
5	20	0.565	45.2	2.26	0.532042357	0.036247969	1.362597131
6	24	1.335	128.16	5.34	0.638450828	0.085647857	3.219587912
7	28	1.835	205.52	7.34	0.7448593	0.117725706	4.425426082
8	32	1.985	254.08	7.94	0.851267771	0.127349061	4.787177532
9	36	2.065	297.36	8.26	0.957676243	0.132481517	4.98011164
10	40	1.979	316.64	7.916	1.064084714	0.126964127	4.772707474
11	44	1.639	288.464	6.556	1.170493185	0.105151189	3.952737519
12	48	1.18	226.56	4.72	1.276901657	0.075703724	2.84577808
13	52	0.855	177.84	3.42	1.383310128	0.054853122	2.06198327
14	56	0.567	127.008	2.268	1.4897186	0.036376281	1.367420484
15	60	0.295	70.8	1.18	1.596127071	0.018925931	0.71144452
16	64	0.2015	51.584	0.806	1.702535542	0.012927373	0.485952782
17	68	0.1248	33.9456	0.4992	1.808944014	0.008006631	0.300977207
18	72	0.044	12.672	0.176	1.915352485	0.002822851	0.106113759
19	76	0.026	7.904	0.104	2.021760957	0.001668048	0.062703585
20	80	0.013	4.16	0.052	2.128169428	0.000834024	0.031351792
21	84	0.024	8.064	0.096	2.234577899	0.001539737	0.057880232
22	88	0.012	4.224	0.048	2.340986371	0.000769868	0.028940116
23	92	0.016	5.888	0.064	2.447394842	0.001026491	0.038586821
24	96	0.022	8.448	0.088	2.553803314	0.001411425	0.053056879
25	100	0.013	5.2	0.052	2.660211785	0.000834024	0.031351792
26	104	0.011	4.576	0.044	2.766620256	0.000705713	0.02652844
27	108	0.0145	6.264	0.058	2.873028728	0.000930258	0.034969307
28	112	0.021	9.408	0.084	2.979437199	0.00134727	0.050645203
29	116	0.017	7.888	0.068	3.085845671	0.001090647	0.040998498
30	120	0.00138	0.6624	0.00552	3.192254142	8.85349E-05	0.003328113
		ΣMti =	*Σti.Mti.Δti =*	*ΣMti.Δt =*	tbar =		
		15.58708	2343.7352	62.34832	37.59099203		

Appendix F - Project Recognition

i. Acceptance from 2nd International Conference on Advanced Materials and Engineering Materials 2012 (ICAMEM2012)

Notification of Acceptance

2nd International Conference on Advanced Materials and Engineering Materials 2012 (ICAMEM 2012)

Beijing, China Dec.16-17 Shanghai, China Dec.29-30

http://www.icamem.org

Dear S. Fauzan Ashri,Chin Yee Sing,Vijay R. Raghavan

Paper ID: 124

Paper Title: Experimental Studies on the Pressure Drop of Multi-Staged Swirling Fluidized Bed

The review process of your paper for 2nd International Conference on Advanced Materials and Engineering Materials 2012 (ICAMEM 2012) has been completed. We are pleased to inform you that your paper has been accepted for presentation. You are cordially invited to present the paper at ICAMEM2012 held on 16-17 December 2012, in Beijing, China. On 29-30 December 2012, in Shanghai, China

This notification serves as our formal acceptance of your paper as well as an invitation to present your work at ICAMEM2012. Please note that this NOTIFICATION will be sent to your co-author(s) (if any), as well.

Important Note:

In order to register the conference successfully, you must finish the following FOUR processes and register by Email. (Before December 7, 2012)

1. Finish the payment of Registration fee according to the Registration Form.
2. Format your paper according to the Template, please download the AuthorInstructions on the website http://icamem.org/Author%20Instructions.rtf
3. Submit **Final Paper** (**BOTH MS Word file and PDF**) and **Copyright Form via TTP** online submission and editing tool after the conference (by the end of December, 2012). Note that we will send your personal login and password information via TTP new online tool at the end of December.
4. Send your

(1)Filled Registration Form;
(2)Final Paper (both .doc and .pdf format);
(3)The Scanned Payment Proof (in jpg format);
(4) Scanned Student Card (in jpg format if any);
(5)Scanned Copyright Agreement (in pdf format)

Please strictly adhere to the format specified in the conference template while preparing your final paper. If you have any problem when preparing the final paper, please feel free to contact us via icamem2012@hotmail.com

If the above requirements are met by the set deadlines, the paper will be published in "Advanced Materials Research" [ISSN:1022-6680, Trans Tech Publications] which should be indexed by Elsevier: SCOPUS www.scopus.comand **Ei Compendex (CPX)** www.ei.org/.Cambridge Scientific Abstracts (CSA) www.csa.com, Chemical Abstracts (CA) www.cas.org, Google and Google Scholar google.com, **ISI (ISTP, CPCI, Web of Science)**www.isinet.com, Institution of Electrical Engineers (IEE) www.iee.org,etc. http://www.ttp.net/1022-6680.html.The full text is online available via platform www.scientific.net.

Please kindly notice that the Conference Program will be available at the website in December 2012. The CD-ROM Proceedings will be available at the conference and online version should be available within 8-10 weeks after receiving the manuscript in full text via TTP platform. Authors will receive free online "author access" via your email address (as it appears in the paper) and from us supplied password. Via this access you will be able to download your papers as PDF and order reprints online. In addition participants will receive full online access to the entire proceedings via TTP platform http://www.scientific.net.Hard copy of Proceedings will be sent to authors about 3-4 months after the time of receipt of the manuscripts by TTP.

Maybe some unforeseeable events could prevent a few authors attending the conference to present their papers, if so, please inform us. And we will send you the official receipt and proceeding after ICAMEM 2012.

Finally, we would like to further extend our congratulations to you and we are looking forward to meeting you in Beijing or Shanghai, China!

Yours sincerely,
ICAMEM2012

ttp trans tech publications inc.
Publishers in Science and Engineering

ii. Acceptance from International Conference on Mechatronics and Computational Mechanics 2012 (ICMCM2012)

ICMCM2012 Notification of Acceptance

http://www.icmcm.org/

***Dear** S. Fauzan Ashri and Chin Yee Sing*

***Paper ID:** 126*

***Paper Title:** Experimental Studies on the Pressure Drop of Multi-Staged Swirling Fluidized Bed*

The review process of your paper for 2012 International Conference on Mechatronics and Computational Mechanics (ICMCM 2012) has been completed. We are pleased to inform you that your paper has been accepted for presentation. You are cordially invited to present the paper at ICMCM 2012 held on 20 - 21 December 2012, in Dubai, UAE.

This notification serves as our formal acceptance of your paper as well as an invitation to present your work at ICMCM 2012. Please note that this NOTIFICATION will be sent to your co-author(s) (if any), as well.

Important Note:

Please kindly notice that the paper will not be published in the proceedings unless the author pays the registration fee. In order to register the conference successfully, you must finish the following FOUR processes and register by Email. (Before December 6, 2012).

1. Finish the payment of Registration fee according to the Registration Form)
2. Format your paper according to the Template http://www.icmcm.org/downloads/AuthorInstructions.rtf
3. Send your (1) filled Registration Form (You can download Registration Form from the website http://www.icmcm.org/reg.html), (2) Final Paper (BOTH MS Word file and PDF), (3) the Scanned Payment Proof (in jpg format), (4) Scanned Student Card (in jpg format if any) and (5) COPYRIGHT Agreement FORM (.pdf) to us by email cfp@icmcm.org.
4. Submit Final Paper (BOTH MS Word file and PDF) and Copyright Form via TTP online submission and editing tool in late December 2012. Note that we will send your personal login and password information via TTP new online tool in late December.

Please strictly adhere to the format specified in the conference template while preparing your final paper. If you have any problem when preparing the final paper, please feel free to contact us via cfp@icmcm.org.

If the above requirements are met by the set deadlines, the paper will be published in Applied Mechanics and Materials [ISSN:1660-9336, Trans Tech Publications].Applied Mechanics and Materials is indexed by Elsevier: SCOPUS www.scopus.com and Ei Compendex (CPX) www.ei.org/. Cambridge Scientific Abstracts (CSA) www.csa.com,Chemical Abstracts (CA) www.cas.org, Google and Google Scholar google.com, ISI (ISTP, CPCI, Web of Science)www.isinet.com, Institution of Electrical Engineers (IEE) www.iee.org, etc. http://www.ttp.net/1660-9336.html

Please kindly notice that the Conference Program will be available at the website in December, 2012. The CD-ROM Proceedings will be available at the conference and online version should be available within 8-10 weeks after receiving the manuscript in full text via TTP platform. Authors will receive free online "author access" via your email address (as it appears in the paper) and from us supplied password. Via this access you will be able to download your papers as PDF and order reprints online. In addition participants will receive full online access to the entire proceedings via TTP platform http://www.scientific.net. Hard copy of Proceedings will be sent to authors about 3-4 months after the time of receipt of the manuscripts by TTP.

Maybe some unforeseeable events could prevent a few authors attending the conference to present their papers, if so, please inform us. And we will send you the official receipt and proceeding after ICMCM 2012.

Finally, we would like to further extend our congratulations to you and we are looking forward to meeting you in Dubai, UAE!

Yours sincerely,

ICMCM 2012

Appendix G - Calculation of Superficial Velocity

According to Sreenivasan and Raghavan [7], superficial velocity in ms^{-1} is obtained by dividing the measured air flow rate by the distributor ring area.

$$V_{Superficial} = \frac{\text{Flow rate } (m^3/s)}{\text{Bed area } (m^2)}$$

The flow rate (Q) is obtained from the orifice flow rate, which is represented by:

$$\text{Flow rate} = \frac{C_d \times \sqrt{2 \times g \times \Delta p_{air}} \times \text{Orifice Area}}{\sqrt{1 - (d/D)^4}}$$

Given:

1. Pipe diameter, D = 0.1 m
2. Orifice diameter hole, d = 0.062 m
3. Coefficient of discharge, $C_d = 0.068$
4. Air density, $\rho_{air} = 1.2\ kg/m^3$
5. Beta Ratio, $\beta = \frac{d}{D} = \frac{0.062}{0.1} = 0.62$
6. Orifice area, $A = \frac{\pi d^2}{4} = \frac{\pi (0.062)^2}{4} = 0.003019\ m^2$
7. Bed Area, $A_{bed} = \frac{\pi}{4}\left(Bed\ Outer\ Diameter, D_o^2 - Bed\ Inner\ Diameter, D_i^2\right) = 0.039$

   Thus, superficial velocity yields,

$$V_{sup} = \frac{0.668 * 0.003019 * \sqrt{2 * 9.81 * \frac{Orifice\ Pressure\ Difference, \Delta P}{\rho_{air}}}}{\sqrt{1 - \left(\frac{d}{D}\right)^4}} * \frac{1}{0.039}$$

   Superficial Velocity, $V_{sup} = 0.225 \sqrt{Orifice\ Pressure\ Difference, \Delta P}$